1521-0081/65/4/1214–1256$25.00
PHARMACOLOGICAL REVIEWS

http://dx.doi.org/10.1124/pr.113.007625
Pharmacol Rev 65:1214–1256, October 2013

ASSOCIATE EDITOR: MICHAEL G. ROSENBLUM

Interrogating Tumor Metabolism and Tumor Microenvironments Using Molecular Positron Emission Tomography Imaging. Theranostic Approaches to Improve Therapeutics

Orit Jacobson and Xiaoyuan Chen

Laboratory of Molecular Imaging and Nanomedicine, National Institute of Biomedical Imaging and Bioengineering, National Institutes of Health, Bethesda, Maryland

This work is supported by the Intramural Research Program of the National Institutes of Health [National Institute of Biomedical Imaging and Bioengineering].

Address correspondence to: Xiaoyuan Chen, Laboratory of Molecular Imaging and Nanomedicine, National Institute of Biomedical Imaging and Bioengineering, National Institutes of Health, Bethesda, MD. E-mail: shawn.chen@nih.gov

dx.doi.org/10.1124/pr.113.007625.

***Abstract*——Positron emission tomography (PET) is a noninvasive molecular imaging technology that is becoming increasingly important for the measurement of physiologic, biochemical, and pharmacological functions at cellular and molecular levels in patients with cancer. Formation, development, and aggressiveness of tumor involve a number of molecular pathways, including intrinsic tumor cell mutations and extrinsic interaction between tumor cells and the microenvironment. Currently, evaluation of these processes is mainly through biopsy, which is invasive and limited to the site of biopsy. Ongoing research on specific target molecules of the tumor and its microenvironment for PET imaging is showing great potential. To date, the use of PET for diagnosing local recurrence and metastatic sites of various cancers and evaluation of treatment response is mainly based on [^{18}F]fluorodeoxyglucose ([^{18}F]FDG), which measures glucose metabolism. However, [^{18}F]FDG is not a target-specific PET tracer and does not give enough insight into tumor biology and/or its vulnerability to potential treatments. Hence, there is an increasing need for the development of selective biologic radiotracers that will yield specific biochemical information and allow for noninvasive molecular imaging. The possibility of cancer-associated targets for imaging will provide the opportunity to use PET for diagnosis and therapy response monitoring (theranostics) and thus personalized medicine. This article will focus on the review of non-[^{18}F]FDG PET tracers for specific tumor biology processes and their preclinical and clinical applications.**

I. Introduction

A. Nuclear Medicine

Nuclear medicine is a noninvasive imaging modality that harnesses the properties of radioactive isotopes to enable visualization of biologic components under normal and pathologic conditions in living subjects. Depending on the properties of the radiotracer, various aspects of biochemical processes can be targeted and visualized by single-photon emission computed tomography (SPECT) or positron emission tomography (PET). Although both modalities are used for cancer diagnosis and imaging, they have relatively low spatial resolution and thus provide limited anatomic information of the lesions. On the other hand, the high sensitivity of these modalities makes them an appropriate molecular imaging technology of choice.

Magnetic resonance imaging (MRI), computed tomography (CT), and ultrasound can precisely visualize the morphology of lesions and provide the exact localization of malignant sites. In addition, functional MRI provides functional imaging data, such as changes in perfusion of neural activity in the brain (Vanzetta, 2006). However, these technologies are not able to give specific information on the biochemical processes within a given tissue, nor can they image specific target macromolecules within the human body because of their low sensitivity (Nishimura et al., 1988; Spanaki et al., 1999; Ryu et al., 2002). The increasing availability of PET and SPECT fused/coregistered with CT and MRI for precise anatomic localization, coupled with the discovery of a multitude of new biochemical targets that characterize a specific disease, has led to tremendous

ABBREVIATIONS: Akt/AKT, protein kinase B; AR, androgen receptor; ATSM, diacetyl-bis(N^4-methylthiosemicarbazone; [^{11}C]MET, [^{11}C]methionine; BBNR, bombesin receptor; CDK, cyclin-dependent kinases; c-EGF, Cys-tagged epidermal growth factor; CT, computed tomography; CXCR4, CXC chemokine receptor 4; DHT, dihydrotestosterone; DFO, desferrioxamine B; ECM, extracellular matrix; EGFR, epidermal growth factor receptor; [^{18}F]EF-5, [^{18}F]2-(2-nitro-1*H*-imidazol-1-yl)-*N*-(2,2,3,3,3-pentafluoropropyl)-acetamide; [^{18}F]FAZA, [^{18}F]fluoroazomycinarabinoside; [^{18}F]FBEM, *N*-[2-(4-[^{18}F]fluorobenzamido)ethyl]maleimide]; [^{18}F]FDOPA, 6-[^{18}F]fluoro-L-dopa; [^{18}F]FET, [^{18}F]fluoroethyl-L-tyrosine; anti-[^{18}F]FACBC, anti-1-amino-3-[^{18}F]fluorocyclobutane-1-carboxylic acid; [^{18}F]FMISO, [^{18}F]fluoromisonidazole; [^{18}F]HX4, 3-[^{18}F]fluoro-2-(4-((2-nitro-1*H*-imidazole-1-yl)methyl)-1*H*-1,2,3-triazole-1-yl)-propan-1-ol; FDA, Food and Drug Administration; FDG, fluorodeoxy glucose; FLT, fluorothymidine; GPCR, G-protein-coupled receptor; GRPR, gastrin releasing peptide receptor; HGF, hepatocyte growth factor; HER, human epidermal growth factor receptor; HIF, hypoxia induced factor; HNSCC, head and neck squamous cell carcinoma; Hsp, heat shock protein; hTR, human telomerase RNA; hTERT, human telomerase reverse transcriptase; MAP, mitogen-activated protein; MAPK, mitogen activated protein kinase; MVD, microvessel density; MMPs, matrix metalloproteases; MRI, magnetic resonance imaging; NET, neuroendocrine tumor; NPs, nanoparticles; NSCLC, non–small cell lung cancer; OC, octreotide; PET, position emission tomography; PD153035, 4-[(3-bromophenyl)amino]-6,7-dimeth-oxyquinazoline hydrochloride; PI3K, phosphatidylinositol 3-kinase; PS, phosphatidylserine; PSMA, prostate-specific membrane antigen; Rb, retinoblastoma; RBC, red blood cells; ROI, region of interest; RTK, receptor tyrosine kinase; SA, specific activity; SPECT, single-photon emission computed tomography; SPIO, superparamagnetic iron oxide; SST, somatostatin; SStR, somatostatin receptor; SUV, standardized uptake value; TCTP-1, tumor cell targeting peptide; TGF, transforming growth factor; TK, tyrosine kinase; TK1, thymidine kinase 1; uPA, urokinase plasminogen activator; VEGFR, vascular endothelial growth factor; VLA-4, very late antigen 4.

interest in molecular imaging in oncology (Schillaci and Simonetti, 2004).

Nuclear medicine approaches to cancer imaging can be divided into three main domains: 1) imaging metabolic processes, which is generally called "metabolic imaging"; 2) "functional imaging" that measures blood flow, oxygen consumption, and other functionalities (Gil-da-Costa et al., 2006); and 3) "molecular imaging" methods aimed at more specific biochemical targets (Jager et al., 2005).

Currently, PET imaging tracers in the clinical setting are mainly designed to target general metabolic processes within cancer cells. For example, [^{18}F]fluorodeoxyglucose ([^{18}F]FDG), a glucose analog, is injected in patients and accumulates in tumor cells because of an upregulation of hexokinase, which among other mechanisms, induces high glucose uptake by these cells. Nevertheless, these tracers are not specific, and major research efforts are aimed at the development of specific molecular tracers that will provide information on the biochemistry of the tumor. In the field of oncology, various biochemical components can potentially be targeted and quantitatively imaged to study tumor biology, such as cell surface receptors, proteins involved in signal transduction pathways, apoptosis markers, proliferation markers, proteolytic enzymes, and extracellular matrix targets. The use of specific markers may thus allow personalized treatments for patients and may facilitate and assist the evaluation of treatment.

B. Positron Emission Tomography

PET, a noninvasive molecular imaging modality, is based on nuclear medicine imaging technology and short-lived positron emitting bioprobes. PET enables four-dimensional (three-dimension spatial and temporal) and quantitative determination of the distribution of radioactivity within the human body. PET has been used for in vivo noninvasive biochemical investigations in several medical fields such as oncology, cardiology, and neurology (Wang and Maurer, 2005).

The fundamental physics that allow dynamic detection and three-dimensional localization of PET is based on a process called annihilation. Upon decay, PET radioisotope emits a positron that thereafter collides with an electron in the surrounding medium. The annihilation that occurs due to the collision converts the mass of the positron and electron into electromagnetic radiation, where two photons with equal energy of 511 keV are emitted simultaneously at ~180° to each other. The patient injected with the PET tracer is surrounded by a ring of scintillation detectors, and only readings detected at the same time at 180° to each other are registered (Saleem et al., 2006). PET results are calculated from the scans by drawing a region of interest (ROI) that includes the organ or tissue of interest, for example a tumor. Standardized uptake value (SUV) then is calculated as activity concentration in the ROI/ (injected dose/body weight) (Adams et al., 2010). SUV can be calculated as the average of pixels per area of the ROI (SUV_{mean}) or as the highest pixels within the ROI (SUV_{max}). SUV can be affected by image noise, low image resolution, and subjective user ROI selection (Adams et al., 2010). In preclinical settings, percent injected dose per gram tissue (%ID/g) is often used instead of SUV.

Another nuclear medicine technology that will not be discussed in this article is SPECT. Similar to PET, SPECT uses radioactive isotopes. However, SPECT isotopes emit only one photon upon decay. Detection of a single photon requires physical collimators, which exhibit low geometric efficiencies, to reject scattered photons and to increase or decrease the field of view, depending on the needs of the study. SPECT is less sensitive than PET and does not allow absolute quantitative measurements of tracer accumulation (Rahmim and Zaidi, 2008).

The use of PET requires the administration of a molecule labeled with a positron-emitting radionuclide, such as ^{15}O, ^{13}N, ^{11}C, ^{68}Ga, ^{18}F, ^{64}Cu, ^{89}Zr, and ^{124}I, which have half-lives of 2.037 minutes, 9.965 minutes, 20.39 minutes, 68 minutes, 109.8 minutes, 12.7 hours, 3.27 days, and 4.176 days, respectively (Bonasera et al., 2001; Zhang et al., 2011b). Positron emitting isotopes are produced mainly by a cyclotron, but several PET isotopes can be produced by a generator (e.g., ^{68}Ga, ^{82}Rb). Ideally, the addition of the isotope to the tracer should have negligible or at least quantitatively predictable effect on the biologic properties of the tracer. It is also crucial to avoid saturation of the target being imaged; therefore, the radiotracer should have high specific activity (activity per mole, SA).

The high sensitivity of PET and the low concentration of the tracers used for imaging allow visualization of low-capacity systems such as ligand binding to the receptor. However, to be suitable for PET, there are several requirements for the radiotracer, such as high affinity and selectivity toward the receptor, low nonspecific binding, and optimal biologic half-life.

Some known radiotracers that have been used in the clinic for measuring different processes in the human body are [^{18}F]FDG (Jhanwar and Straus, 2006; Tafti et al., 2012), 3′-deoxy-3′-[^{18}F]fluorothymidine ([^{18}F]FLT) (Enslow et al., 2012; Kishino et al., 2012), and [^{11}C]choline (Gofrit et al., 2006; Rodari et al., 2011) for the measurements of energy, proliferation, and cell membrane metabolism, respectively; ^{13}N-NH_3 for perfusion imaging (Niemeyer et al., 1993; Fiechter et al., 2012, 2013); ^{15}O-H_2O for cerebral blood flow (Ter-Pogossian and Herscovitch, 1985; Gruner et al., 2011; Komar et al., 2012); [^{11}C]raclopride (Montgomery et al., 2007; te Beek et al. 2012; Urban et al., 2012); and [^{18}F]FDOPA (6-[^{18}F]fluoro-L-dopa) (Ishida et al., 2004) for the measurements of dopamine system and ^{68}Ga-*N*-[[4,7,10-tris (carboxymethyl)-1,4,7,10-tetraazacyclododec-1-yl]acetyl]-D-phenylalanyl-L-cysteinyl-3-(1-naphthalenyl)-L-alanyl-D-tryptophyl-L-lysyl-L-threonyl-*N*-[(1*R*,2*R*)-2-hydroxy-1-

(hydroxymethyl)propyl]-, cyclic (2-7)-disulfide (DOTA-NOC) for the detection of neuroendocrine tumors (NETs) (Krausz et al., 2011).

Small molecules or biomolecules such as peptides, proteins, affibodies, antibodies, aptamers, and oligonucleotides can be labeled with PET isotopes and evaluated for their potential as diagnostic imaging agents. Whether a suitably labeled molecule can act as a tracer will depend on the desired chemical and biologic properties. Small molecules usually have rapid clearance from the blood. Lipophilic molecules often clear through liver and intestine and will mask these organs. Peptides typically have rapid clearance from the blood and relatively high concentration in the target tissue (Jacobson and Chen, 2010). Peptides are relatively easy to synthesize "in house" with chemical modifications if needed. Moreover, peptides can often tolerate harsh chemical conditions for modification or radiolabeling. Another advantage of the small size is that peptides penetrate tumors fairly easily and may have low nonspecific binding, leading to high accumulation in target tissue (Jacobson and Chen, 2010). Affibody molecules are small proteins with a scaffold that consists of 58 amino acids and three-helix bundle, display a binding surface as large as antibodies, and have characteristics similar to peptides. Larger biomolecules, such as antibodies, have slow pharmacokinetics (slow clearance from the blood), high nonspecific binding and are not optimal for short imaging timetable, requiring labeling with longer half-life isotopes (Jacobson and Chen, 2010). In addition, the large size of the antibodies (~150 kDa) limits intratumoral diffusion to a penetration rate of approximately 1 mm every 2 days, leading to heterogeneous deposition within the tumor (Niu et al., 2012). An approach to overcome the disadvantages of antibodies for PET imaging is by antibody engineering. On the basis of the sequence and structure, the size of an antibody can be reduced to create single-chain variable fragment. In addition, naturally occurring heavy-chain antibodies that lack the first constant domain of the heavy-chain (C_H1) and the complete light-chain (Hamers-Casterman et al., 1993) provide an attractive alternative because it contains a complete Fc yet is approximately only half the size of IgG. The antigen-binding fragments of such heavy-chain antibodies are confined in a single domain, referred to as single domain antibody, variable heavy chain, or nanobody (Niu et al., 2012; Oliveira et al., 2010). These modifications that change the size of the tracer will probably affect the target binding affinity and specificity and pharmacokinetics compared with the parent antibody and should be analyzed individually for each engineered molecule.

Another type of biomolecules studied as potential PET tracers are oligonucleotides, based on antisense sequences of target mRNA. These molecules, both for imaging and therapy, require delivery of stable oligonucleotides in vivo. The tracer needs to be resistant to nucleases degradation and should have low binding to plasma proteins in circulation. These tracers are also required to overcome biologic barriers, including the immune systems of the body, before they can be taken up by the cells of interest and subsequently hybridized with the target mRNA. The main drawback of antisense oligonucleotides as tracers is that the specificity of the tracer plays a role only after the oligonucleotide is taken up by cells that may or may not have the targeted mRNA. It is unclear whether the labeled oligonucleotide will be secreted or washed if there is no target mRNA. Another unanswered question is whether the antisense oligonucleotide tracer that does bind target mRNA will remain in the cell and how long it will stay after being processed by cellular components.

A very interesting oligonucleotide form, which has not been applied thus far as a tracer for PET imaging, is the aptamer. Aptamers are short strands of RNA or DNA, which undergo selection in vitro by binding to the desired target, removal of unwanted oligonucleotides, and thereafter amplification by PCR, a process called systematic evolution of ligands by exponential enrichment (McKeague and Derosa, 2012). The ability to use aptamers in vivo is not straightforward: the oligonucleotide folding is highly dependent on the environment, such as pH, and it undergoes rapid degradation in the blood. However, these limitations might be overcome by chemical modifications.

The possibility of targeting receptors for imaging is an attractive concept, because it may provide the opportunity to evaluate agents for the diagnosis of several disorders and allow conducting experiments with agonists or antagonists for guiding and monitoring treatment. Overexpression of various receptors was found to be related to the initiation and progression of cancer. Several examples are estrogen receptor in breast cancer, androgen receptor (AR) in prostate cancer, integrin $\alpha_v\beta_3$, vascular endothelial growth factor receptor (VEGFR), and epidermal growth factor receptor (EGFR), all playing a major role in the development of a broad range of human tumors. Overexpressed receptors can be targeted for diagnostic and therapeutic approaches. Developing specific molecules that bind to the overexpressed receptors in vivo with high affinity and specificity will allow the visualization of the tumor based on its biochemical properties using PET. This diagnostic tool may serve as guidance to a specific treatment and monitoring of treatment efficacy.

C. Requirements of Radiotracers for Positron Emission Tomography Molecular Imaging

To perform in vivo molecular imaging and quantitation of low-capacity systems using PET, an appropriate PET biomarker is required. The accumulation of

radioactivity in target organs is dependent on the interaction of the radiotracer with its target.

A suitable PET radiotracer requires the following characteristics.

- High affinity for its target to obtain high-contrast PET images. The desired affinity of the radiotracer depends on the concentration of the target. As a rule of thumb, low capacity systems such as transporters and receptors require target concentration/dissociation constant ratio (B_{max}/K_d) of at least 4 to obtain sufficient contrast. If B_{max}/K_d is lower than 1, the radiotracer will not accumulate over plasma levels, and therefore, it will not be possible to detect the target (Elsinga, 2002; Mishani and Abourbeh, 2007). Imaging low capacity systems, such as enzymes, transporters, and receptors, require a sufficient target concentration to produce a detectable signal.
- High specificity of the radiotracer to its target is necessary to reduce background noise.
- The radiotracer must be stable in vivo, otherwise undesirable metabolites might form and bind other molecules or take part in unknown biochemical processes to give nonspecific accumulation of radioactivity.
- If the target molecule is intracellular, the lipophilicity of a radiotracer is an important parameter, because it determines the ability of the molecule to cross cell membranes. For optimal passage of lipid bilayers, a log$P$ of 1.5–3 is required. Higher values of log$P$ are undesired because they might result in high nonspecific binding caused by hydrophobic interactions between lipids and proteins.
- Clearance of nonspecifically bound radioactivity within the time scale of measurement for PET is necessary to distinguish between specific and nonspecific uptakes. In addition, the clearance of the unbound radiotracer should not interfere with the target organ (i.e., the bladder and prostate cancer).

There are some radiochemistry demands that ought to be considered, such as the following.

Labeling position within the molecule: it should neither interfere with the binding nor change the affinity of the bioprobe to the target. Furthermore, the labeling position should be metabolically inert to avoid cleavage of the radioactive isotope from the intact bioprobe.

Duration of the radiosynthesis and expected radiochemical yield: it is expected to achieve high radiochemical yield and high specific activity within short reaction time (on the order of one physical half-life of the radioisotope or less).

High specific activity: high activity in minimum mass is needed to avoid saturation of binding sites. Under saturating conditions, it would be impossible to measure changes in the concentration of available binding sites.

Choice of radioisotope: when choosing a radioisotope, several considerations need to be taken into account for: 1) optimally, replacing an atom that already exists in the molecule, for example carbon-11 instead of carbon-12. In this manner, the properties of the molecule do not change. If this choice is not possible, the labeling will have to be by replacing an atom or addition of the radioisotope, which might change molecular properties. 2) Optimal radiochemical decay, which is reflected in the positron energy. Higher positron energies result in the positron traveling farther before an annihilation event, thus decrease the PET image resolution. In contrast, lower energy of the positron may result in absence of the signal. 3) Optimal half-life—the optimal half-life of the isotope should be as long as (or longer than) the biologic system that is being investigated. For example, ligands binding to receptors may reach an equilibrium state after 3 hours. In this case, the use of a short half-lived isotope, such as carbon-11, is not favored.

Favorable dosimetry: dosimetry is affected by the radioisotope energy and also by the other routes of decay. For example, some PET isotopes such as copper-64 also undergo β decay and electron capture, which can be more harmful to the tissue.

II. Imaging of Tumor Biology and Development

Several molecular pathways are responsible for the formation, development, and aggressiveness of cancer. Cancer cells possess a deregulation in their normal proliferation and homeostasis, resulting in constant replication and genetic instability.

Hanahan and Weinberg (2000, 2011) described several essential alteration steps in cell physiology that collectively dictate tumor development: sustaining proliferative signaling, evading growth suppression, resisting cell death (apoptosis), limitless replicative potential, inducing angiogenesis, and tissue invasion and metastasis. Acquisition of each of these physiologic changes during tumor development represents the successful breaching of an anticancer defense mechanism hardwired into cells and tissues. Increasing data show that in addition to mutations within the tumor cells, the tumor microenvironment, consisting of normal cells recruited to the tumor, supports tumor development and metastasis, for example, by providing proliferation and anti-apoptotic signals, facilitating angiogenesis, and suppressing the immune system. Some of the processes involved in tumor development

and the interaction of tumor cells with stroma are potential targets for PET imaging, as will be discussed below.

A. Sustaining Proliferative Signaling

Most of the cells in the human body are somatic and do not proliferate. Of the cells that do proliferate, mainly tissue stem cells, environmental signals have an important role in regulating cell growth, proliferation, and homeostasis. Normal cells interact with their environment by different mechanisms, including cell-cell contact and soluble growth factors or hormones, for receiving proliferation signals. These growth factors can act through cell surface receptors or internally via cytoplasmic receptors (Daughaday and Deuel, 1991).

Tumor development requires a combination of defects that allow cells to become self-sufficient for cell proliferation and insensitive to signals that normally restrain cell growth. Many of the proliferation growth factors exert their function by binding to surface receptor tyrosine kinases (RTKs), which are transmembrane proteins involved in the regulation of cell proliferation, as well as other fundamental cellular processes such as survival, migration, metabolism, and differentiation (Choura and Rebai, 2011; Takeuchi and Ito, 2011). RTKs consist of an extracellular domain for ligand binding, a transmembrane domain, and a cytoplasmic domain, which starts the signal transduction using its tyrosine kinase domain.

In normal cells, RTK activity is strictly regulated; but dysregulation or constitutive activation of RTK has been found in a wide range of cancers. The deregulated activation occurs by gain-of-function mutation (Parma et al., 1993; Shenker et al., 1993), gene rearrangement, gene amplification, and overexpression or abnormal autocrine, endocrine, or paracrine stimulation of both the receptor and the ligand (Porter and Vaillancourt, 1998; McCubrey et al., 2008a,b; Steelman et al., 2008; Takeuchi and Ito, 2011). Inasmuch as RTKs have been implicated in many aspects of the malignant phenotype, they emerged as promising therapeutic targets (Takeuchi and Ito, 2011).

Binding of growth factors to RTK induces dimerization and autophosphorylation on one or both of the dimer subunits. This phosphorylation induces intracellular signaling via adaptor proteins to recruit multiple proteins to RTKs, thus amplifying the signal transduction induced by activated RTKs (Porter and Vaillancourt, 1998). Mutations in these and other signaling pathways can lead to uncontrolled regulation and aberrant signaling. Two of such pathways, which have been shown to be involved in signaling in cancer cells, are the Ras/Raf/mitogen-activated protein kinase Kinase (MEK)/mitogen-activated protein kinase (MAPK) and Ras/phosphatidylinositol 3-kinase (PI3K)/PTEN/Akt/mammalian target of rapamycin (Chappell et al., 2011). Activation of PI3K/AKT signaling pathway is a key regulator of normal cell growth and cell fate decisions by processes, such as proliferation, invasion, apoptosis, and induction of hypoxia-related proteins, and this pathway is frequently overactivated in cancers (Schuurbiers et al., 2009).

Another group of receptors that were found to be involved in cancer formation and progression is the cell surface proteins, G-protein-coupled receptors (GPCR) (Spiegelberg and Hamm, 2007; Lin, 2012). GPCRs are one of the largest receptor proteins family (Kumar, 2011), and their discovery earned Robert Lefkowitz and Brian Kobilka the 2012 Nobel Prize in Chemistry. Cross-talk between GPCR and growth factor receptors has a role in downstream signaling activation of proteins that are implicated in cancer growth, angiogenesis, and metastasis (Lappano and Maggiolini, 2011). Dimerization of GPCR is receptor ligand dependent and is not always a necessary mechanism in GPCR activation (Kumar, 2011).

Overexpression and/or disregulation of RTKs and GPCRs in tumors led to extensive research and numerous attempts for developing PET tracers that will allow the detection of the receptors and guide and monitor anticancer treatment.

1. Epidermal Growth Factor Receptor. The EGF family comprises six known structurally related polypeptides, namely EGF, transforming growth factor (TGF)-α, amphiregulin, heparin binding EGF, betacellulin, and epiregulin. This family of growth factors is distinguishable by the fact that their soluble forms are proteolytically derived from their integral membrane precursors and that they all contain a conserved three-loop compact structure known as the EGF-like domain (Lee et al., 1995).

The EGFR belongs to the human epidermal growth factor receptor (HER) family of tyrosine kinase (TK) receptors, which consists of four members: EGFR (HER1 or ErbB1), HER-2/neu (ErbB2), HER3 (ErbB3), and HER4 (ErbB4) (Abourbeh et al., 2007). Members of the HER family of TK receptors have extracellular ligand-binding domains, transmembrane regions, and multifunctional cytoplasmic tails. The tail has an ATP-binding site and TK activity and is capable of phosphorylating itself (autophosphorylation) as well as other proteins (Carpenter et al., 1991; Prigent and Lemoine, 1992; Fantl et al., 1993). Upon ligand binding, the EGFR functions as a branch in the signaling network and forms active homodimers or heterodimers with one of the three related proteins, ErbB2/c-neu, ErbB3, and ErbB4 followed by autophosphorylation of the receptor at the intracellular TK domain. This process initiates a cascade of cellular signaling that increases cell division and influences other aspects associated with malignant progression—angiogenesis, metastasis, and inhibition of apoptosis (Hunter, 1984; Prenzel et al., 2001; Yarden and Sliwkowski, 2001).

Under nonpathologic conditions, EGFR has moderate expression levels in the liver and kidneys

(approximately 10^5 receptors per cells), and its expression in normal epithelial tissues is lower (10^4 receptors per cells). EGFR is also expressed by a subpopulation of bone marrow stem cells (Chen et al., 2003).

Overexpression of EGFR has been found in numerous human cancers, such as non-small-cell lung carcinoma, squamous-cell carcinoma, colorectal, gastric, pancreatic, ovarian, breast, and prostate cancers (Arteaga, 2002; Mendelsohn and Baselga, 2003; Ritter and Arteaga, 2003). The number of receptors per cell varies, for example, for breast cancer, MDA-MB-468 cell line was reported to express 10^6 receptors per cells and MCF-7 cell line was found to express only 10^4 receptors per cell (Chen et al., 2003). Furthermore, overexpression has been found to correlate with therapy resistance, metastasis formation, and poor prognosis. It is important to emphasize that with a microarray analysis, different human cancer cell lines exhibit different levels of EGFR, which reflect on their sensitivity to EGFR targeted therapies. This finding suggests that cancers in human patients may also have different EGFR expression levels, and it is crucial to determine receptor expression before deciding on the appropriate treatment (Eiblmaier et al., 2008). Another element that influences the response to anti-EGFR therapy is mutations within the receptor gene, which will be discussed below.

Thus, EGFR is an attractive therapeutic target for the design and development of compounds that specifically inhibit its TK activity and its signal transduction pathway in cancer cells. Such compounds can serve as potential PET agents when labeled with an appropriate isotope. 4-(Anilino)- and 4-[(phenylmethyl)amino]quinazolins have been shown to potently and selectively inhibit EGFR kinase activity by reversibly binding to the intracellular ATP binding domain of EGFR. The prototype for such compounds, the EGFR reversible inhibitors, gefitinib (Iressa; AstraZeneca, London, UK; and Teva, Petah Tikva, Israel) and erlotinib (Tarceva; Genentech, South San Francisco, CA; and OSI Pharmaceuticals, Mellville, NY) (Cohen et al., 2003; Herbst, 2003; Herbst and Kies, 2003), were approved by the Food and Drug Administration (FDA) for the treatment of non-small cell lung cancer (NSCLC). However, clinical trials using gefitinib did not show significantly improved survival (Comis, 2005). Moreover, clinical trials with erlotinib showed effective results on survival in only a small percentage of patients in whom EGFR possesses activating mutations in the kinase domain (Cohen et al., 2003; Memon et al., 2011). Accurate measurements of EGFR phosphorylation level in human tumors are lacking, making it hard to distinguish whether poor response to drugs such as gefitinib or erlotinib is due to the lack of specific activating mutations, to the absence of a survival function of EGFR, or to insufficient long-term occupancy of the receptor by reversible inhibitors (Cohen et al., 2003).

Imaging of EGFR and EGFR TK inhibitor by nuclear medicine modalities has been summarized in a number of excellent review articles (Cai et al., 2008b; Mishani et al., 2008). This article will only highlight the most recent updates.

There has been a growing interest in using EGFR-TK inhibitors as radiotracers for molecular imaging of EGFR overexpressing tumors via PET. Gefitinib was labeled with ^{11}C and ^{18}F and evaluated in vitro and in vivo in xenografted mouse models (Su et al., 2008; Kawamura et al., 2009; Zhang et al., 2010). [^{18}F]Gefitinib had high nonspecific cellular uptake in vitro and did not correlate with EGFR expression levels in vivo (Su et al., 2008). On the other hand, [^{11}C]gefitinib appears to be able to measure EGFR level in fibrosarcoma-bearing mice (Zhang et al., 2010). [^{11}C]Gefitinib had about 3.5%ID/g uptake in subcutaneous tumors at 1 hour postinjection, which was reduced upon blocking with gefitinib (100 mg/kg), indicating a specific binding (Zhang et al., 2010). However, [^{11}C]gefitinib had ~10 times higher accumulation in the small intestine, and high uptake was also observed in the liver, heart, lung, and kidneys (Zhang et al., 2010), limiting the application of [^{11}C]gefitinib for the diagnosis of lesions in these organs.

Memon et al. (2009) labeled erlotinib with ^{11}C and tested its use in mice bearing subcutaneous human lung cancer tumors that had low expression (A549 and NCI358) and high expression (HCC827) of EGFR (Memon et al., 2009). They showed that xenografts from the erlotinib-sensitive HCC827 cells could be visualized by micro-PET scanning with 3.66%ID/g, whereas xenografts from A549 and NCI358 cells could not (1.62 and 0.69%ID/g, respectively) at 1 hour postinjection. The researchers pointed out that HCC827 cells with high expression of EGFR also have a deletion gene mutation (delE746-A750) in exon 19. The presence of this mutation is believed to further increase the sensitivity of the HCC827 cells to erlotinib treatment (Chang et al., 2007). Further analysis of the data showed correlation between EGFR expression and sensitivity to erlotinib and uptake of [^{11}C]erlotinib in the tumors. It is important to note that although [^{11}C]erlotinib seems to be a potential biomarker, it also exhibits very high uptake in the liver.

[^{11}C]Erlotinib was evaluated in clinical trial in 13 patients with NSCLC (Memon et al., 2011) to test the feasibility of using [^{11}C]erlotinib to visualize tumor, metastases, and malignant lymph nodes before treatment and to compare it with [^{18}F]FDG. [^{11}C]Erlotinib successfully visualized NSCLC lung tumors, including metastases to the lymph nodes that were not identified by [^{18}F]FDG (Fig. 1). The ratios between [^{11}C]erlotinib uptake of lung tumor-to-lung tissue were about 1.3, and those of the lymph nodes-to-lung tissue were around 2, which allows a clear visualization of tumor lesions (Memon et al., 2011)

Fig. 1. [^{11}C]Erlotinib accumulation in lymph nodes that were negative on [^{18}F]FDG PET/CT in a human patient. Left, transaxial slice of CT; middle, [^{18}F]FDG PET; right, [^{11}C]Erlotinib PET. White arrows indicate the lymph node metastases.[Adapted by permission from Macmillan Publisher Ltd on behalf of Cancer Research UK: Memon AA, Weber B, Winterdahl M, Jakobsen S, Meldgaard P, Madsen HH, Keiding S, Nexo E, and Sorensen BS (2011) PET imaging of patients with non-small cell lung cancer employing an EGF receptor targeting drug as tracer. *Br J Cancer* **105:**18050–1855.]

[^{11}C]Erlotinib was able to distinguish molecular heterogeneity between tumors in the same patient, which suggests that [^{11}C]erlotinib PET/CT can be used to classify tumors accumulating erlotinib. Importantly, this imaging method may prove useful for the selection of patients suitable for erlotinib treatment and should be further evaluated in a larger population of patients (Memon et al., 2011). PD153035 [4-[(3-bromophenyl)amino]-6,7-dimeth-oxyquinazoline hydrochloride)] is another EGFR TK inhibitor that was labeled with ^{11}C and evaluated in tumor-bearing mice (Wang et al., 2007b), healthy human volunteers (Liu et al., 2009), and in 21 patients with advanced chemotherapy-refractory NSCLC using PET/CT (Meng et al., 2011). NSCLC patients were treated with erlotinib (150 mg daily) and imaged with [^{11}C]PD153035 before treatment (baseline), and 1–2 weeks, and 6 weeks after treatment. Overall survival and progression free survival times were correlated with the [^{11}C]PD153035 SUV. The researchers found a strong correlation between patients with higher SUV_{max} and survival, whereas patients who had higher SUV_{max} at the baseline point survived much longer than patients with lower baseline SUV_{max} (Meng et al., 2011). On the other hand, no correlation was found at 6 weeks after treatment between baseline SUV_{max} and overall survival or progression free survival (Meng et al., 2011). The researchers suggested that [^{11}C]PD153035 PET/CT may be a rapid way for identifying patients, with refractory advanced NSCLC likely to respond to the EGFR-TK inhibitors but not for monitoring treatment response. It is also important to note that [^{11}C]PD153035 distribution in human patients showed that accumulation in the tumor ranged from SUV_{max} 1.26 to 5.93 compared with accumulation in the bladder (5.29 ± 1.09), gallbladder (2.67 ± 1.06), kidneys (2.15 ± 0.69), small intestine (1.88 ± 0.78), and liver (1.09 ± 0.81) (Liu et al., 2009), making the tracer inappropriate for imaging EGFR expression of tumors in these organs. The researchers did not evaluate activating mutations in the EGFR for the patients in this study, suggesting that their results are independent of EGFR mutations.

Another study reported by Yeh et al. (2011) described the preclinical study of small molecule TK-inhibitor, [^{18}F]F-PEG6-IPQA [4-[(3-iodophenyl)amino]-7-{2-[2-{2-(2-[2-{2-([18F]fluoroethoxy)-ethoxy}-ethoxy]-ethoxy)-ethoxy}-ethoxy]-quinazoline-6-yl-acrylamide], which has increased selectivity and irreversible binding to the active mutant L858R EGFR kinase for imaging EGFR-mutant in tumor-bearing mice. [^{18}F]F-PEG6-IPQA was evaluated in four different NSCLC cell lines with different sensitivity to the drug gefitinib: H441 and PC14 cells that are wild type and should have high resistance to gefitinib, H3255 cells expressing L858R mutant EGFR that are the most sensitive to the treatment, and H1975 cells that express two mutations, L858R and T790M, should have more resistance to gefitinib. Micro-PET/CT was done before and after treatment with gefitinib (100 mg/kg, 1 hour before injection of the tracers). Before treatment (Fig. 2), [^{18}F]F-PEG6-IPQA had the highest accumulation in genfitinib-sensitive H3255 tumors (2.34 ± 0.13%ID/g at 2 hour postinjection) and to less degree in genfitinib-resistant H441 tumors (1.59 ± 0.44%ID/g), whereas uptake in H1975 and PC14 tumors was low and similar to muscle background (Yeh et al., 2011). [^{18}F]F-PEG6-IPQA uptake was significantly reduced after treatment with gefitinib (1.38 ± 0.43%ID/g) in H3255 tumors. As expected, gefitinib treatment did not affect the drug-resistant tumor cells, H441, which had

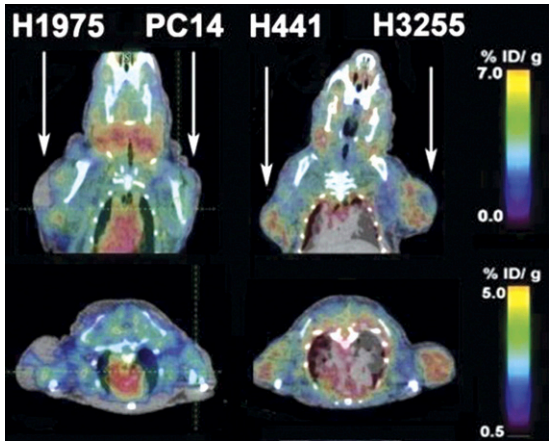

Fig. 2. Representative coronal and axial micro-PET/CT images in 2 mice 2 hours after injection of [^{18}F]F-PEG6-IPQA. Each mouse bears two different subcutaneous tumors on the opposite shoulders. Arrows indicate tumors. [Adapted from Cai W, Chen K, He L, Cao Q, Koong A, and Chen X (2007) Quantitative PET of EGFR expression in xenograft-bearing mice using ^{64}Cu-labeled cetuximab, a chimeric anti-EGFR monoclonal antibody. *Eur J Nucl Med Mol Imaging* **34:**850–858. Used with permission.]

similar uptake of 1.58 ± 0.01%ID/g. [^{18}F]F-PEG6-IPQA uptake was also decreased in H1975 and PC14 tumor xenograft models. H1975 cells have the L858R mutation, which is sensitive to gefitinib, but they also have second mutation, T790M, which gives resistance to gefitinib by interfering its binding to the ATP binding site of EGFR kinase (Yeh et al., 2011). This tracer may allow detection of EGFR-positive tumors expressing L858R mutation and help distinguish patients who will respond to EGFR-TK inhibitors such as gefitinib and erlotinib.

Most of the TK inhibitor-based tracers are small molecules that have shown the value of screening EGFR positive tumors in patients, but also displayed undesired uptakes in metabolic organs such as liver, kidneys, and intestine and limit their wide clinical use for lesion detection and receptor quantification.

Cetuximab (Bristol-Myers Squibb, New York, NY; and Eli Lilly and Company, Indianapolis, IN) was the first antibody approved by the FDA for the treatment of colorectal cancer and head and neck cancer. Cetuximab binds to the extracellular domain of EGFR with nanomolar affinity, similar to that of the natural ligand EGF (Fan et al., 1993). It was found to be effective in prolonging survival in conjunction with either radiation or chemotherapy treatments in locally advanced tumors and recurrent and metastatic tumors (Bonner et al., 2010; Kabolizadeh et al., 2012). However, cetuximab was found to work only in cases where KRAS (Kirsten rat sarcoma) protein is not mutated. Cetuximab has been conjugated with macrocyclic chelator DOTA and labeled with ^{64}Cu for PET imaging of EGFR. In one study, ^{64}Cu-DOTA-cetuximab was tested in seven xenograft models, and a good linear correlation was found between the tumor uptake measured by PET scans and the EGFR expression level ex vivo measured by Western blot (Fig. 3) (Cai et al., 2007). In another study, five cervical cancer xenograft models were used. Positive correlation between EGFR mRNA expression levels, cell-surface expression of the EGFR, and the internalization degree of ^{64}Cu-DOTA-cetuximab was found (Eiblmaier et al., 2008). Nevertheless, the pharmacokinetics of ^{64}Cu-DOTA-cetuximab was characteristic of antibodies and displayed very slow clearance from nontarget organs such as the blood, spleen, heart, lung, and liver. At 24 hour postinjection these organs still had high uptake, suggesting that optimal contrast might be observed at late time points.

A more potent monoclonal antibody of the EGFR, panitumumab, approved for the treatment of colorectal cancer by the FDA, was conjugated with DOTA and labeled with ^{64}Cu (Niu et al., 2009). The ability of ^{64}Cu-DOTA-panitumumab to image EGFR expression levels was tested in three human head and neck squamous cell carcinoma (HNSCC) cell lines, which had different levels of EGFR expression, determined by flow cytometry in the order of UM-SCC-22B < SAS < SQB20. Interestingly, there was no correlation between

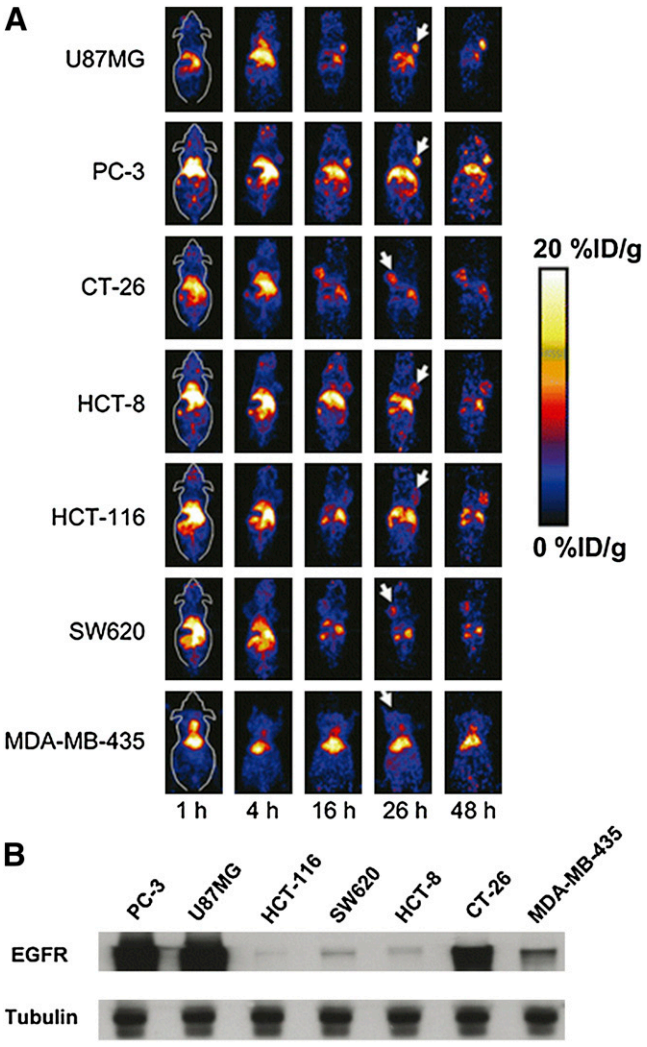

Fig. 3. (A) Micro-PET coronal images at different time points of seven subcutaneous xenograft models after intravenous injection of ^{64}Cu-DOTA-Cetuximab. White arrows indicate tumors; (B) Western blot of EGFR expression in the seven tumor types tested. [Adapted from Niu G, Li Z, Xie J, Le QT, and Chen X (2009) PET of EGFR antibody distribution in head and neck squamous cell carcinoma models. *J Nucl Med* **50:**1116–1123. Used with permission.]

PET quantification and EGFR protein expression level. The tumor cell lines that had the lowest EGFR protein expression (UM-SCC-22B) among the three cell lines tested, showed the highest accumulation of ^{64}Cu-DOTA-panitumumab (34.80 ± 9.26%ID/g at 48 hour postinjection), whereas the tumor cell line with the highest EGFR expression (SQB20) showed the lowest accumulation of ^{64}Cu-DOTA-panitumumab (9.39 ± 1.44%ID/g at 48 hour postinjection; Fig. 4) (Niu et al., 2009). The tumors were excised and immunofluorescence staining was performed to determine EGFR expression in the tumors ex vivo. EGFR expression was found to be correlated with the flow cytometry results. However, after in vivo injection of fluorescein isothiocyanate-labeled panitumumab, the staining profile was significantly different, whereas UM-SCC-22B had uniform staining, SQB20 slides had patchy staining, suggesting

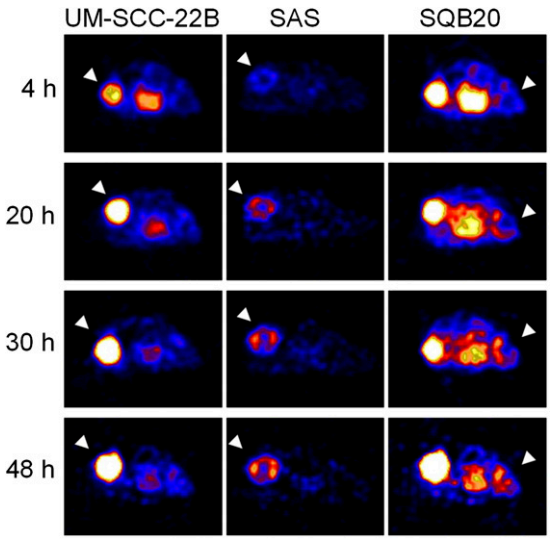

Fig. 4. Micro-PET images of HNSCC tumor-bearing mice at different time points after intravenous injection of ^{64}Cu-DOTA-panitumumab. White arrowheads indicate tumor. [Adapted from Niu G, Li Z, Xie J, Le QT, and Chen X (2009) PET of EGFR antibody distribution in head and neck squamous cell carcinoma models. *J Nucl Med* **50:**1116–1123. Used with permission.]

low penetration of the antibody in the SQB20 tumors. In an attempt to explain these results, the vascularity of each tumor type was examined, and it turned out that the microvascular density of SQB20 was the lowest (Niu et al., 2009). The researchers suggested that the vascular density can be a determining factor for antibody diffusion and binding and subsequently influence treatment efficacy. To ensure their idea, the researchers repeated the experiment with another antibody tracer, ^{64}Cu-DOTA-cetuximab, that showed similar results to those obtained with ^{64}Cu-DOTA-panitumumab in this model of HNSCC (Niu et al., 2009). Similar disparity results were also shown by Aerts et al. (2009) using ^{89}Zr-Cetuximab. This study provides evidence for the lack of an observed correlation between therapeutic efficacy of cetuximab and panitumumab and EGFR expression level as determined by immunohistochemistry and emphasizes the superiority of PET imaging for determining drug accumulation in target organ.

Panitumumab was also labeled with a longer half-lived PET isotope ^{89}Zr ($t_{1/2}$ = 78.4 hour) (Nayak et al., 2012). Labeling with ^{89}Zr allows imaging for 4–5 days postinjection, when most of the antibody was cleared from the blood and gave very high tumor-to-blood and tumor-to-muscle ratios (Ramos-Suzarte et al., 1999). Panitumumab was conjugated to the chelator *p*-isothiocyanatobenzyl-desferrioxamine B for ^{89}Zr labeling. ^{89}Zr-panitumumab was injected into mice bearing human colorectal adenocarcinoma, using EGFR-positive (LS-174T) and EGFR-negative (A375) cell lines (Nayak et al., 2012). Micro-PET of ^{89}Zr-panitumumab combined with MRI showed significant differences between the positive and negative tumors and was able to detect distant metastatic lesion sites. ^{89}Zr-Panitumumab accumulated in positive tumors with a peak tumor uptake of 42.89 ± 4.49%ID/g 3 days postinjection and was proven to be specific to EGFR by blocking with unlabeled panitumumab.

Another biomarker for targeting EGFR is anti-EGFR Affibody protein ($Z_{EGFR:1907}$), which has been site specifically labeled with ^{18}F and ^{64}Cu and evaluated in tumor-bearing mice (Miao et al., 2010, 2012). The labeled Affibody molecule showed good pharmacokinetics in vivo with fast accumulation in EGFR-positive tumors but also displayed very high uptake in the liver (Fig. 5). ^{64}Cu-Affibody also had extremely high renal uptake and retention, although this issue was partially resolved by ^{18}F labeling (Miao et al., 2010, 2012). Surprisingly, liver uptake was reduced and tumor uptake was increased when the labeled Affibody was administered as low SA form, with 45–50 μg of unlabeled Affibody (Fig. 5). High uptake in the liver may be explained by high concentration of normally expressed EGFR available for binding in the liver, which could retain significant amount of the radiolabeled ligand (Jungbluth et al., 2003; Miao et al., 2010). When a small amount of unlabeled Affibody is injected, perhaps due to blood flow difference in the liver and tumor, receptors in the liver were blocked more than those in the tumor, to give better PET images. However, using low SA Affibody for imaging will reduce the ability to quantify the receptor in a clinical setting (Miao et al.,

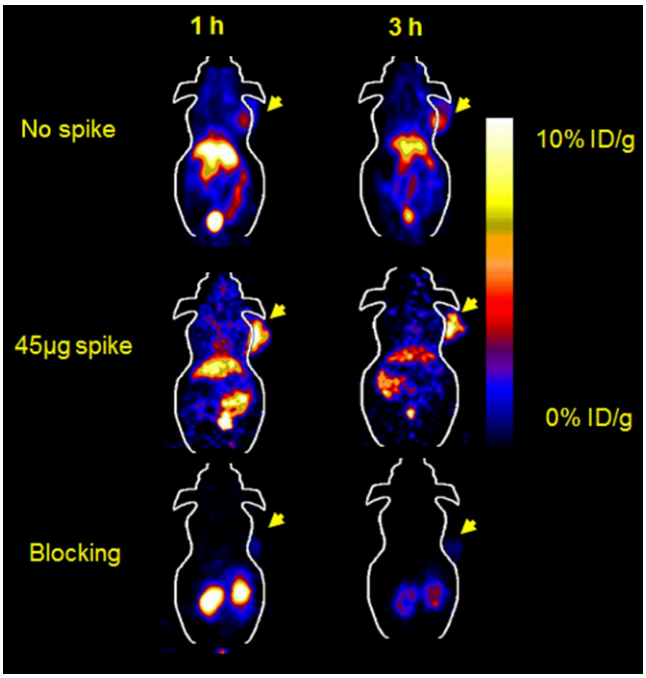

Fig. 5. Micro-PET of [^{18}F]FBEM-Cys-$Z_{EGFR:1907}$ in an A431 xenograft model co-injected with 0, 45, and 500 μg of Ac-Cys-ZEGFR:1907.[Adapted from Miao Z, Ren G, Liu H, Qi S, Wu S, and Cheng Z (2012) PET of EGFR expression with an ^{18}F-labeled affibody molecule. *J Nucl Med* **53:** 1110–1118. Used with permission.]

2010). Tumor specificity of the labeled Affibody was confirmed by coinjection with 500 μg of unlabeled Affibody (Fig. 5).

PET imaging of EGFR was also evaluated by labeling the natural ligand EGF (Li et al., 2012a). Cys-tagged EGF (cEGF) was labeled with ^{18}F by coupling the free thiol group of the cysteine residue tag with *N*-[2-(4-[^{18}F]fluorobenzamido)ethyl]maleimide] ([^{18}F]FBEM). [^{18}F]FBEM-cEGF was evaluated in vivo in mice bearing UM-SCC1 tumors (Li et al., 2012a) and successfully visualized the tumors at early time points of (e.g., 2.60 ± 0.59%ID/g at 0.5 hour). Unfortunately, very high uptake was detected in the liver and kidneys (7.23 ± 0.51 and 15.5 ± 1.21%ID/g, respectively). To overcome liver accumulation, the researchers coinjected unlabeled cEGF with the labeled derivative. Injection of 50 and 500 μg both significantly reduced liver uptake, but coinjection with 50 μg of ice-cold EGF resulted in higher tumor uptake, coinjection with 500 μg of ice-cold EGF resulted in lower tumor uptake, probably due to the blocking of receptor-specific binding in both the liver and tumor (Li et al., 2012a). Further dynamic scans of [^{18}F]FBEM-cEGF in the same animal model confirmed that the ligand is cleared through both the hepatobiliary and renal routes. This fast clearance resulted in a suitable tumor-to-background contrast required for an imaging agent (Li et al., 2012a).

2. Human Epidermal Growth Factor Receptor-2/neu. Human epidermal growth factor receptor-2 (HER-2) is another member of the RTKs and is involved in regulating cell growth, survival, and differentiation through interlinked signal transduction pathways, such as PI3K/Akt and Ras/Raf/MEK/MAPK (Yarden and Sliwkowski, 2001). High expression of HER-2 on the cell membrane results in a constitutive signaling of downstream cascades that contributes to the resistance of cancer cells to apoptosis and leads to their survival improvement (Yarden and Sliwkowski, 2001; Ferretti et al., 2007).

Overexpression of HER-2 was found in a wide variety of human cancers and was associated with high-grade aggressiveness of the tumor and poor prognosis (Meric-Bernstam and Hung, 2006; Ferretti et al., 2007). The HER receptor family is involved in the regulation of normal breast growth and development and overexpression of HER-2 is associated with 20% of breast cancer and aggressive phenotype (Yarden and Sliwkowski, 2001). Overexpression of the HER-2 gene was also suggested to be significantly associated with multiple drug resistance in NSCLC cell lines (Tsai et al., 1993). Collectively, the data from the literature suggest that HER-2 has a great potential as a target for diagnosis and therapy.

One of the therapies targeting HER-2 is the humanized, recombinant antibody, trastuzumab, which binds to the extracellular domain of HER-2 and has been shown to selectively exert antitumor effects in cancer models and patients with HER-2-amplified breast cancer, but not in tumors with normal HER-2 expression (Vogel et al., 2002; Seidman et al., 2008). Trastuzumab was approved by the FDA for the treatment of patients with HER-2-positive metastatic breast cancer and as a combination treatment with paclitaxel for the treatment of patients with HER-2 expressing metastatic breast cancers who have not received chemotherapy for their metastatic disease (Milenic et al., 2010).

Because several excellent review articles on HER-2 imaging have been published (Niu et al., 2008; Smith, 2010), we will only discuss some of the recent updates on antibodies and affibodies based PET tracers.

Trastuzumab was labeled with ^{64}Cu and ^{89}Zr using chelators conjugated to the antibody (Dijkers et al., 2010; Oude Munnink et al., 2010; Paudyal et al., 2010). In a study that was done with human patients (n = 14), Dijkers et al. (2010) evaluated the optimal dosage and time of administration of ^{89}Zr-trastuzumab to enable PET imaging of HER-2 in patients with metastatic breast cancer (Dijkers et al., 2010). Patients who were not pretreated with trastuzumab were injected with doses of 10 or 50 mg of ^{89}Zr-trastuzumab, and patients who received trastuzumab treatment were injected with 10 mg of ^{89}Zr-trastuzumab. The patients underwent at least two PET scans between days 2 and 5 post-tracer injection. The best time for assessing ^{89}Zr-trastuzumab uptake by tumors was found to be 4–5 days after the injection. In addition, for optimal PET scan results in patients who did not receive pretreatment with trastuzumab a dose of 50 mg of ^{89}Zr-trastuzumab was required, whereas for patients that had the treatment a dose of 10 mg of ^{89}Zr-trastuzumab was sufficient (Dijkers et al., 2010). ^{89}Zr-trastuzumab was also successful in imaging bone, liver, and brain metastases (Fig. 6). Quantification of the PET images confirmed a dose dependency of trastuzumab clearance and revealed significantly higher uptake in metastatic tumor lesions compared with the corresponding normal tissue (Fig. 6) (Dijkers et al., 2010).

An interesting experiment that was done in mice using labeled trastuzumab for HER-2 expression imaging was to evaluate anti-heat shock protein (Hsp) 90 treatment using its inhibitor NVP-AUY922 [5-(2,4-dihydroxy-5-isopropyl-phenyl)-*N*-ethyl-4-[4-(morpholinomethyl)phenyl]isoxazole-3-carboxamide]. In vivo evaluation was done in a HER-2-positive xenograft model using mice treated with 50 mg/kg i.p. 5-(2,4-dihydroxy-5-isopropyl-phenyl)-*N*-ethyl-4-[4-(morpholinomethyl)phenyl]isoxazole-3-carboxamide (NVP-AUY922) every other day, and an imaging study was done using ^{89}Zr-Trastuzumab 6 days before and after treatment. Micro-PET imaging was performed at 1, 3, and 6 day post-^{89}Zr-trastuzumab injection and showed reduction of tracer accumulation posttreatment that was confirmed by biodistribution (Oude Munnink et al., 2010). HER-2 immunohistochemistry performed on the

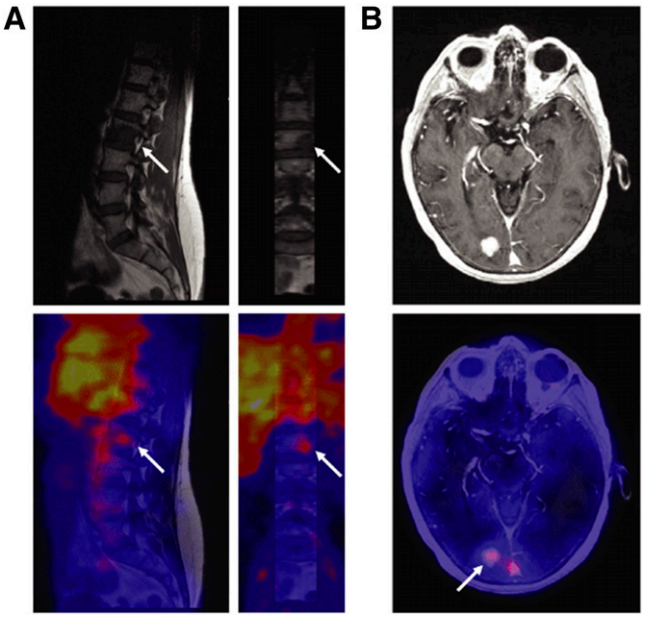

Fig. 6. Images from HER-2 PET and MRI scans of a human patient. (A) In a vertebral metastasis seen on MRI but unapproachable for biopsy, HER-2 status was revealed by ^{89}Zr-trastuzumab uptake on PET imaging. (B) Example of HER-2-positive brain lesion undetected by conventional scans, revealed by 89Zr-trastuzumab PET imaging and subsequently confirmed by MRI. White arrows indicate lesions. [Adapted by permission from Macmillan Publishers Ltd: Dijkers EC, Oude Munnink TH, Kosterink JG, Brouwers AH, Jager PL, de Jong JR, van Dongen GA, Schroder CP, Lub-de Hooge MN, and de Vries EG (2010) Biodistribution of ^{89}Zr-trastuzumab and PET imaging of HER2-positive lesions in patients with metastatic breast cancer. *Clin Pharmacol Ther* **87:** 586–592.]

excised tumors confirmed downregulation of HER-2 in the NVP-AUY922-treated group, showing the feasibility of ^{89}Zr-trastuzumab as a biomarker for Hsp90 inhibition in HER-2-positive xenograft (Fig. 7) (Oude Munnink et al., 2010).

High-affinity HER-2-binding Affibody molecules were obtained by use of phage display technology and affinity maturation, and several of them were labeled for PET imaging. Cheng et al. (2008) developed a method for site-specific radiofluorination of Affibody molecules using anti-HER-2 Affibody molecules [$Z_{HER-2:477}$ and $(Z_{HER-2:477})_2$] as model proteins. These Affibody molecules were designed to contain free cysteine residue at the C terminus and were labeled with 4-[^{18}F](fluorobenzylidene)oxime ([^{18}F]FBO). In vitro and in vivo studies were done along with micro-PET imaging in mice bearing HER-2-positive tumors (Cheng et al., 2008). Cell uptake studies showed that the dimer [^{18}F]FBO-$(Z_{HER-2:477})_2$ had a twofold higher affinity than the monomer [^{18}F]FBO-$Z_{HER-2:477}$ but also showed higher nonspecific cell uptake. In vivo [^{18}F]FBO-$(Z_{HER-2:477})_2$ showed poor results as an imaging agent, displaying low tumor uptake and slow clearance from normal tissues such as blood, muscle, liver, lung, and spleen (Cheng et al., 2008). On the other hand, imaging using the monomer [^{18}F]FBO-$Z_{HER-2:477}$ was rather successful and clearly visualized the HER-2-positive tumors. This study emphasizes the importance of the fine balance between good affinity and size effects, which could influence penetration, as seen from the comparison between the monomer and the dimer (Cheng et al., 2008).

Another anti-HER-2 Affibody was labeled with ^{18}F by cysteine conjugation through [^{18}F]FBEM (Kramer-Marek et al., 2009). [^{18}F]FBEM-$Z_{HER-2:342}$ enabled quantitative assessment of HER-2 downregulation after anti-HER-2 therapy with 17-demethoxygeldanamycin, which is an Hsp90 inhibitor and downregulates HER-2 levels (Kramer-Marek et al., 2009). [^{18}F]FBEM-$Z_{HER-2:342}$ was tested in five xenograft models with various HER-2 expression levels, and indeed there was a good correlation between HER-2 expression and activity. The effect of therapeutic regimens on HER-2 expression after 17-demethoxygeldanamycin treatment was compared in mice bearing high and low HER-2-expressing tumors. The change of HER-2 protein level upon Hsp90 inhibitor treatment was successfully

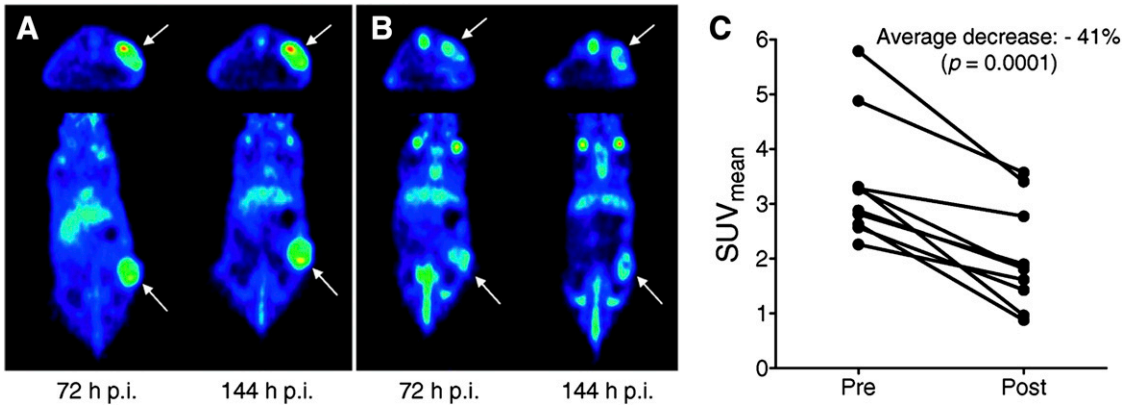

Fig. 7. Transversal and coronal PET images of a representative mouse scanned with ^{89}Zr-trastuzumab before (A) and after (B) treatment with NVP-AUY922. Arrows indicate tumors. (C) PET quantification of 89Zr-trastuzumab tumor uptake at 144 hour postinjection. [Adapted from Oude Munnink TH, Korte MA, Nagengast WB, Timmer-Bosscha H, Schroder CP, Jong JR, Dongen GA, Jensen MR, Quadt C, Hooge MN, and Vries EG (2010) ^{89}Zr-trastuzumab PET visualizes HER2 downregulation by the HSP90 inhibitor NVP-AUY922 in a human tumor xenograft. *Eur J Cancer* **46:**678–684. Used with permission from Elsevier.]

measured by quantitative [^{18}F]FBEM-$Z_{HER-2:342}$ PET, suggesting that this tracer is appropriate for monitoring therapy effects on HER-2 expression noninvasively and for optimizing therapy for patients on individual basis (Kramer-Marek et al., 2009). The same Affibody was also labeled with ^{64}Cu and ^{68}Ga for imaging HER-2-positive tumors (Cheng et al., 2010; Kramer-Marek et al., 2011).

3. Somatostatin Receptors. SStRs are GPCRs, which characteristically comprise a single polypeptide chain with seven transmembrane-spanning domains. Most neuroendocrine tumors (NET) express a high density of SStR; therefore, SStR is a suitable target for PET imaging and targeted therapy. SStR ligand, somatostatin (SST), is a small regulatory peptide widely distributed in the human body that functions as a neurotransmitter in the hypothalamus and also has antiproliferative effects as well as inhibitory effects on the production of several exocrine hormones in the gastrointestinal tract (Koopmans et al., 2009). SST has two isoforms, one with 14 amino acids and the other with 28 amino acids, both of which bind with high affinity for all five SStR subtypes. Upon ligand activation, the SStR on the cell membrane is phosphorylated; thereafter, the ligand-receptor complex is internalized and directed to the endosomes. The receptor then undergoes dephosphorylation and the vesicles fuse with lysosomes, resulting in an increase of hormone degradation, reduced mRNA and receptor protein synthesis, and receptor recycling (Hofland and Lamberts, 2003; Koopmans et al., 2009).

Five different human SStR subtype genes have been cloned and named sst_1, sst_2, sst_3, sst_4, and sst_5. Depending on the cell type, the five sst_s are coupled to a variety of signal transduction pathways (Hofland and Lamberts, 2003). One of the most commonly used analogs of SST is octreotide (OC), which consists of eight amino acids and has increased metabolic stability over SST. Although SST has a very short plasma half-life (~3 minutes), which makes it unsuitable for PET tracer development, OC has a longer plasma half-life (1.7 hours) (Lamberts et al., 2002). All of the OC analogs bind with high affinity to sst_2 and sst_5 and with varying affinity to the sst_3 and sst_4 receptors (Koopmans et al., 2009).

Overall, SStR PET tracers based on OC analogs were successfully evaluated in the clinic and were able to differentiate tumor physiology as well as detect NET with high accuracy. OC conjugation to chelators, such as DOTA (1,4,7,10-tetraazacyclododecane-1,4,7,10-tetraacetic acid), NOTA (1,4,7-triazacyclononane-1,4,7-triacetic acid), and TETA (1,4,8,11-tetraazacyclotetradecane-1,4,8,11-tetraacetic acid), etc., allows labeling with isotopes such as ^{68}Ga and ^{64}Cu for PET imaging (Lamberts et al., 2002). Several SST/OC analogs have been evaluated in clinical PET imaging studies. One study described a comparison between ^{68}Ga-DOTA-TOC (PET imaging) and ^{111}In-DTPA-OC (SPECT imaging) as agents for detection of NET in 27 patients with histologically proven untreated NETs (Buchmann et al., 2007). ^{68}Ga-DOTA-TOC appeared to be superior and imaged more positive lesions than ^{111}In-DTPA-OC, although the calculated SUV_{max} of ^{68}Ga-DOTA-TOC in positive lesions had a broad range from 0.9 to 34.4. The researchers concluded that PET imaging with ^{68}Ga-DOTA-TOC was clinically more relevant,, and in one case of this cohort, the data obtained by ^{68}Ga-DOTA-TOC imaging were clinically helpful in the decision to change the patient's surgical management (Buchmann et al., 2007).

Another study that was published recently by Krausz et al. (2012) described the imaging of NETs in the pancreas by SST/OC analog ^{68}Ga-DOTA-NOC. Ninety-six patients with pathologically proven pancreatic NET (n = 40), nonpancreatic NET, or with biochemical suspicion of NET (n = 63) underwent PET scans with ^{68}Ga-DOTA-NOC. From a total of 103 ^{68}Ga-DOTA-NOC PET scans of NET, increased tracer uptake was seen in one or more areas of the pancreas in 76 scans, with SUV_{max} ranging from 5.5 to 165. Of the 76 positive pancreatic cancer cases, the tracer was clearly visualized in 35 lesions of pancreatic tumor sites (Krausz et al., 2012). Among 63 cases without previous known pathology in the pancreas, uptake was significantly higher than the adjacent background activity but no anatomically identifiable tumors were seen by CT. In 38 sites, the accumulation was judged as physiologic, generally lower relative to adjacent structures. In 24 scans with suspected tumor and in 37 of 38 scans with physiologic uptake, diagnostic CT or MRI or endoscopic ultrasonography failed to detect tumor (Fig. 8) (Krausz et al., 2012).

Haug et al. (2012) reported on the clinical evaluation of another SST analog, ^{68}Ga-DOTA-octreotate (TATE) in 104 patients with suspected, nonlocalized NET. NET-positive tumors were verified by histology. ^{68}Ga-DOTA-TATE detected NETs in 29 of the 36 cases and excluded the presence of a NET in 61 of the 68 non-NET patients, indicating a sensitivity of 81% and specificity of 90%. PET/CT gave a false-positive result in seven patients and a false-negative result in another seven patients, indicating positive and negative predictive values of 81 and 90%, respectively, and an accuracy of 87% (Haug et al., 2012).

To allow a longer imaging time window during the clearance of nonspecific binding, which is expected to allow better tumor-to-background ratio, DOTA-TATE was also labeled with ^{64}Cu (Pfeifer et al., 2012). ^{64}Cu-DOTA-TATE was injected into 14 patients with a history of NET, and the patients were scanned at 1, 3, and 24 hour postinjection. As a comparison, these patients were also injected with the SPECT tracer, ^{111}In-DTPA-OC. Imaging SStR using ^{64}Cu-DOTA-TATE gave higher quality and better spatial resolution than ^{111}In-DTPA-OC, resulting in a higher detection

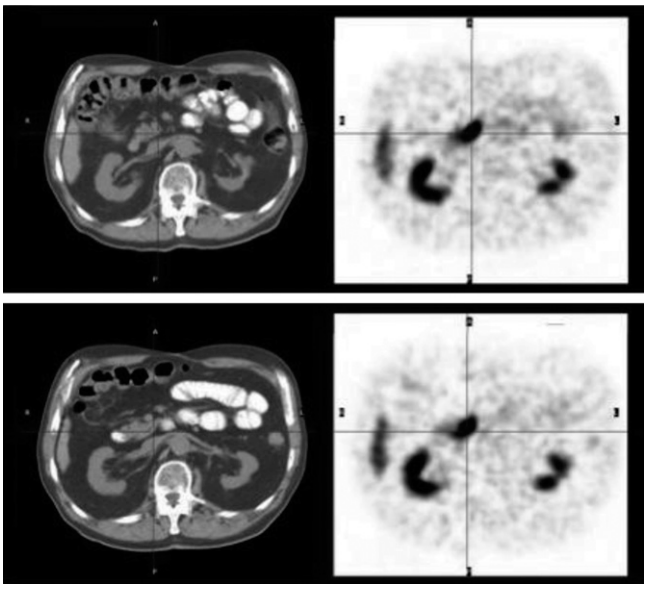

Fig. 8. Transaxial PET/CT scans of a patient injected with 68Ga-DOTA-NOC studied for follow up of midgut carcinoid. PET images (right) show intense uptake in the uncinate process (black cross) with no CT findings in the pancreas (left). [Adapted from Krausz Y, Rubinstein R, Appelbaum L, Mishani E, Orevi M, Fraenkel M, Tshori S, Glaser B, Bocher M, Salmon A, Chisin R, Gross DJ, and Freedman N (2012) Ga-68 DOTA-NOC uptake in the pancreas: pathologic and physiologic patterns. *Clin Nucl Med* **37:**57–62. Used with permission.]

rate (Fig. 9) (Pfeifer et al., 2012). ^{64}Cu-DOTA-TATE showed uptake in additional lesions in 6 of 14 patients, and in 5 patients, the tracer allowed detection of metastatic lesions in organs that were not previously known as metastatic sites (Pfeifer et al., 2012).

4. Bombesin Receptor. BBNR family consists of four receptor subtypes: neuromedin B receptors (BB_1), gastrin releasing peptide receptor (GRPR, BB_2) and BBNR BB_3 and BB_4 (Koopmans et al., 2009). BBNR belongs to GPCR family and undergoes internalization after the receptor-agonist complex has been formed. Bombesin is a 14 amino acid amphibian homolog peptide of the mammalian GRP, a member of the brain-gut peptides, and binds with high affinity to GRPR (Anastasi et al., 1971; Koopmans et al., 2009). All BBNR subtypes are overexpressed at different levels by NET; however, to date the majority of PET tracers developed for BBNR imaging in vivo target GRPR (Reubi and Waser, 2003)

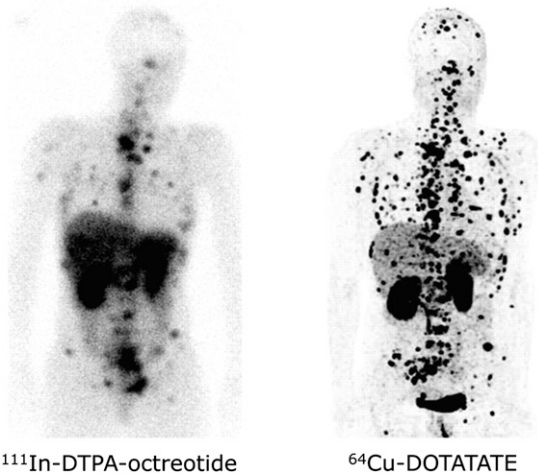

Fig. 9. Comparison of ^{111}In-DTPA-OC (left) and 64Cu-DOTA-TATE (right) in a patient with multiple bone and soft tissue metastases. [Adapted from Pfeifer A, Knigge U, Mortensen J, Oturai P, Berthelsen AK, Loft A, Binderup T, Rasmussen P, Elema D, Klausen TL, Holm S, von Benzon E, Højgaard L, and Kjaer A (2012) Clinical PET of neuroendocrine tumors using ^{64}Cu-DOTATATE: First-in-humans study. *J Nucl Med* **53:** 1207–1215. Used with permission.]

Several bombesin analogs (agonists and antagonists) for the GRPR have been radiolabeled with various PET isotopes and evaluated in vivo for tumor imaging, most of which focus on AR-independent prostate cancer. This is based on the idea that it might detect neuroendocrine differentiation, characteristic of high grade and high stage tumors, and might improve lymph node staging and recurrence detection (Koopmans et al., 2009; Abiraj et al., 2011; Lears et al., 2011). Nanda et al. (2012) recently reported on the design, development, ^{64}Cu labeling, and evaluation of new bombesin antagonist analogs, ^{64}Cu-(NO2A-X-D-Phe^{6}-BBN(6–13)NHEt. These peptides have different linker groups that determine the hydrophobicity that reflects on their pharmacokinetics in vivo. The analogs were first evaluated in normal mice and showed relatively high specific uptake in the pancreas, which normally express GRP cell-surface receptors in mice. Thereafter, the analogs were injected in mice bearing subcutaneous prostatic tumors that express high levels of GRPR. Biodistribution studies showed high uptake and retention in the tumors and rapid urinary excretion to give very high tumor to background ratios. Micro-PET/CT imaging showed clear visualization of tumors 15 hours postinjection, whereas the more hydrophilic peptide had the highest accumulation in GRPR-expressing tumor and the most efficient clearance of radiotracer from whole body via the renal urinary excretion pathway (Fig. 10) (Nanda et al., 2012).

Another study evaluated several bombesin antagonists [D-Phe-Gln-Trp-Ala-Val-Gly-His-Leu-NHCH2CH3 (ATBBN) and Gly-Gly-Gly-Arg-Asp-Asn-D-Phe-Gln-Trp-Ala-Val-Gly-His-Leu-NHCH2CH3 (MATBBN)] and agonists [Gln-Trp-Ala-Val-Gly-His-Leu-MetNH2 (AGBBN) and Gly-Gly-Gly-Arg-Asp-AsnGln-Trp-Ala-Val-Gly-His-Leu-MetNH2 (MAGBBN)] and labeled them with ^{18}F for testing in prostate cancer tumor-bearing mice (Yang et al., 2011b). Some of the peptide analogs contained a hydrophilic linker consisting of six amino acids (Gly-Gly-Gly-Arg-Asp-Asn) with the aim to improve their hydrophilicity and tumor uptake. Indeed, the most lipophilic antagonist had almost no tumor uptake, but rather rapid and prominent activity accumulation in the liver and intestines. Insertion of the hydrophilic linker to agonist and antagonist peptides resulted in high quality images with high tumor-to-background contrast as early as 0.5 hour postinjection (Yang et al., 2011b). The distinct

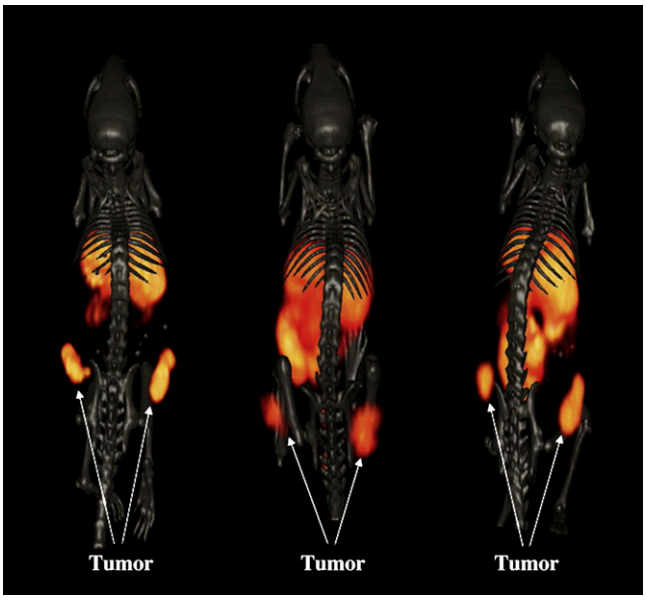

Fig. 10. Coronal micro-PET/CT images in GRPR-positive tumor-bearing mice 15 hours postinjection of three ^{64}Cu-bombesin peptide-based antagonists. The most hydrophilic peptide was presented on the left and the most hydrophobic on the right. [Adapted from Nanda PK, Pandey U, Bottenus BN, Rold TL, Sieckman GL, Szczodroski AF, Hoffman TJ, and Smith CJ (2012) Bombesin analogs for gastrin-releasing peptide receptor imaging. *Nucl Med Biol* **39:**461–471. Used with permission from Elsevier.]

difference between linker-modified and unmodified tracers signifies the profound impact of lipophilicity on the pharmacokinetics of the tracers. Overall, multiple receptors and proteins were targeted using PET tracers to evaluate proliferation of cancer cells. Most of the tracers were tested in animal models, and some gave promising results. As for many of the reported PET tracers, the transition from bench to bedside seems to be lacking. Four clinical studies of EGFR imaging are ongoing, including the antibody ^{89}Zr- etuximab, the two TK inhibitors, [^{18}F]F-PEG6-IPQA and [^{11}C]erlotinib, and ^{111}In-ABT-806 (antibody for SPECT). Clinical trials for HER-2 include trastuzumab antibody labeled with PET isotopes ^{64}Cu, ^{89}Zr, or SPECT isotope ^{111}In, and the F(ab′)$_2$ fragment of trastuzumab labeled with ^{68}Ga. SStr, on the other hand, has been evaluated in many human clinical trials, all of which were based on OC derivatives labeled with ^{68}Ga or ^{111}In. BBNR tracer was only evaluated once using bombesin antagonist BAY86-7548 [DOTA-4-amino-1-carboxymethyl-piperidine-D-Phe-Gln-Trp-Ala-Val-Gly-His-Sta-Leu-NH$_2$] labeled with ^{68}Ga. In our opinion, with the great number of proliferation tracers available for human studies, more efforts are needed to be directed into human trials rather than further development of more tracers and evaluating them in mouse models.

B. Imaging of Apoptosis Pathways

Apoptosis (programmed cell death) is a form of cell death that is highly conserved throughout evolution and plays an important role in the control of development and tissue homeostasis. Apoptosis is precipitated by sequential activation of cysteine proteases of the caspase family and can be activated by a wide range of stimuli, originating from the outside of the cell (extrinsic) by ligation of transmembrane death receptors, such as tumor necrosis factor (TNF)-related apoptosis-inducing ligand (TRAIL), Fas, TNF, DR3–6, and their ligands or cytotoxic agents, or from intracellular signals (intrinsic), such as p53 activation after DNA damage (Adams, 2003; Shi, 2006; Adams and Cory, 2007; Wang and Youle, 2009).

In the extrinsic pathway, upon activation of caspase-8 and caspase-10, each receptor can form a death-inducing signaling complex by recruiting the adaptor protein Fas-associated protein with death domain (FADD) and the caspases into multiprotein complexes (Adams and Cory, 2007; Wang and Youle, 2009). The intrinsic mitochondrial pathway occurs in response to diverse stresses, including cytokine deprivation and DNA damage; activates caspase-9 on the scaffold protein Apaf-1; and cytochrome *c* is released from damaged mitochondria (Wang and Youle, 2009). As a consequence, these initiator caspases cleave and activate effector caspases such as caspase-3, -6, and -7 (Wang and Youle, 2009).

Caspases are cysteine proteases that are synthesized as inactive proenzymes and become activated upon cleavage (Degterev et al., 2003; Fulda, 2009). In caspase-dependent apoptosis, activation of apoptosis pathways eventually leads to the activation of caspases that function as common death effector molecules (Degterev et al., 2003).

Cancer cells can acquire resistance to signals initiating apoptosis. Such resistance can be achieved by, for example, the blockage of tumor suppressor p53 pathway. p53 is a transcription factor that regulates the expression of several proapoptotic proteins (e.g., Bax, Bak), caspases, death receptors (e.g., Fas), DNA repair proteins, or the cell cycle inhibitor (Essmann and Schulze-Osthoff, 2012) and plays a critical role in response to various cellular stresses by modulating transformation, cell growth, DNA synthesis and repair, differentiation and apoptosis (Zhao et al., 2012). Under cellular stress, p53 accumulates in the cytosol and leads to direct activation of Bax and/or Bak, which leads to activation of apoptosis (Mihara et al., 2003; Chipuk et al., 2004; Leu et al., 2004).

Other than blocking of proapoptotic pathways, cancer cells can upregulate antiapoptotic pathways such as the phosphatidylinositol 3-kinase (PI3K)/Akt signaling pathway. This pathway is important for cellular regulation functions such as proliferation, growth, transcription, translation, cell cycle, and apoptosis (Vanhaesebroeck and Alessi, 2000; Cantley, 2002). PI3K/Akt signaling is found to be disrupted in many human cancers and plays a major role not only in

tumor growth but also in the response to anticancer treatment (Vivanco and Sawyers, 2002; Maddika et al., 2007). Imaging apoptosis can be useful for cancer patients as a method of monitoring the effectiveness of therapies that induce apoptosis.

To date, the most widely used agent to evaluate cell death by PET is ^{18}F-labeled Annexin V. Annexin V is a 36-kDa human protein with high affinity for cell membrane of apoptotic cells and binds phosphatidylserine (PS). Induction of apoptosis results in externalization of PS from the inner leaflet of the plasma membrane to its outer surface as a marker for phagocytes for clearance of apoptotic cells (Corsten et al., 2006). A downside of PS imaging is that PS can also bind Annexin V under necrosis because of the disruption in the plasma membrane integrity. Another possible drawback of Annexin V is that tumor cells under stress, for example, chemotherapy, can transiently exhibit PS on their membrane but it does not necessarily show commitment to apoptosis later on (Blankenberg, 2002).

^{99m}Tc-Annexin V was evaluated in patients with NSCLC and non–Hodgkin's lymphoma in phase II clinical trials and showed higher accumulation of tracer in the lesion postchemotherapy. However, there was very high background and the use of SPECT does not allow for the quantification of the results (Blankenberg, 2008). Nevertheless, Annexin V and its derivatives have been extensively evaluated in xenograft models when labeled with PET isotopes (Li et al., 2008; Zhang et al., 2009; Bauwens et al., 2011; Cheng et al., 2012; Hu et al., 2012). The results of one interesting study was recently published by Hu et al. (2012), describing the ability of [^{18}F]Annexin V to visualize and evaluate cell death induced by the chemotherapy drug doxorubicin in a HNSCC tumor xenograft model (Hu et al., 2012). Tumor-bearing mice were treated with two doses of doxorubicin (10 mg/kg) at 1-day intervals, and PET imaging studies using [^{18}F]Annexin V were performed at 0 hour, 6 hours, 24 hours, 3 days, and 7 days after treatment started. Two doses of doxorubicin effectively inhibited the growth of tumors by inducing cell death, including apoptosis. The cell death was clearly visualized by [^{18}F]Annexin V using micro-PET as early as at 6 hours after therapy and reached peak uptake at day 3 (1.56 ± 0.23%ID/g in a comparison with the PBS-treated group that had tumor uptake of 0.89 ± 0.31%ID/g; Fig. 11) (Hu et al., 2012). These results suggest that cell death induced by doxorubicin treatment occurs shortly after the treatment begins and persists for several days. Tumor growth curves showed no significant change at day 3 after therapy started; however, there was complete eradication of several tumors by day 7. The researchers also used an apoptosis reporter gene (Niu et al., 2013) and bioluminescence imaging and observed strong caspase-3 activity in a doxorubicin-treated group at day 5 after therapy initiation. They hypothesized that the ratio of apoptotic

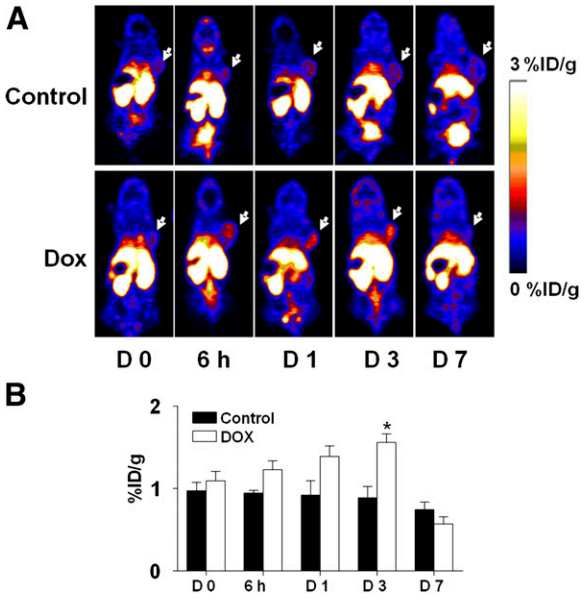

Fig. 11. (A) Coronal PET images of tumor-bearing mice injected with [^{18}F]SFB-Annexin-V at different time points after doxorubicin treatment started. White arrows indicate tumors. (B) Quantification of [^{18}F]SFB-Annexin V tumor uptake before and after treatment. [Adapted from Hu S, Kiesewetter DO, Zhu L, Guo N, Gao H, Liu G, Hida N, Lang L, Niu G, and Chen X (2012) Longitudinal PET imaging of doxorubicin-induced cell death with ^{18}F-Annexin V. *Mol Imaging Biol* **14:**762–770. Used with permission.]

cells among the tumor kept increasing with time within the first several days. At day 7, the treated tumor showed decreased Annexin V uptake, partially because of the removal of the majority of apoptotic and necrotic cells. This may also be explained by the possibility of disruption to tumor vascularization that reduced Annexin V availability (Hu et al., 2012).

As can be seen from this and other publications, both chemotherapy and radiation therapy induce apoptosis in tumor cells (Blankenberg, 2002; Hu et al., 2012). PET imaging, with its ability to provide information on the rate and extent of apoptosis, is of great interest in monitoring the efficacy of anticancer treatment. However, labeled Annexin V is still suboptimal for clinical evaluation because of its high uptake in the abdominal region and the inability to distinguish apoptosis from necrosis. In addition, uptake of radiolabeled Annexin V appears to have modest change in response to therapy, which may be due to nonspecific uptake of protein tracers caused by enhanced permeability of blood vessels (discussed under the angiogenesis chapter) and poor lymphatic drainage of tumors (Cheng et al., 2012).

Other tracers for imaging apoptosis by PET have been developed and are under evaluation. [^{18}F]2-(5-Fluoropentyl)-2-methyl malonic acid ([^{18}F]ML10) is a small molecule and has been evaluated in eight healthy human subjects (Hoglund et al., 2011). Although its target on the cell membrane of apoptotic cells is unknown, ML10 has shown selective passage through the membrane and accumulation within the cytoplasm of apoptotic cells from the early stages of the

death process without entering viable cells (Aloya et al., 2006). One requirement for apoptosis tracers is the lack of binding to viable cells and tissues; therefore, in healthy subjects it should have fast distribution and clearance. Indeed, [^{18}F]ML10 showed rapid distribution and fast clearance through the urine (Hoglund et al., 2011). [^{18}F]ML10 was further evaluated in nine human patients for the early detection of response of brain metastases to whole-brain radiation therapy (Allen et al., 2012). The primary tumors of the patients were small cell lung cancer, uterine sarcoma, melanoma, and breast cancers, and the minimal size of lesions was determined to be ≥1.5 cm in diameter. [^{18}F]ML10 was administered intravenously to each patient before and after irradiation, followed by PET/CT scans. [^{18}F]ML10 visualized brain metastasis lesions before treatment, which reflects on the basal apoptosis in cancers. After the radiation therapy, [^{18}F]ML10 uptake was significantly increased in tumors with good signal-to-background ratios of 8.76 ± 5.59 (calculated from SUV_{mean}) at 130–150 minutes postinjection (Allen et al., 2012). The signal-to-background ratio increased over time after injection, reflecting tracer accumulation at its target while being cleared from nontarget organs (Fig. 12) (Allen et al., 2012). A correlation between [^{18}F]ML10 uptake after treatment and the reduction of tumor size as detected by MRI was found (Allen et al., 2012).

[^{18}F]ML10 seems to be a promising PET tracer for early apoptosis detection and tumor response to radiotherapy and warrants studies at a larger scale. Nevertheless, it exhibited high accumulation in the kidneys, ovaries, heart wall, liver, and pancreas, which limits detection of apoptosis in tumors within these organs (Hoglund et al., 2011). The mechanism of tracer uptake by apoptotic cells remains unknown.

Another PET tracer that is under evaluation for apoptosis imaging is a small molecule inhibitor of caspase-3 labeled with F-18, isatin-5-sulfonamide ([^{18}F]ICMT-11) (Nguyen et al., 2009). [^{18}F]ICMT-11 was administered into mice bearing murine lymphoma tumors treated with the chemotherapy drug cyclophosphamide (CPA, 100 mg/kg) to induce apoptosis 24 hours prior to imaging. [^{18}F]ICMT-11 uptake in the tumor was increased by 1.5-fold after CPA treatment (Fig. 13). Histologic analysis of tumor tissues showed that CPA treatment significantly increased apoptosis and active caspase-3 (Nguyen et al., 2009). As seen in several other tracers, [^{18}F]ICMT-11 also had high uptake in the liver, small intestine, kidneys, and urine. Overall, [^{18}F]ICMT-11 seems to be a good tracer for imaging caspase-3 activity, but further research is required to improve the pharmacokinetics and sensitivity of the tracer for apoptotic cells.

Although imaging of apoptosis is very insightful for evaluation of different therapies, clinical trials attempting PET imaging of apoptosis were done only with [^{18}F]ML10 for brain tumors or metastasis. In addition, SPECT imaging of apoptosis was evaluated in human patients using Annexin V labeled with ^{99m}Tc. We believe that this field has not fulfilled its potential and requires more basic research, which should include the development of tracers with better pharmacokinetics and more accurate reflection of early events during the apoptosis cascase.

C. Imaging Limitless Replicative Potential

Continuous replication of chromosomes in cells is regulated by the length of telomeres. Telomeres have several protecting functions of chromosome DNA ends

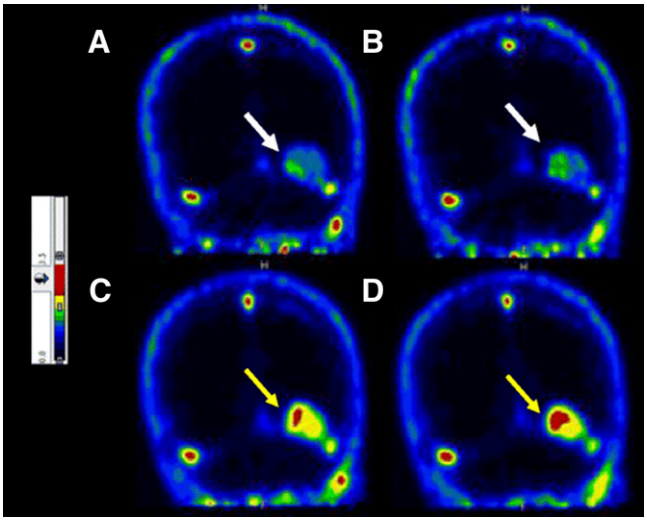

Fig. 12. Coronal brain PET images of patient with brain metastasis using [^{18}F]ML10 before whole-brain radiation therapy (A and B) and after 10 fractions of radiation (C and D). Arrows indicate metastatic lesions. [Adapted from Allen AM, Ben-Ami M, Reshef A, Steinmetz A, Kundel Y, Inbar E, Djaldetti R, Davidson T, Fenig E, and Ziv I (2012) Assessment of response of brain metastases to radiotherapy by PET imaging of apoptosis with ^{18}F-ML-10. *Eur J Nucl Med Mol Imaging* **39:**1400–1408. Used with permission.]

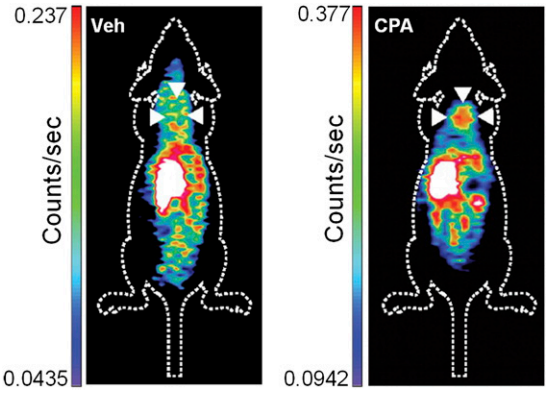

Fig. 13. [^{18}F]ICMT-11 coronal PET images of tumor-bearing mice nontreated (left) or treated with CPA (right). White arrowheads indicate the tumors. [Adapted from Nguyen QD, Smith G, Glaser M, Perumal M, Arstad E, and Aboagye EO (2009) Positron emission tomography imaging of drug-induced tumor apoptosis with a caspase-3/7 specific [^{18}F]-labeled isatin sulfonamide. *Proc Natl Acad Sci USA* **106:**16375–16380. Used with permission.]

from degradation and fusion (Deng and Chang, 2007). The length of the telomeres is regulated by the expression of telomerase, an enzyme that synthesizes telomeric repeats onto chromosomal DNA end and thus compensates for progressive telomere shortening caused by the end-replication problem (Lingner et al., 1995).

Human telomerase activity is associated with the expression of human telomerase RNA (hTR) and human telomerase reverse transcriptase (hTERT) (Feng et al., 1995; Nakamura et al., 1997). In contrast to hTR, which is commonly expressed in both nonproliferating cells and cancers, hTERT expression is found solely in proliferating cells, including tumor cells. Telomerase activity is correlated with resistance to induction of apoptosis.

The majority of cancer cells maintain their telomeres mainly by expression of hTERT, yet some cancer cells use indeterminate pathways that allow telomere maintenance in the absence of active telomerase (Nakamura et al., 1997). Because hTERT expression is found in more than 85% of solid tumors but is undetectable in most normal somatic cells, it has become an attractive target for imaging and therapy (Shay and Bacchetti, 1997; Hiyama and Hiyama, 2003; Wirth et al., 2005; Liu et al., 2007).

Numerous studies have shown indirect imaging of hTERT in mice using luciferase or green fluorescent protein as reporter genes (Yu et al., 2010; Xie et al., 2012). The sole study that was reported for imaging telomerase expression by PET used human sodium iodide symporter (hNIS), a PET reporter gene that was introduced to the tumors by recombinant adenoviruses (Groot-Wassink et al., 2004). The researchers used promoter fragments from the telomerase genes (hTR or hTERT) to drive the expression of the NIS.

To evaluate the applicability of this method, ovarian carcinoma tumor-bearing mice were injected intratumorally with Ad-hTERT-NIS, Ad-hTR-NIS, or the negative controls Ad-hNIS and Ad-luciferase followed by intravenous injection of $Na^{124}I$, and PET imaging was performed 72 hours later. PET images showed that in all animals receiving injection with a NIS-expressing virus, the tumors had heterogeneity of expression within a tumor (Fig. 14), perhaps because of uneven virus diffusion from the point of injection. Another possibility suggested by the researchers is that there was heterogeneity of telomerase promoter activity in different parts of the tumor (Groot-Wassink et al., 2004).

An attempt to image hTERT mRNA using SPECT was done by ^{99m}Tc-labeled *S*-acetylmercaptoacetyltriglycine antisense oligonucleotide, ^{99m}Tc-MAG3-ASON (Liu et al., 2007). As a control, ^{99m}Tc-labeled *S*-acetylmercaptoacetyltriglycine sense bioprobe, ^{99m}Tc-MAG3-SON, was also tested. The design of antisense oligonucleotides is based on the complementary sequence of the oligonucleotide to the appropriate target mRNA. In the described study,

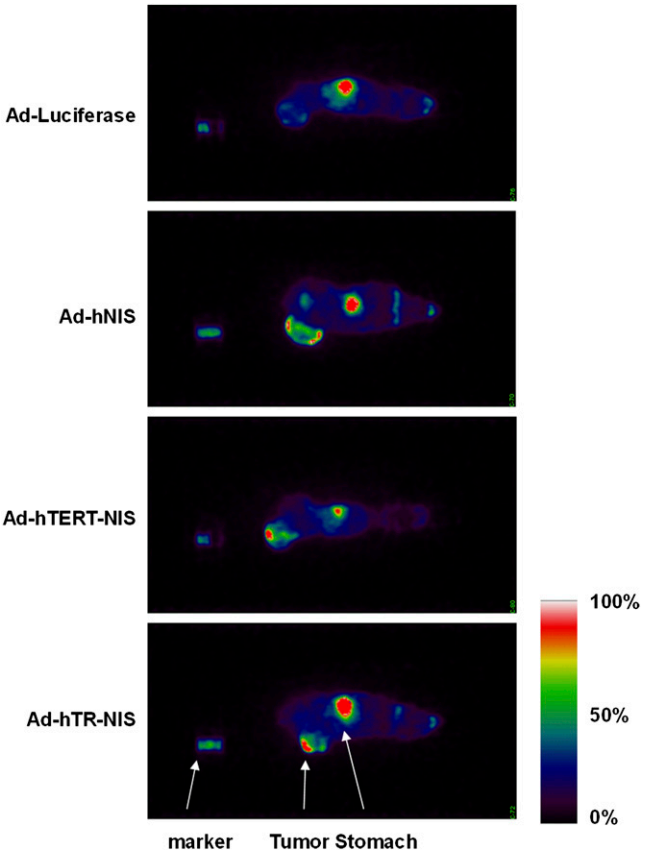

Fig. 14. PET imaging of tumor-bearing mice after injection of various recombinant adenoviruses into the tumors followed by injection of Na124I 72 hours later. [Adapted from Groot-Wassink T, Aboagye EO, Wang Y, Lemoine NR, Keith WN, and Vassaux G (2004) Noninvasive imaging of the transcriptional activities of human telomerase promoter fragments in mice. *Cancer Res* **64:**4906–4911. Used with permission.]

the researchers used 18-mer antisense oligonucleotide; 5′-TAGAGACGTGGCTCTTGA-3′, which is complementary only to the hTERT mRNA. Primary amine on the terminal 3′-phosphate group was conjugated to *S*-acetyl NHS-MAG3 for ^{99m}Tc labeling (Gauchez et al., 1999). Biodistribution of ^{99m}Tc-MAG3-ASON was evaluated in mice bearing human mammary tumor xenografts by tail vein injection and compared with ^{99m}Tc-MAG3-SON. ^{99m}Tc-MAG3-ASON uptake in the tumor increased over time and was higher at all the examined time points than ^{99m}Tc-MAG3-SON, and both bioprobes accumulated similarly in metabolic organs such as kidneys and liver (Fig. 15).

Another attempt to measure mRNA hTERT levels in tumors in vivo using ^{99m}Tc-radiolabeled duplex siRNA was reported (Kang et al., 2010). 2′-*O*-methyl modification on the duplex siRNA was used to protect it from harsh physical and chemical conditions and nuclease degradation. ^{99m}Tc-hTERT-siRNA showed significantly higher tumor accumulation in HepG2 xenograft model than a nonspecific probe, ^{99m}Tc-siRNA, indicating specific delivery of ^{99m}Tc-hTERT-siRNA (Kang et al., 2010). Overall, although imaging using oligonucleotides

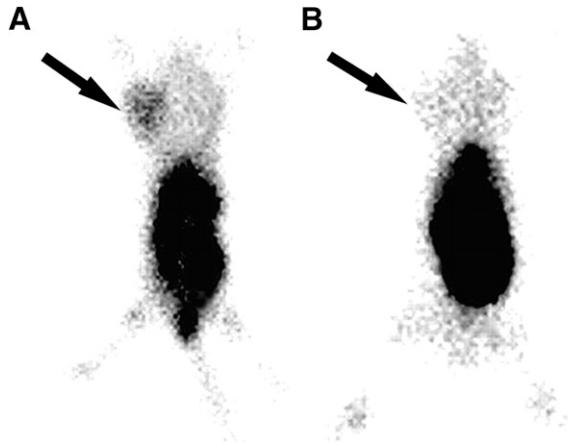

Fig. 15. SPECT imaging of hTERT expression in mammary tumor xenografts in mice using ^{99m}Tc-MAG3-ASON (A) or ^{99m}Tc- MAG3-SON (B). [Adapted from Liu M, Wang RF, Zhang CL, Yan P, Yu MM, Di LJ, Liu HJ, and Guo FQ (2007) Noninvasive imaging of human telomerase reverse transcriptase (hTERT) messenger RNA with ^{99m}Tc-radiolabeled antisense probes in malignant tumors. *J Nucl Med* **48**:2028–2036. Used with permission.]

can visualize positive tumors, the technique is suboptimal because of high background.

A direct imaging of telomerase expression in tumors at the protein level is still absent. From a clinical point of view, it would be preferable to image hTERT levels in the tumors noninvasively before treatment and, in the case of high expression of hTERT, to have treatment with antisense oligodeoxyribonucleotides or siRNA molecules.

D. Cell Cycle Imaging

The cell cycle is an ordered set of events that normally leads to replication. Cells are released from the quiescent phase (G_0), enter into the first gap G_1, and prepare for DNA replication in the synthetic phase (S). Thereafter the cells pass through the second gap (G_2) followed by the mitosis phase (M). At the end of M phase, the cell splits into its two identical daughter cells, which enter either G_1 or G_0. The transition from one phase to the other is regulated by proteins responsible for cell cycle, including cyclin-dependent kinases (CDK), cyclins, CDK inhibitors, and CDK substrates.

A mechanism that regulates cell cycle arrest is the transcription factor p53, already mentioned earlier, which is a tumor suppressor that undergoes activation in response to cancer-associated stress signals. In normal cells, p53 level is low and is degraded via the E3 ubiquitin ligase Mdm2. Oncogenic stress induces the expression of Arf, which inhibits Mdm2 and activates p53. Activation of p53 can induce several cellular responses, including cell cycle arrest, senescence, and apoptosis (Polager and Ginsberg, 2009; Larsson, 2011).

Another transcription factor family that regulates cell fate and cell cycle progression is the E2F family, whose members are downstream of the tumor suppressor protein retinoblastoma (Rb) (Polager and Ginsberg, 2009). One member of this family is E2F1, which can induce apoptosis by both p53-dependent and p53-independent pathways (Stanelle and Putzer, 2006; Polager and Ginsberg, 2008).

The CDK inhibitor p21 is responsible for inhibition of cell cycle proliferation, mainly by interfering with cyclin E/Cdk2 activity, and is one of the major transcriptional targets of p53 and may play the role of a tumor suppressor in cancer. Nevertheless, p21 was also shown to act as an oncogene, because it inhibits apoptosis and may promote cell proliferation in various tumors (Gartel, 2009).

Another pathway involved in cell cycle is transforming growth factor β (TGF-β) signaling. TGF-β has both inhibitory and stimulatory effects on cell proliferation and acts both as a tumor suppressor and oncogene. Under normal conditions, TGF-β promotes cell differentiation and inhibits proliferation. However, during cancer progression, TGF-β secreted from tumor cells often has oncogenic activity while losing its inhibitory function (Siegel and Massague, 2003; Li et al., 2006). TGF-β growth inhibition pathway is mediated through upregulation of cell cycle inhibitors such as p15 and p21 and through downregulation of cell cycle stimulators such as c-myc Cdk4 and Cdk6 (Li et al., 2006). TGF-β also signals through other pathways such as mitogen activated protein kinase (MAPK) and protein phosphatase 2A.

Increased cell cycle, growth, and metabolism of tumor cells can be a target for many chemotherapeutic drugs and these processes can be measured by PET.

1. Nucleoside Imaging. Shields et al. (1998b) reported on the synthesis of thymidine nucleoside with ^{11}C as a means to image proliferating cells and its evaluation in lymphoma patients. PET studies using [^{11}C]thymidine clearly visualized the tumors and the uptake was reduced post chemotherapy, demonstrating its potential as a biomarker of tumor proliferation and response to therapy (Shields et al., 1998b). However, its rapid metabolism along with the short half-life of ^{11}C (20 minutes) makes it less favorable for clinical practice (Mankoff et al., 1998; Shields et al., 1998b). The same group also reported an ^{18}F analog, 3′-deoxy-3′-[^{18}F]fluorothymidine ([^{18}F]FLT) (Shields et al., 1998a). [^{18}F]FLT is taken up by cells and then phosphorylated by thymidine kinase 1 (TK1), a modification that leads to intracellular trapping and retention of [^{18}F]FLT within the cell (Shields et al., 1998a). Because TK1 is overexpressed in various tumors, there is preferential trapping of radiolabeled thymidine by malignant tumors over normal tissues, and indeed [^{18}F]FLT accumulation correlates with TK1 expression and activity. TK1 is the first enzyme in DNA salvage pathway and is activated during the S phase of cell cycle; thus, accumulation of [^{18}F]FLT in the cells can also be used as a marker for cells at the

S-phase in normal cells (Buck et al., 2009; Soloviev et al., 2012).

To date, [^{18}F]FLT is the most widely used PET nucleoside tracer and has shown very good results in the clinic for the visualization of cancers and monitoring treatments (Kenny et al., 2007; Li et al., 2012b; Inubushi et al., 2013). An interesting example of using [^{18}F]FLT was published recently by Leonard et al. (2012). The researchers evaluated the ability of [^{18}F]FDG (imaging metabolism) and [^{18}F]FLT (imaging proliferation/S-phase) to monitor the treatment of patients with relapsed mantle cell lymphoma (MCL). MCL is associated with enhancement of cyclin-D1 expression and cyclin D1-dependent kinase activity to promote cell cycle progression (Leonard et al., 2012). Unfortunately, it has poor prognosis and requires new treatment strategies. The researchers used a selective CDK4/6 inhibitor PD0332991, which causes cell cycle arrest at G_1 in cancer cell lines by blocking phosphorylation of Rb at CDK4/6-specific sites (Leonard et al., 2012). The patients were scanned before and after treatment along with lymph node biopsies to assess Rb protein phosphorylation and markers of proliferation and apoptosis. Extensive reduction was observed in tumor-cell proliferation (reduction in [^{18}F]FLT uptake) and minor reduction in tumor metabolism ([^{18}F]FDG uptake) within the first 3 weeks of treatment compared with the baseline scans (Fig. 16). The reduction in proliferation was also demonstrated by decreased number of phosphorylated Rb within the cells and reduced proliferation (evaluated by Ki-67 staining) in the lymph nodes (Leonard et al., 2012). This work signifies the importance of imaging cell proliferation over metabolism in evaluating tumor potential progression and risks due to the possibility that nonproliferating tumor cells will still exhibit high metabolic state and, hence, high [^{18}F]FDG uptake.

The drawbacks of [^{18}F]FLT are its uptake in the liver and bone marrow due to catabolism as well as its uptake by the proliferating bone marrow cells, which limit the use of [^{18}F]FLT to assess therapy response to diseases involving these organs (Kenny et al., 2005). In addition, [^{18}F]FLT may be less sensitive for tumors with low TK1 expression levels. Therefore, it is unclear whether the sensitivity of [^{18}F]FLT imaging of primary and metastatic tumor lesions is sufficient for reliable assessment of therapy response (Chen and Chen, 2011).

[^{18}F]1-(2′-Deoxy-2′-fluoro-β-D-arabinofuranosyl)thymine ([^{18}F]FMAU), an uracil analog, is also phosphorylated by thymidine kinases and incorporated into DNA but not into RNA or protein (Sun et al., 2005a). In one study, [^{18}F]FMAU was injected into human patients with different types of cancers and had lower normal bone marrow uptake, which enabled visualization of bone metastases; however it also had higher uptake in the liver, kidney, and myocardium in comparison with [^{18}F]FLT (Sun et al., 2005b). PET imaging with [^{18}F]FMAU seems to be promising, and it would be of interest to use this tracer for assessment of anticancer treatment response in preclinical and clinical studies for bone metastases and diseases not related to liver, kidneys, or myocardium.

2. Androgen Receptor. AR is a member of the steroid/thyroid hormone receptor superfamily that plays a critical role in the development and maintenance of male secondary sexual phenotypes such as muscle, hair and bone mass, prostate growth, and spermatogenesis (Dalton et al., 1998; Yin et al., 2003). The AR is a cellular regulatory protein that, upon androgen binding, migrates into the nucleus, binds to specific DNA sequences called androgen response elements, and modulates the transcription of target genes to induce cell proliferation and apoptosis (Heinlein and Chang, 2004). Two of the natural ligands for AR are testosterone and 5α-dihydrotestosterone (5α-DHT), which are natural steroids and are given as replacement therapy for androgen deficiency (Wu, 1992; Bagatell and Bremner, 1996).

AR is also believed to be involved in prostate carcinogenesis, and amplification of AR is present in most advanced prostate cancer specimens (Comuzzi et al., 2004; Santos et al., 2004). Males who are castrated at a young age do not develop prostate cancer, implying that androgens are risk factors for prostate cancer development (Santos et al., 2004). Approximately 80–90% of prostate cancers are androgen-dependent upon initial diagnosis, and endocrine therapy of prostate cancer is directed toward the reduction of serum androgens and inhibition of AR (Heinlein and Chang, 2004). On the other hand, some very aggressive forms of prostate cancer lose AR expression and are insensitive to inhibition of the AR (Heinlein and Chang, 2004; Santos et al., 2004).

Although AR is a specific target for prostate cancer treatment, loss of expression of AR has been observed in several aggressive tumors. Therefore, it is critical to determine its role in individual patients to guide and monitor treatment modalities. DHT was labeled with fluorine-18 to give 16β-[^{18}F]fluoro-5α-dihydrotestosterone ([^{18}F]FDHT), which competes with DHT for binding to AR (Liu et al., 1992). Larson et al. (2004) reported on a comparative clinical study of seven castrated patients with low circulating testosterone levels who had progressive metastatic prostate cancer and were imaged with [^{18}F]FDG and [^{18}F]FDHT. [^{18}F]FDG uptake was positive in 97% of the lesions with SUV_{max} of 5.22, whereas [^{18}F]FDHT was positive in 78% of the lesions with SUV_{max} of 5.28, and [^{18}F]FDHT also displayed heterogeneity in accumulation at different areas of the tumors (Larson et al., 2004). The reason for heterogeneity of tracer uptake in this study is unknown but might be because of the variation in AR expression versus glucose metabolism rate. Such heterogeneity might be indicative of prostate cancer and should

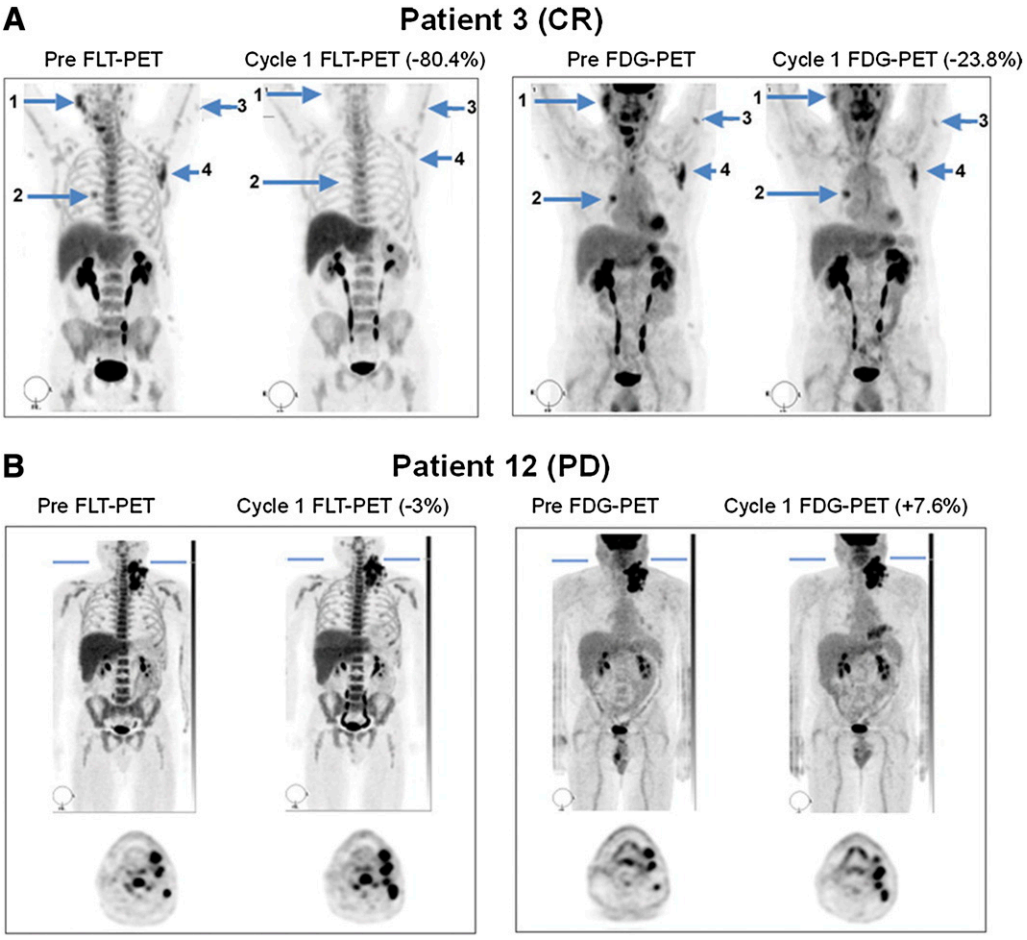

Fig. 16. Representative [^{18}F]FLT-PET/CT and [^{18}F]FDG-PET/CT images from two patients before and during the third week of treatment with PD0332991 in responding (A) and progressing patients (B). [Adapted from Leonard JP, LaCasce AS, Smith MR, Noy A, Chirieac LR, Rodig SJ, Yu JQ, Vallabhajosula S, Schoder H, English P, Neuberg DS, Martin P, Millenson MM, Ely SA, Courtney R, Shaik N, Wilner KD, Randolph S, Van den Abbeele AD, Chen-Kiang SY, Yap JT, and Shapiro GI (2012) Selective CDK4/6 inhibition with tumor responses by PD0332991 in patients with mantle cell lymphoma. *Blood* **119:**4597–4607. Used with permission.]

be evaluated for response to therapy and disease progression.

Two patients in this study were under testosterone treatment and had diminished [^{18}F]FDHT uptake at the tumor site as expected. In another scan done to a patient treated with an Hsp90 inhibitor that indirectly reduces cellular concentration of AR, new lesions were detected by both [^{18}F]FDG and [^{18}F]FDHT in scans that were performed 4–5 weeks postinitial scans (Larson et al., 2004). [^{18}F]FDHT was further evaluated in patients with progressive metastatic castration-resistant prostate cancer (Scher et al., 2010). The patients received different doses of an AR antagonist, MDV3100 (Enzalutamide; Medivation, San Francisco, CA), which inhibits AR nuclear translocation and subsequent binding to the response element on the DNA (Larson et al., 2004). Patients underwent PET scans before and 4 weeks after treatment with MDV3100 was initiated. PET imaging showed a decrease in [^{18}F]FDHT uptake in all patients who received treatment compared with scans done before therapy. An obstacle for interpreting these results and for imaging AR post-MDV3100 treatment is that the antagonist prevents the binding of [^{18}F]FDHT to AR. Therefore, in this setting, the best use of [^{18}F]FDHT is as a method for evaluating the optimal dose of antiandrogen required for complete blockade of the AR, on a patient-by-patient basis.

Another promising PET tracer reflecting the downstream effects of AR signaling is the monoclonal antibody, J591, that targets the extracellular domain of prostate-specific membrane antigen (PSMA) (Mease et al., 2008; Holland et al., 2010). PSMA is a transmembrane glycoprotein mainly expressed on benign and malignant prostatic epithelial cells, and its expression level was found to correlate with tumor aggression, metastatic spread, and the development of castration resistance or resistance to hormone-based therapies (Morris et al., 2005). J591 was previously evaluated in a clinical trial as a therapy for localized metastatic prostate cancer and induced antibody-dependent cellular cytotoxicity and reduced PSA levels (Morris et al., 2007). ^{111}In-DOTA-J591 has been tested in castrated patients with progressive metastatic prostate cancer who received J591 as therapy (Morris

et al., 2005). J591 was also labeled with ^{90}Y and ^{177}Lu for radioimmunotherapy (Morris et al., 2007).

Holland et al. (2010) reported on the labeling and evaluation of J591 with ^{89}Zr using the chelator desferrioxamine B (DFO) and evaluated the labeled antibody ^{89}Zr-DFO-591 in mice bearing PSMA-positive and PSMA-negative tumors. ^{89}Zr-DFO-591 had higher and more specific uptake in PSMA-positive tumors than that in PSMA-negative tumors (Fig. 17). ^{89}Zr-DFO-J591 is currently under clinical study for the detection of PSMA-positive lesions in castration-resistant prostate cancer patients. Preliminary results showed that the tracer accumulates in primary tumors and metastatic lesions (Deri et al., 2013).

As described above, a number of PET tracers are available to image the cell cycle, with the lead compound being [^{18}F]FLT, which is being evaluated in many clinical trials around the world. The tracer seems to be close to getting approval for clinical use by the FDA. It is unclear whether there is a place for more tracers designed based on nucleosides. Other tracers for the cell cycle, which are being evaluated in clinical trials, are more specific and tumor-type directed. These include [^{18}F]FDHT (for AR imaging) and two PSMA tracers ^{89}Zr-DFO-J591 (antibody) and [^{18}F]DCFBC (small molecule inhibitor). Obviously, tracers imaging proliferation, which were discussed above, can also fit into the definition of cell cycle tracers. We believe that imaging the cell cycle will be a corner stone in tumor imaging in the future and should be used for drug development as well as for guiding specific therapies.

3. Sigma-2 Receptor Imaging. Sigma receptors were identified initially as a subclass of opioid receptors, but because of their different neuropharmacological properties and because they are expressed throughout the mammalian body, they were classified as unique family of receptors that include σ-1 and σ-2 (Hornick et al., 2012). Part of the σ-2 receptor complex includes human progesterone receptor membrane-binding component 1, which was used for development of compounds that bind σ-2. Expression of σ-2 receptor is highly upregulated by dividing cells including cancer cells, and the expression is downregulated upon quiescence. In some tissues, the σ-2 can serve as a therapeutic target, because its human progesterone receptor membrane binding component 1 part binds to

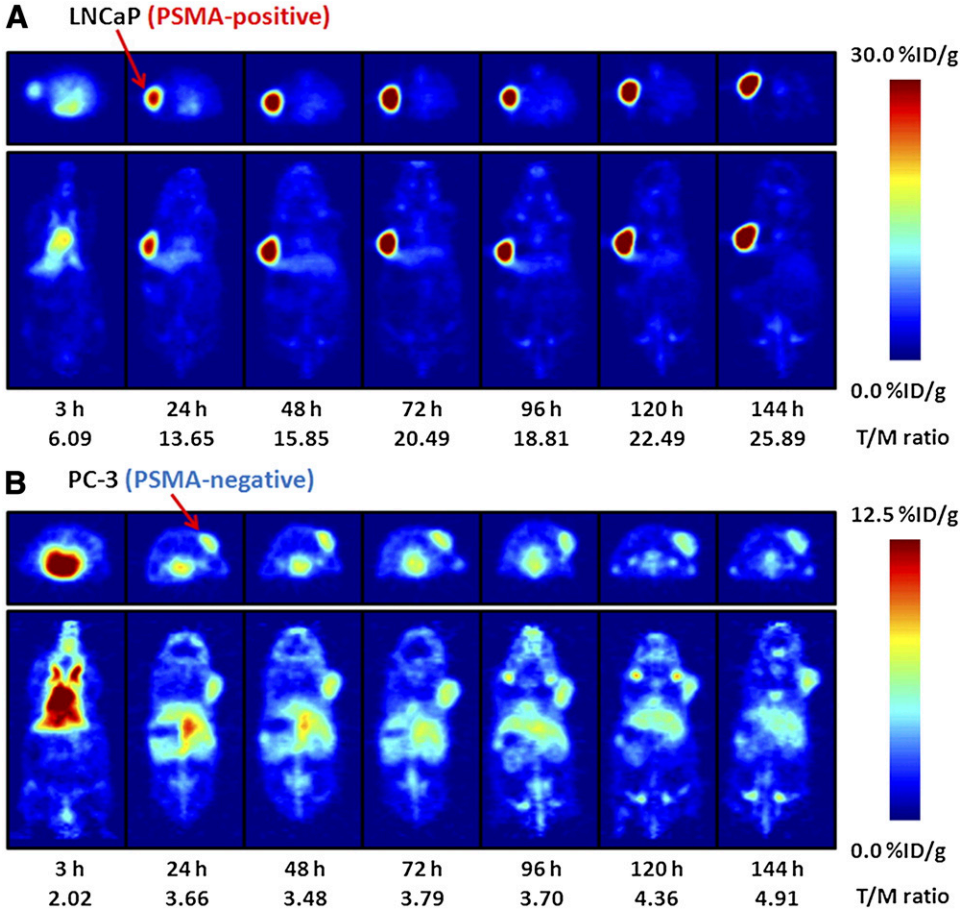

Fig. 17. Transaxial and coronal micro-PET images of mice bearing PSMA-positive (A) and PSMA-negative (B) tumors after injection of ^{89}Zr-DFO-591 over time. Tumor-to-muscle ratio (T/M) was calculated from PET images. [Adapted from Holland JP, Divilov V, Bander NH, Smith-Jones PM, Larson SM, and Lewis JS (2010) ^{89}Zr-DFO-J591 for immunoPET of prostate-specific membrane antigen expression in vivo. *J Nucl Med* **51:**1293–1300. Used with permission.]

cytochrome P450 and reduces its drug metabolism activity. Several cancers, including pancreatic cancer, are sensitive to σ-2 agonists, which inhibit proliferation and induce apoptosis by various mechanisms with little effect on normal tissues (Bem et al., 1991; Vilner et al., 1995). A possible mechanism for the action of σ-2 agonists is by eliminating P-glycoprotein-mediated drug resistance and at subtoxic doses (van Waarde et al., 2010). A large number of radiolabeled σ-2 ligands have been prepared for PET imaging (Abate et al., 2011; Dehdashti et al., 2013).

Dehdashti et al. (2013) recently reported on the first study in humans using a small σ-2 ligand, [^{18}F]ISO-1. In this study, [^{18}F]ISO-1 PET imaging was performed in 30 patients with primary breast cancer, lymphoma, or head and neck cancer. Tumor SUV_{max} and tumor-to-muscle ratio were positively correlated with immunohistochemical staining of the proliferation marker Ki-67 (Dehdashti et al., 2013). It appears that [^{18}F] ISO-1 is a promising tracer that warrants further tests in bigger cohorts of patients as a potential imaging marker to replace biopsies for assessing tumor cell proliferation and monitoring response to chemotherapies that target cycling cells (Dehdashti et al., 2013).

E. Metabolism Imaging

Tumor growth requires high amount of energy for cellular processes such as cell cycle, growth, and proliferation, and the source of the energy comes from high metabolic rate. Metabolic imaging of tumor can be complicated with background from kidneys, liver, and bone marrow because of high metabolic rates in these organs. In addition, heterogeneous metabolic states during tumorigenesis can cause low tracer uptake or difficulties to decipher imaging with unclear margins and metastases.

To date, the use of PET for diagnosing local recurrence and metastatic sites of various cancers is mainly based on [^{18}F]FDG, which measures glucose metabolism. After malignant transformation and probably because of high proliferation rate, a range of tumors can be characterized by elevated glucose consumption and subsequent increased uptake of [^{18}F]FDG. The transport of FDG through the cell membrane via glucose transport proteins and subsequent intracellular phosphorylation by the enzyme hexokinase have been identified as key steps for the accumulation of FDG in the tissue (Saleem et al., 2006). In contrast to glucose, FDG-6-phosphate cannot be further metabolized, thus it is accumulated in cells and can be visualized by PET.

However, the use of [^{18}F]FDG is suboptimal because it is cancer-specific. It also accumulates in normal tissues such as brain and bladder and in inflammatory lesions. Hence, there is an increasing need for more specific and selective biologic radiotracers, which will yield specific biochemical information and allow for noninvasive molecular imaging. Several PET tracers other than FDG have been used in the clinic for metabolism measurement.

1. Lipid Synthesis Imaging

a. [^{11}C] and [^{18}F]choline. Choline is one of the components of phosphatidylcholine, which is a major component in the cell membrane. Accumulation of phosphatidylcholine during membrane biosynthesis occurs during the S phase, and the absence of choline results in cell arrest during G_1 phase (Jackowski, 1994). Choline labeled with ^{11}C or ^{18}F is incorporated into the cells, undergoes phosphorylation, and is then integrated into phospholipids (Jadvar, 2012; Picchio and Castellucci, 2012; Schwarzenbock et al., 2012). Thus, accumulation of radiolabeled choline in tumors is indicative of membrane lipid synthesis and proliferation activity of cells (Shiue and Welch, 2004). Unlike [^{18}F]FDG, radiolabeled choline does not accumulate in the brain or in the bladder, and clinical studies using [^{11}C]choline or [^{18}F]choline showed their superiority over [^{18}F]FDG for imaging cancers of bladder and prostate and their metastases (de Jong et al., 2002; Gofrit et al., 2006), brain tumors (Tan et al., 2011), and lung cancer and its metastases (Hara et al., 2000). The main downside of [^{11}C]choline imaging is its short half-life, which requires onsite radiosynthesis. On the other hand, using [^{18}F]choline eliminates this disadvantage but creates a different limit—[^{18}F]choline and its metabolites have higher urinary clearance—reducing its usage for imaging lesions in the prostate region but still allowing detection of metastases to the bone (Beheshti et al., 2009). Beheshti et al. (2009) reported on the usage of [^{18}F]choline in 70 patients with progressive prostate cancer with 318 bone lesions: 262 lesions showed increased uptake of [^{18}F]choline with an average SUV_{max} of 8.1 $\pm$ 3.9. Some of the lesions showed no abnormality in CT but still had a clear accumulation of [^{18}F]choline.

b. [^{11}C]Acetate. Acetate is a fatty acid, mainly used by cells in the form of acetyl coenzyme-A, which is important in metabolism. For example, acetyl-coenzyme A is a part of aerobic respiration as a substrate of tricarboxylic acid cycle (TCA cycle, also known as Krebs cycle). Because of the TCA cycle pathway in the myocardium, [^{11}C]acetate was originally used in imaging cardiac oxidative metabolism. In the myocardium, [^{11}C]acetate was shown to be metabolized to $^{11}CO_2$ (Yoshimoto et al., 2001; Yun et al., 2009). [^{11}C]Acetate serves as an alternative radiotracer for detecting tumors not seen on [^{18}F]FDG scans, such as bladder, prostate, and metastatic sites, in part because of lower excretion of [^{11}C]acetate into the urinary tract (Orevi et al., 2012; Yu et al., 2011). It is not clear whether in tumors [^{11}C]acetate is also metabolized to $^{11}CO_2$ as seen in myocardium. In fact, a study done by Yoshimoto et al. (2001) suggests that in vitro, the acetate labeled with ^{14}C is incorporated into the lipid soluble fraction of the cells, mainly into phosphatidylcholine and neutral lipids. The

difference between acetate metabolism by myocardium and tumor cells can be attributable to the high lipid synthesis and proliferation observed in tumor cells, which is absent in the myocardium (Yoshimoto et al., 2001). These results were also confirmed in prostate tumor models in mice using an inhibitor of fatty acid synthesis (Vāvere et al., 2008).

2. Amino Acid Imaging. During the enhanced metabolic state and protein synthesis characteristic of tumors, the need for amino acids for protein synthesis is elevated, and their increased uptake by cells is believed to be via several different transport systems (Hyde et al., 2003). The expression of these transporters was found to be enhanced in cancer development (la Fougère et al., 2011). One of the limiting factors of amino acid imaging is that amino acid transporters, which are upregulated on tumor cell membranes, are independent of tumor growth and are more indicative of metabolism (la Fougère et al., 2011).

Several amino acids were labeled with ^{11}C and ^{18}F and evaluated as PET-imaging agents, such as [^{11}C]methionine ([^{11}C]MET), [^{18}F]fluoroethyl-L-tyrosine ([^{18}F]FET), 6-[^{18}F]fluoro-L-*m*-tyrosine, L-3-[^{18}F]α-methyl-tyrosine, and a few other derivatives (Laverman et al., 2002).

Weber et al. (2000) described a comparative study between [^{11}C]MET and [^{18}F]FET in 16 patients with primary or recurrent intracerebral tumors (Fig. 18). Both tracers clearly visualized the brain lesion with similar uptake and high image contrast (SUV_{mean} of 2.9 ± 1.3 for [^{11}C]MET and 2.4 ± 1.0 for [^{18}F]FET).

L-3-[^{18}F]α-Methyl-tyrosine was also evaluated in 37 patients with NSCLC, and its uptake in tumors was compared with [^{18}F]FDG (Kaira et al., 2009). The patients underwent both scans before surgery. The excised tumors were tested for VEGFR and L-type amino acid transporter-1 by immunohistochemical staining. SUV_{max} for [^{18}F]FDG of primary tumor was significantly higher (ranging from 1.30 to 16.4) than that of L-3-[^{18}F]α-methyl-tyrosine (ranging from 0.81 to 3.60). VEGFR expression was found to be more correlated with L-3-[^{18}F]α-methyl-tyrosine uptake in the tumor than [^{18}F]FDG. In addition, VEGF level had a strong correlation with the expression of L-type amino acid transporter. The amino acid transport system appears to be related to tumor angiogenesis in NSCLC, and therefore L-3-[^{18}F]α-methyl-tyrosine may also be used to monitor anti-VEGF therapy and for assessing metastatic potential and prognosis in patients with NSCLC (Kaira et al., 2009).

Another amino acid analog that was evaluated in human patients is anti-1-amino-3-[^{18}F]fluorocyclobutane-1-carboxylic acid (anti-[^{18}F]FACBC). This synthetic L-leucine analog displayed high uptakes by prostate cancer cells both in vitro and in vivo (Schuster et al., 2007). It was proposed that the uptake of anti-[^{18}F]FACBC is mediated via the sodium-independent L large-neutral amino acid transport system. Fifteen patients with a recent diagnosis of prostate carcinoma (n = 9) or suspected recurrence (n = 6) underwent PET scans with anti-[^{18}F]FACBC (Schuster et al., 2007). The tracer accumulated in both primary and metastatic prostate carcinoma on initial staging as well as uptake in recurrent prostate carcinoma and allowed one to distinguish between benign and malignant tumors. Anti-[^{18}F]FACBC was also compared with a SPECT tracer, anti-PSMA antibody ^{111}In-capromab pendetide (ProstaScint; Cytogen Corporation, Princeton, NJ), and was able to detect recurrent neoplasia that was not revealed by SPECT. Another advantage of anti-[^{18}F]FACBC is that it has little renal excretion compared with [^{18}F]FDG (Schuster et al., 2007).

3. Dopamine Metabolism Imaging. Another labeled amino acid used in the clinic is [^{18}F]FDOPA that can cross the blood-brain barrier. It was initially developed to study the dopamine system, but it appears that [^{18}F]FDOPA is rapidly metabolized in the human body to 3-*O*-*methyl*-6-[^{18}F]fluoro-L-dopa, which makes the quantification of the biologic system complicated. [^{18}F]FDOPA was found to be a good imaging agent for glioma and NET (Heiss et al., 1996; Jora et al., 2011; Lopci et al., 2012). 6-[^{18}F]fluoro-L-tyrosine has a simpler metabolism and was developed to improve the quantification of the dopamine system (Shiue and Welch, 2004).

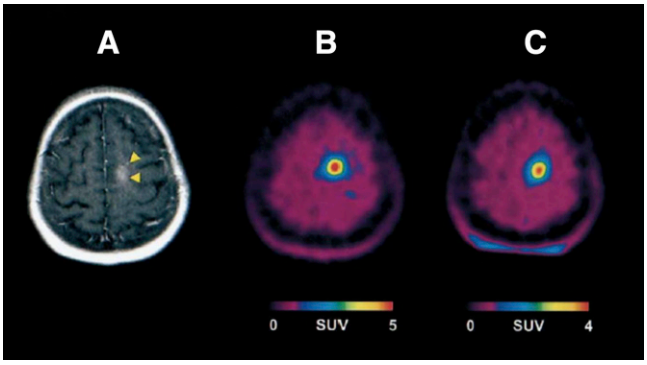

Fig. 18. Brain image of a patient with glioblastoma. (A) MRI shows small area of contrast enhancement (arrowheads); (B) [^{11}C]MET PET imaging; (C) [^{18}F]FET PET imaging. [Adapted from Weber WA, Wester HJ, Grosu AL, Herz M, Dzewas B, Feldmann HJ, Molls M, Stocklin G, and Schwaiger M (2000) *O*-(2-[^{18}F]fluoroethyl)-L-tyrosine and L-[*methyl*-^{11}C] methionine uptake in brain tumors: initial results of a comparative study. *Eur J Nucl Med* **27**:542–549. With kind permission of Springer Science +Business Media.]

F. Tumor Microenvironment Imaging

Angiogenesis is defined as the formation and sprouting of new blood vessels from pre-existing ones. This process is a crucial for tumor growth and metastasis. To induce angiogenesis, angiogenic factors are released by the tumor or cells in its microenvironment to activate endothelial cells in established blood vessels and induce endothelial proliferation and migration (Backer and Backer, 2012).

Angiogenic factors consist of a diverse array of molecules that regulate the maintenance and destruction of both extracellular matrix and perivascular cells as well as those that stimulate endothelial cell division and migration. The main condition that induces angiogenesis is hypoxia, a reduction of oxygen levels. Oxygen diffusion in the tissue is only 1 mm diameter, therefore, when the size of tumor is larger than 2 mm, the cells in the center of the tumor are under a hypoxic microenvironment. Hypoxia induces profound changes in the gene expression profile of tumor cells that initiates tumor angiogenesis and vasculogenesis (Otrock et al., 2009; Miles et al., 2011; Shang et al., 2012). However, the new vasculature within the tumor is disorganized, with distinct morphologic and molecular characteristics that are different from normal blood vessels. Tumor vasculature consists of irregular branches with arteriovenous shunts and lacks pericytes that normally cover the vessels and maintain vascular integrity. Hence, tumor vessels are highly permeable to plasma and plasma proteins, and tumor microenvironment often shows local edema, bleeding, and insufficient clearance of CO_2 and metabolites, leading to an acidic microenvironment. These conditions also contribute to overexpression of genes regulating angiogenesis, tumor growth, and metastasis (Otrock et al., 2009; Miles et al., 2011; Shang et al., 2012). Importantly, high permeability of tumor vessels and relatively high blood volume flow in the tumor can contribute to nonspecific tracer accumulation in the tumor (Goel et al., 2011).

1. Hypoxia Imaging. Hypoxia induced factor 1 (HIF-1) is a heterodimer composed of HIF-1α and HIF-1β subunits. At normal oxygen levels, HIF-1α subunits are hydroxylated at conserved proline residues. This directs its recognition by the tumor suppressor Von Hippel-Lindau protein, which leads to ubiquitination and proteasomal degradation (Greer et al., 2012; Semenza, 2012). Under hypoxic conditions, Von Hippel-Lindau does not tag HIF for degradation. HIF-1α and HIF-1β form a dimer and translocate into the nucleus, where this dimer functions as a transcription factor encoding the transcription of many proangiogenic genes including VEGF gene. VEGF is a secreted protein that stimulates angiogenesis and thereby increases O_2 delivery (Bader and Hsu, 2012; Semenza, 2012). In addition, activation of HIF-1 was found to upregulate CXC chemokine receptor 4 (CXCR4) and its ligand stromal cell-derived factor (CXCL12), which were both shown to be involved in tumor progression and metastasis (Staller et al., 2003; Bader and Hsu, 2012). Hypoxia imaging enables evaluation of treatment response for different therapies that induce hypoxia and can help guide appropriate dosage of treatment (Sun et al., 2011).

A widely used PET agent for imaging hypoxia in tumor is [^{18}F]fluoromisonidazole ([^{18}F]FMISO), a 2-nitroimidazole derivative that enters the cell via passive diffusion. Once it enters the cell, the nitro group is reduced by nitro-reductase enzymes, resulting in radical anion (Lee and Scott, 2007). If the oxygen pressure inside the cells is high, as within normal cells, this radical anion will be reoxidized and converted back to the nitro group, and [^{18}F]FMISO will be diffused out of the cell. In case of low oxygen levels, as typical to cells under hypoxic stress, [^{18}F]FMISO cannot be reoxidized, and its metabolites accumulate inside the cell (Lee and Scott, 2007). [^{18}F]FMISO has been studied in a number of clinical trials in patients with various types of cancer (Rasey et al., 1996; Thorwarth et al., 2006; Zimny et al., 2006; Lee and Scott, 2007). Overall, [^{18}F]FMISO has a relatively low uptake in hypoxic tissue and slow clearance from nonhypoxic tissues, which result in low tumor-to-background contrast (Rajendran and Krohn, 2005).

Another derivative based on 2-nitroimidazole pharmacophore is 3-[^{18}F]fluoro-2-(4-((2-nitro-1*H*-imidazole-1-yl)methyl)-1*H*-1,2,3-triazole-1-yl)-propan-1-ol ([^{18}F]HX4). [^{18}F]HX4 was evaluated in 12 head and neck patients who were also injected with [^{18}F]FMISO for a comparison (Chen et al., 2012). [^{18}F]HX4 exhibited lower uptake than [^{18}F]FMISO in the hypoxic tissues and had slightly higher tumor-to-muscle ratio. However it had lower liver and gastrointestinal uptake, which resulted in overall better tumor-to-background ratio than [^{18}F]FMISO. In addition, [^{18}F]HX4 had a fast clearance from normal tissue, and it was predominantly cleared through kidneys and gallbladder, implying that it could be potentially useful for gastrointestinal tract tumor imaging (Chen et al., 2012).

An additional 2-nitroimadazole derivative that was evaluated in animal models and recently in patients is [^{18}F]2-(2-nitro-1*H*-imidazol-1-yl)-*N*-(2,2,3,3,3-pentafluoropropyl)-acetamide ([^{18}F]EF-5) (Lin et al., 2012). [^{18}F]EF-5 contains five fluorine atoms and is a very lipophilic molecule in comparison with other nitroimidazole derivatives (Koch et al., 2010; Lin et al., 2012). In a research reported by Koch et al. (2010), three patients with gliobastoma were assessed by [^{18}F]EF-5 PET. Binding was also measured ex vivo on tumor biopsies by immunohistochemistry using fluorescent anti-EF-5 monoclonal antibody (Koch et al., 2010). [^{18}F]EF-5 uptake could recognize regions with high EF-5 binding; however, no independent assessment of hypoxia in these patients was done. Because of to its high lipophilicity, [^{18}F]EF-5 displayed high uptake in the gallbladder, liver, and intestine (Koch et al., 2010; Lin et al., 2012).

An additional 2-nitroimidazole nucleoside analog is [^{18}F]fluoroazomycinarabinoside ([^{18}F]FAZA). [^{18}F]FAZA has rapid clearance from nonhypoxic tissue, leading to higher tumor-to-background ratios than [^{18}F]FMISO (Mortensen et al., 2012). In addition, it is more hydrophilic, hence it has more rapid diffusion through tissue and faster renal excretion. [^{18}F]FAZA was evaluated in several human cancer patients (Grosu et al., 2007;

Schuetz et al., 2010; Havelund et al., 2013). Havelund et al. (2013) recently reported on the evaluation of [^{18}F]FAZA in 14 patients with locally advanced rectal cancer. [^{18}F]FAZA uptake was significantly higher in rectal tumors than in normal tissues such as muscle and intestine walls. Unfortunately, there was extremely high accumulation in the bladder, with spillover to the surrounding tissues, including the area of the tumor (Havelund et al., 2013).

Diacetyl-bis(N^4-methylthiosemicarbazone) (ATSM) was labeled with the short half-lived PET isotope ^{62}Cu ($t_{1/2}$ = 9.7 minutes). ^{62}Cu-ATSM was evaluated in 22 glioma patients at different stages (Tateishi et al., 2013). ^{62}Cu-ATSM uptake in the tumors was qualitatively evaluated and compared with MR imaging and HIF-1 expression levels (Tateishi et al., 2013). Higher ^{62}Cu-ATSM uptake and higher tumor-to-blood ratios were found in grade IV than those in grade III gliomas, whereas no significant difference was found between grade III and grade II gliomas (Tateishi et al., 2013). In addition, ^{62}Cu-ATSM uptake was predictive of HIF-1α expression levels in the tumors. ATSM can also be labeled with the longer half-lived PET isotope, ^{64}Cu ($t_{1/2}$ = 12.7 hour). Lewis et al. (2008) reported on the clinical evaluation of ^{64}Cu-ATSM in 10 patients with uterine cervix carcinoma and compared it with ^{60}Cu-ATSM. ^{60}Cu is another PET isotope that has a half-life of 0.395 hour. The image quality with ^{64}Cu-ATSM was much better than ^{60}Cu-ATSM (Fig. 19), probably attributable to the fact that the positron range of ^{60}Cu is approximately five times greater than ^{64}Cu. Nevertheless, both ^{60}Cu-ATSM and ^{64}Cu-ATSM clearly visualized the tumors and tumor-to-muscle ratios for both tracers were similar and both tracers had prominent accumulation in the hypoxic tissues (Lewis et al., 2008).

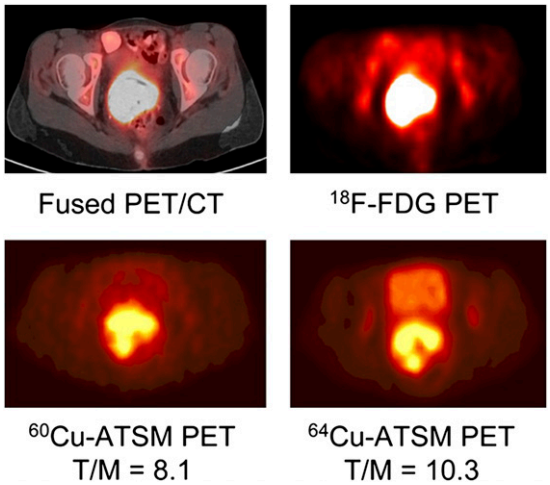

Fig. 19. Transaxial images of pelvis of a cervical cancer patient injected with [^{18}F]FDG (top right), fused image PET/CT (top left), ^{60}Cu-ATSM (bottom left) and ^{64}Cu-ATSM (bottom right). [Adapted from Lewis JS, Laforest R, Dehdashti F, Grigsby PW, Welch MJ, and Siegel BA (2008) An imaging comparison of ^{64}Cu-ATSM and ^{60}Cu-ATSM in cancer of the uterine cervix. *J Nucl Med* **49:**1177–1182. Used with permission.]

^{64}Cu-ATSM was also evaluated in tumor xenograft models (Hansen et al., 2012; McCall et al., 2012; Yuan et al., 2006). Overall, ^{64}Cu-ATSM appears to be good choice for hypoxia imaging in terms of 1) ease of synthesis (compared with ^{18}F labeling, which is more complicated) and 2) fast clearance rate from normoxic tissue allowing a short interval between injection and imaging. However, retention of ^{64}Cu-ATSM in well-perfused areas was also found, indicating that tissue uptake is not related only to hypoxia (Yuan et al., 2006).

2. Vascular Endothelial Growth Factor/Vascular Endothelial Growth Factor Receptor Imaging. The VEGF gene family in mammals consists of five VEGF glycoproteins (VEGF-A, -B, -C, -D, and -E) and placental growth factor (Ichihara et al., 2011; Sakurai and Kudo, 2011). The five growth factors bind to three RTKs, denoted as VEGFR-1, -2, and -3. VEGF-A is considered a key angiogenic factor and has been the most characterized one among the VEGF family. Although it has one order of magnitude higher affinity to VEGFR-1 than to VEGFR-2, VEGFR-A signaling is mainly interceded by VEGFR-2, probably because of its higher kinase activity than that of VEGFR-1. Under hypoxic conditions, the expression levels of VEGF-A and its receptors VEGFR-1 and -2 are dramatically upregulated (Olsson et al., 2006). Several PET imaging tracers, including small molecules, proteins, and antibodies have been developed and evaluated for their ability to measure VEGF/VEGFR expression in tumors.

In several preclinical studies, bevacizumab, a monoclonal antibody that inhibits VEGF-A, was conjugated to different chelators and was labeled with different PET isotopes such as ^{64}Cu, ^{86}Y, and ^{89}Zr (Nagengast et al., 2010; Nayak et al., 2011; Paudyal et al., 2011). Labeled bevacizumab had accumulation in VEGF-positive tumors corroborating with VEGF levels. Nagengast et al. (2010) reported on the usage of ^{89}Zr-bevacizumab as a PET imaging biomarker for the detection of early antiangiogenic therapeutic effect of the Hsp90 inhibitor NVPAUY922 [5-(2,4-dihydroxy-5-isopropyl-phenyl)-*N*-ethyl-4-[4-(morpholinomethyl)phenyl]isoxazole-3-carboxamide] in two ovarian carcinoma xenograft models derived from A2780 and CP70 cell lines. Tumor-bearing mice were injected intraperitoneally with NVPAUY922 (50 mg/kg) twice a week for 2 weeks. ^{89}Zr-bevacizumab allowed in vivo visualization and quantification of early antiangiogenic response to treatment with Hsp90 inhibition (Fig. 20) (Nagengast et al., 2010). Several clinical trials using ^{89}Zr-bevacizumab are currently ongoing in patients with various cancer types.

Wang et al. (2007a) described the ^{64}Cu-labeling and evaluation of two VEGFR-2 ligands: wild-type $VEGF_{121}$ and its mutant $VEGF_{DEE}$. $VEGF_{121}$ is the shortest VEGF-A isoform that exists in nature. The VEGFR-2 ligands were with ^{64}Cu using DOTA chelator

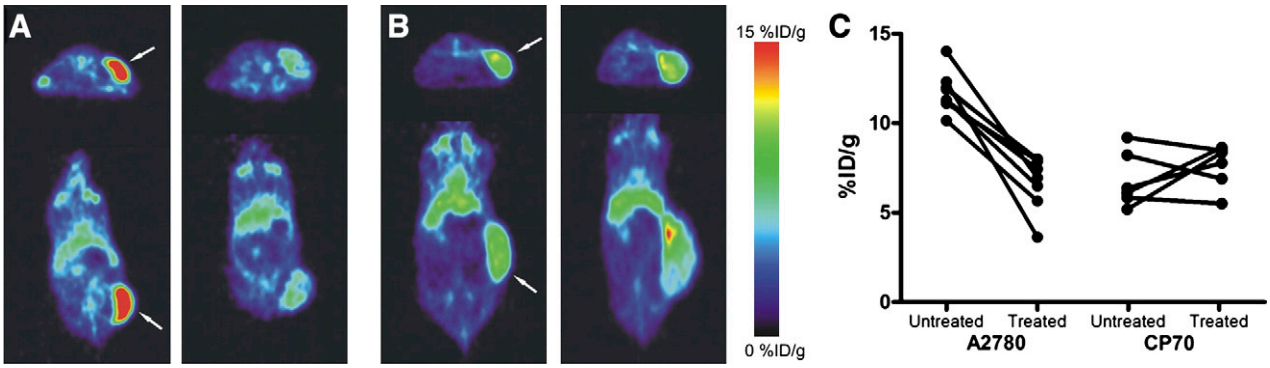

Fig. 20. Representative transaxial and coronal micro-PET images of ^{89}Zr-bevacizumab 6 days postinjection before treatment of A2780 (A) and CP70 (B) xenografts (left) and after NVP-AUY922 treatment (right). Tumors are indicated by arrows. (C) Micro-PET quantification of A2780 and CP70 xenografts before and after NVP-AUY922 treatment. [Adapted from Nagengast WB, de Korte MA, Oude Munnink TH, Timmer-Bosscha H, den Dunnen WF, Hollema H, de Jong JR, Jensen MR, Quadt C, Garcia-Echeverria C, van Dongen GA, Lub-de Hooge MN, Schröder CP, and de Vries EG (2010) ^{89}Zr-bevacizumab PET of early antiangiogenic tumor response to treatment with HSP90 inhibitor NVP-AUY922. *J Nucl Med* **51:**761–767. Used with permission.]

and compared in mice bearing VRGFR-2-positive murine breast tumor (Wang et al., 2007a). $VEGF_{DEE}$ had 20-fold lower binding affinity to VEGFR-1 and slightly lower affinities to VEGFR-2 than $VEGF_{121}$. Both ^{64}Cu-DOTA-$VEGF_{121}$ and ^{64}Cu-DOTA-$VEGF_{DEE}$ had rapid and specific uptake in VEGFR-2-expressing tumors (3 ± 0.4 and 4.6 ± 1.4%ID/g at 1 hour postinjection, respectively). They also had high uptake in the liver (>10%ID/g at all the time points examined). It is interesting that renal uptake of ^{64}Cu-DOTA-$VEGF_{DEE}$ was significantly lower than that of ^{64}Cu-DOTA-$VEGF_{121}$ because kidneys express high levels of VEGFR-1 (Wang et al., 2007a). The researchers concluded that ^{64}Cu-DOTA-$VEGF_{DEE}$ is a better candidate for VEGFR-2 and angiogenesis imaging in the clinic because of the high renal uptake of ^{64}Cu-DOTA-$VEGF_{121}$.

Recently, the same group described the site-specific labeling of single-chain scVEGF protein containing an N-terminal Cys-tag with [^{18}F]FBEM, without affecting its binding affinity. [^{18}F]FBEM-scVEGF was evaluated in several xenograft models (Wang et al., 2012). [^{18}F]FBEM-scVEGF had relatively low uptake in VEGFR-2-positive tumors (1.38 ± 0.38%ID/g at 2 hours postinjection; Fig. 21) compared with other labeled VEGF derivatives. Nevertheless, its tumor-to-background ratio increased over time (1.06 ± 0.14 at 0.5 hour to 1.74 ± 0.29 at 2.0 hours postinjection). [^{18}F]FBEM-Sc-VEGF also had uptake in the gallbladder, which was explained by its instability in vivo. The researchers suggested that the hydrophobic group in the tracer was chopped off and accumulated in the gallbladder (Wang et al., 2012).

3. Metalloproteinase Imaging. Human matrix metalloproteinases (MMP) family consists of at least 23 distinct structurally related, zinc-dependent endopeptidases. Normally, MMPs are expressed only when and where they are needed for tissue remodeling that accompanies various processes. However, MMPs were found to play crucial roles in tumor invasion and metastasis. They regulate signaling pathways that control cell growth, survival, invasion, inflammation, and angiogenesis, hence providing a favorable microenvironment for the tumor (Rundhaug, 2003; Sakurai and Kudo, 2011; Bauvois, 2012). MMPs selectively degrade various components of the extracellular matrix (ECM). In that process, proangiogenic growth factors and cytokines that reside in the ECM are released. Moreover, for some growth factors and cytokines secreted as an inactive form, such as pro-IL-1b, cleavage by MMPs renders them active (Rundhaug, 2003; Sakurai and Kudo, 2011; Bauvois, 2012). Upregulation of MMPs (e.g., MMP-2 and MMP-9) in several human cancers was found to be correlated with invasiveness, metastasis, and poor prognosis (Coussens et al., 2002; Egeblad and Werb, 2002; Turpeenniemi-Hujanen, 2005; Yu and Han, 2006; Hua et al., 2011).

Ujula et al. (2010) reported on the evaluation of MMP-9 ligand, tumor cell targeting peptide (TCTP-1), and its two derivatives, lactam-TCTP-1 and linear-TCTP-1. The peptides were conjugated to DOTA, labeled with ^{68}Ga, and injected into a rat melanoma model. Among the three peptides, ^{68}Ga-DOTA-TCTP-1 had the highest uptake in MMP-9-positive tumors with 0.2%ID/g. ^{68}Ga-DOTA-lactam-TCTP-1 also visualized the tumors and had a better clearance profile from the tumor than ^{68}Ga-DOTA-TCTP-1. ^{68}Ga-DOTA-linear-TCTP-1 distribution was less favorable, with high uptake in the liver and heart. All three peptides had high uptake in the kidneys and urinary bladder. ^{68}Ga-DOTA-TCTP-1 and ^{68}Ga-DOTA-lactam-TCTP-1 also exhibited uptake in the liver and heart, but less intense than ^{68}Ga-DOTA-linear-TCTP-1 (Ujula et al., 2010). MMP-9 expression in the tumors was verified by immunohistochemistry and zymography measurements (Ujula et al., 2010). However, no in vivo specificity of these peptides was examined.

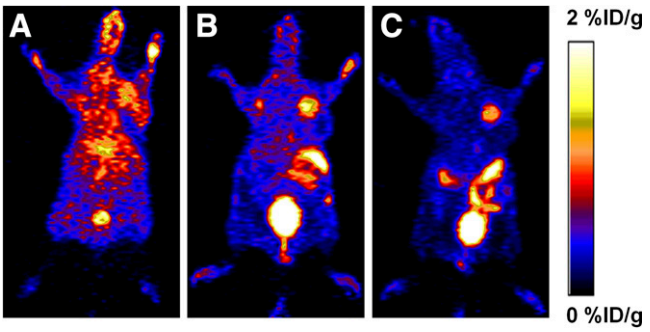

Fig. 21. Micro-PET images of MDA-MB-435 tumor-bearing mice at 0.5 (A), 1 (B), and 2 hours (C) postinjection of [^{18}F]FBEM-sc-VEGF. [Adapted from Wang H, Gao H, Guo N, Niu G, Ma Y, Kiesewetter DO, and Chen X (2012) Site-specific labeling of scVEGF with fluorine-18 for positron emission tomography imaging. *Theranostics* **2**:607–617. Used with permission.]

Other tracers, small molecules, or peptides against MMPs have been developed. Some of them were labeled with PET isotopes for their biodistribution evaluation and for detection of MMP-expressing tumors. However, most of them have low uptake in the tumor and very high uptake in the liver, gatrointestinal tract, kidneys, and lungs (Furumoto et al., 2003; Zheng et al., 2003, 2004; Sprague et al., 2006; auf dem Keller et al., 2010; Ujula et al., 2010). Improved and specific tracers need to be developed and evaluated.

Unlike nuclear medicine imaging, optical imaging with activatable probes might prove to be a better approach for MMP imaging, because these probes will also give information on the activity of the MMPs (Yhee et al., 2012). Such research was reported, for example, by Zhu et al. (2011), who conjugated a substrate of MMP-14 to a near-infrared fluorochrome and to a quencher, and once the probe is cleaved, the fluorochrome can be visualized.

4. Imaging of Integrin $\alpha_v\beta_3$. One promising approach of angiogenesis imaging is the detection of integrin $\alpha_v\beta_3$. Integrins are a family of heterodimeric transmembrane glycoproteins that play an essential role in the regulation of cellular adhesion, migration, proliferation, survival, signal transduction, and differentiation (Chen et al., 2004a,b). One member of this receptor class is the dimeric transmembrane integrin, $\alpha_v\beta_3$, which is expressed at low levels on epithelial cells and mature endothelial cells. Upon activation of endothelial cells, $\alpha_v\beta_3$ is upregulated on the cell membrane. In addition, several tumors including osteosarcomas, neuroblastomas, glioblastomas, melanomas, lung carcinomas, and breast cancers were shown to express this integrin (Felding-Habermann et al., 1992; Bello et al., 2001; Robinson et al., 2004; Zhang et al., 2006). Hence, integrin $\alpha_v\beta_3$ can be targeted for imaging tumor growth, invasion, and metastasis and for the treatment of the rapidly growing and metastatic tumors (Chen, 2006; Liu, 2006; Cai et al., 2008a). Integrin $\alpha_v\beta_3$ interacts with extracellular matrix proteins (e.g., vitronectin, tenascin, fibronectin, and collagen) through their exposed arginine–glycine–aspartic (RGD) amino acid moieties and regulates the migration of endothelial cells through the extracellular matrix during vessel formation (Brooks et al., 1994a,b; Bogler and Mikkelsen, 2003; Hwang and Varner, 2004). For radionuclide imaging of integrin $\alpha_v\beta_3$ expression in vivo, tumor-targeting efficiency and in vivo kinetic profiles are highly related to the receptor-binding affinity and specificity, hydrophilicity, molecular size, and overall molecular charge of the resulting radiotracers (Zhang et al., 2006).

It has been shown that cyclization of RGD peptides via linkers, such as S-S disulfide, thioether, and rigid aromatic rings, often leads to increased receptor binding affinity and selectivity. A number of cyclic RGD peptides have been investigated as PET imaging tracers for monitoring integrin $\alpha_v\beta_3$ expression level in tumors in both clinical and preclinical studies. In addition, dimeric RGD peptides possess better tumor uptake and tumor-to-background contrast than the monomeric analogs. This may be explained by the bivalent binding of the dimer to integrins on the cell surface, which significantly reduces the dissociation of the tracer from its target (Shi et al., 2009). Moreover, addition of PEG groups to the dimeric RGD improves the imaging figure of merit, probably attributable to the longer spacer connecting the two RGD moieties that confers less limitation on the distance between integrins on the cell surface (Shi et al., 2009).

To avoid the hepatobiliary excretion of the labeled RGD peptides, which leads to high nonspecific uptake in the liver and gastrointestinal tract along with low image quality, chemical modifications can be done, such as pegylation, glycosylation, and introduction of more hydrophilic amino acid (for example, substitution of phenylalanine with tyrosine). These modifications lead to renal excretion of the labeled RGD peptides and fast clearance from nonspecific tissue (Gaertner et al., 2012).

One of the most studied RGD-derived PET tracers in human patients is [^{18}F]galacto-RGD (Beer et al., 2005, 2007, 2011; Haubner et al., 2005; Schnell et al., 2009). [^{18}F]Galacto-RGD is based on the monomeric cyclic peptide c(RGDfk) containing a sugar moiety. It has high binding affinity, selectivity, and specificity to $\alpha_v\beta_3$. [^{18}F]Galacto-RGD was tested in a large number of patients and was successful in detecting $\alpha_v\beta_3$ expressing tumors (SUV_{mean} in tumors ranged from 1.2 to 9.0) and had high tumor-to-background contrast (Fig. 22). The tumor expression levels of $\alpha_v\beta_3$ were also confirmed by immunohistochemistry and were in correlation with [^{18}F]galacto-RGD uptake. [^{18}F]Galacto-RGD had rapid clearance from the blood and some uptake in the liver and spleen (Beer et al., 2005, 2007; Haubner et al., 2005; Schnell et al., 2009). The main drawback of this tracer is its complex radiosynthesis,

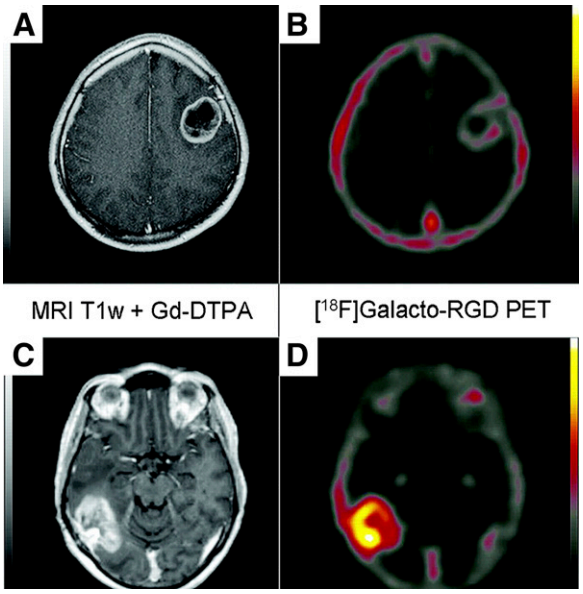

Fig. 22. MRI (A and C) and PET (B and D) images of two patients with glioblastoma. [^{18}F]Galacto-RGD uptake in the upper image (B) shows low accumulation of the tracer in the tumor region (SUV_{max} of 1.2), whereas its uptake is increased in the case of the second patient (D) with a SUV_{max} of 2.8. [Adapted from Schnell O, Krebs B, Carlsen J, Miederer I, Goetz C, Goldbrunner RH, Wester HJ, Haubner R, Popperl G, Holtmannspotter M, Kretzschmar HA, Kessler H, Tonn JC, Schwaiger M, and Beer AJ (2009) Imaging of integrin alpha(v)beta(3) expression in patients with malignant glioma by [^{18}F]Galacto-RGD positron emission tomography. *Neuro-Oncology* **11:**861–870. Used with permission.]

which involves multiple synthetic steps that would complicate routine production. In addition, reducing the liver uptake of these RGD-based imaging agents would be beneficial for imaging tumor or metastases in this organ.

Another c(RGDfk) monomer derivative that was evaluated as a PET tracer for $\alpha_v\beta_3$ expression is [^{18}F]RGD-K5. This derivative contains a highly polar 1,2,3-antitriazole moiety that increases the tracer's excretion via the kidneys into the bladder, thus circumventing unwanted liver uptake (Doss et al., 2012). [^{18}F]RGD-K5 was found to be stable in human blood and cleared rapidly from the blood pool. High uptake of [^{18}F]RGD-K5 was observed in the kidneys, bladder, liver, intestine, and gallbladder in healthy volunteers, indicating that the peptide modification did not achieve its goal (Doss et al., 2012). [^{18}F]RGD-K5 was further evaluated in 12 patients with primary or metastatic breast cancer. All patients underwent scans with both [^{18}F]RGD-K5 and [^{18}F]FDG (Ho Jin Cho et al., 2009). A total of 157 lesions were identified in 10 patients, and among them, 122 lesions had increased uptake of [^{18}F]RGD-K5. [^{18}F]FDG uptake was higher in most of the lesions, and no correlation was found between [^{18}F]RGD-K5 and [^{18}F]FDG uptake. Unfortunately, there was also no correlation between [^{18}F]RGD-K5 uptake in the tumors and the density of microvessels (Ho Jin Cho et al., 2009). This may be explained by the lack of specificity to $\alpha_v\beta_3$ and the binding to other subtypes of integrin that are expressed in breast cancer cells.

Another PET tracer targeting $\alpha_v\beta_3$ that is under clinical evaluation is [^{18}F]fluciclatide. [^{18}F]Fluciclatide is composed of cyclic RGD with multiple disulfide bridges and a polyethylene glycol spacer to stabilize the molecule in vivo with minimal disruption of the RGD pharmacophore (Kenny et al., 2008). Cell studies showed that [^{18}F]fluciclatide was not selective to $\alpha_v\beta_3$ and had 100-fold higher affinity to integrin $\alpha_v\beta_5$. Nevertheless, [^{18}F]fluciclatide biodistribution was assessed in seven human patients with 18 tumor lesions of metastatic breast cancer by PET (Kenny et al., 2008). [^{18}F]Fluciclatide accumulated in all tumors and exhibited two forms of intratumor distribution: homogeneous or only at the tumor rim. Peripheral accumulation could be caused by the necrotic area in the center of the tumor, an issue that should be empirically tested (Kenny et al., 2008). Increased uptake compared with background was demonstrated in metastases in lung, pleura, bone, lymph node, and primary tumor (Fig. 23) (Kenny et al., 2008). It also had uptake in the liver; therefore, liver metastases cannot be distinguished from liver tissue uptake.

Another specific RGD peptide that is under clinical evaluation is [^{18}F]FPPRGD$_2$ (Mittra et al., 2011). [^{18}F]FPPRGD$_2$ is the dimeric peptide PEG$_3$-E[c(RGDyk)]$_2$ coupled with 2-^{18}F-fluoropropionate (Chin et al., 2012). [^{18}F]FPPRGD$_2$ was injected in healthy volunteers to

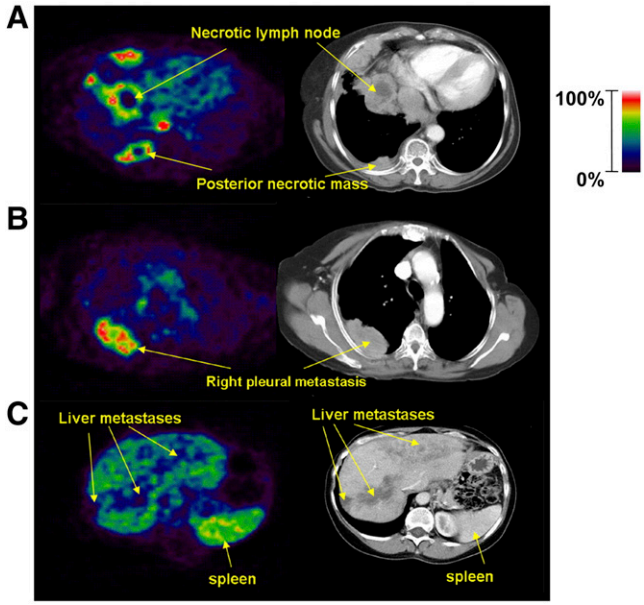

Fig. 23. [^{18}F]Fluciclatide PET/CT images of a patient with lung and pleural metastases showing increased signal in the periphery of lesions. [Adapted from Kenny LM, Coombes RC, Oulie I, Contractor KB, Miller M, Spinks TJ, McParland B, Cohen PS, Hui AM, Palmieri C, Osman S, Glaser M, Turton D, Al-Nahhas A, and Aboagye EO (2008) Phase I trial of the positron-emitting Arg-Gly-Asp (RGD) peptide radioligand ^{18}F-AH111585 in breast cancer patients. *J Nucl Med* **49:**879–886. Used with permission.]

evaluate its biodistribution and the radiation dose (Mittra et al., 2011). [^{18}F]FPPRGD$_2$ had primary uptake in the kidneys, bladder, liver, and gastrointestinal tract and was cleared rapidly through renal and hepatobiliary pathways. [^{18}F]FPPRGD$_2$ seems to have desirable pharmacokinetic properties for a PET tracer and should be further evaluated in cancer patients for tumor staging and evaluating response to antiangiogenesis agents (Mittra et al., 2011). Similar to [^{18}F] galacto-RGD, the radiosynthesis of [^{18}F]FPPRGD$_2$ includes several radioactive steps and results in low yields, which might be an issue for large-scale imaging studies and clinical usage (Chin et al., 2012).

Another promising RGD dimer derivative that was evaluated recently in lung cancer patients is [^{18}F]AlF-NOTA-PRGD$_2$ ([^{18}F]alfatide), which was shown to behave similarly to [^{18}F]FPPRGD$_2$ but allow for straightforward labeling using a kit formulation avoiding HPLC purification (Wan et al., 2013).

A thorough study in the evaluation of angiogenesis therapy by PET was done in mice bearing orthotopic breast tumors (Yang et al., 2011a). In this research they applied several PET tracers to monitor glucose metabolism ([^{18}F]FDG), cellular proliferation ([^{18}F]FLT), tumor hypoxia ([^{18}F]FMISO), and angiogenesis (RGD peptide, [^{18}F]FPPRGD$_2$) during VEGF$_{121}$/rGel therapy of breast cancer (Yang et al., 2011a). Tumor-bearing mice were divided into two groups: a control group and a treated group that received two doses of VEGF$_{121}$/rGel (12 mg/kg i.p.). Treatment resulted in an initial delay of tumor growth and a significant difference in tumor volume was observed at day 7 between the treated and the control groups (Yang et al., 2011a). [^{18}F]FDG uptake did not show significant change after VEGF$_{121}$/rGel treatment. On the other hand, the antiproliferation effect of VEGF$_{121}$/rGel was further demonstrated by decreased [^{18}F]FLT uptake, especially at day 3 after the treatment, suggesting the potential for [^{18}F]FLT to monitor tumor response to cancer therapy. [^{18}F]FMISO uptake was increased by VEGF$_{121}$/rGel treatment at both days 1 and 3 after treatment, indicating that the drug induced tumor hypoxia. Uptake of [^{18}F]FPPRGD$_2$ in the VEGF$_{121}$/rGel-treated mice was decreased at days 1 and 3 after treatment and then resumed to the baseline level at days 7 and 14. Fluorescence immunostaining against murine integrin β3 revealed significant intensity decrease at day 1 and day 3 after VEGF$_{121}$/rGel treatment, which was consistent with [^{18}F]FPPRGD$_2$ uptake. Immunostaining against human integrin $\alpha_v\beta_3$ found no apparent change of integrin expression level in the tumor cells.

The researchers hypothesized that the change of [^{18}F]FPPRGD2 uptake reflects the change of tumor vascular integrin level upon VEGF$_{121}$/rGel treatment rather than tumor cell integrin expression. Moreover, changes of [^{18}F]FMISO and [^{18}F]FPPRGD2 tumor uptake were not correlated, indicating that the tumor uptake of [^{18}F]FPPRGD2 might be affected at least partially by decreased tumor blood supply and hypoxia (Yang et al., 2011a). This research demonstrates the feasibility of using several PET imaging tracers to monitor early tumor responses. This kind of study should accelerate anticancer drug development and promote the clinical translation of molecular imaging.

5. CD105 (Endoglin) Imaging. TGF-β, under some circumstances, requires accessory receptors to modulate its signaling pathway. One such accessory receptor is the endoglin (CD105) that can interact with both type I and type II TGF-β receptors. The critical role of CD105 in healthy formation of blood vessel endothelium is evident from hereditary hemorrhagic telangiectasia, a disease characterized by vascular malformations and is caused by loss-of-function mutations in the human CD105 gene ENG.

In several cancers, CD105 was shown to be upregulated on vascular endothelium of tumors and is involved in cell proliferation, migration, and capillary tube formation and plays a proangiogenic role, although it is expressed at low levels on resting cells (Li et al., 1999; Perez-Gomez et al., 2010). These findings suggested that CD105 might serve as a marker for tumor-related angiogenesis and microvessel density (MVD). MVD assessment contributes to disease prognosis of cancer patients, and high MVD is usually a bad prognosis. Immunohistochemistry staining of antibodies against CD105 is currently being used for MVD measurements (Zhang et al., 2013b).

It is important to note that targeting CD105 for imaging had two potential disadvantages: 1) it is downregulated in some cancers, such as esophageal squamous cell carcinomas, and 2) the extracellular fraction of CD105 can be cleaved, creating a soluble form of CD105 that can limit the application of CD105 as an imaging agent (Perez-Gomez et al., 2010).

No clinical trials were done with PET imaging of CD105 thus far, but an anti-CD105 antibody was investigated as a therapy. TRC105 is a chimeric IgG1 monoclonal antibody that binds CD105 and is being evaluated in patients with advanced refractory solid tumors (Rosen et al., 2012).

TRC105 was labeled with ^{64}Cu and ^{89}Zr and tested in several subcutaneous tumor models (Zhang et al., 2011c, 2012). In addition, an engineered fragment of the antibody, TRC105-Fab was labeled with ^{64}Cu and ^{61}Cu (Zhang et al., 2013b). ^{64}Cu/^{61}Cu-TRC105-F(ab′)$_2$ was compared with the labeled parent antibody in murine breast cancer model (Zhang et al., 2013b). ^{64}Cu/^{61}Cu-TRC105-F(ab′)$_2$ gave higher tumor-to-blood ratios at early time points (up to 24 hours) in comparison to TRC105, as expected. ^{64}Cu/^{61}Cu-TRC105-F(ab′)$_2$, however, had a significantly lower uptake than the full antibody at the 48-hour time point (Zhang et al., 2013b).

6. Mesenchymal-Epithelial Transition Factor Imaging. c-MET is a transmembrane tyrosine kinase receptor that, with its ligand hepatocyte growth factor (HGF), were implicated in multiple cancer processes, including invasion, angiogenesis, and metastasis in a wide variety of neoplastic cells (Martinez-Rumayor et al., 2004). Overexpression of c-MET can be induced by, but not limited to, gene amplification. In some cancers such as breast, ovarian, cervical, gastric, head and neck, and non-small-cell lung cancers, high levels of HGF and/or c-MET were found to be correlated with poor prognosis. Overexpression of c-MET protein confers resistance to EGFR inhibitors, both in preclinical models and in patients (Blumenschein et al., 2012).

c-MET RTK subfamily is structurally distinct from most RTK subfamilies. c-MET is initially expressed as a precursor that undergoes proteolytic cleavage to form the heterodimeric c-MET receptor. Upon ligand binding, the receptor undergoes phosphorylation of the intracellular domain and initiates downstream signaling, mainly through PI3K/Akt, MAPK, and signal transducers and activators of transcription pathways (Bhardwaj et al., 2013).

c-MET was identified as a potential target for cancer treatment, and numerous inhibitors of the HGF/c-Met axis are currently available. These agents include both small-molecule inhibitors and monoclonal antibodies and are being tested in a variety of solid tumors (Bhardwaj et al., 2013).

Onartuzumab (MetMAb; Genentech, South San Francisco, CA) is a c-Met inhibitor in the form of humanized 1-armed monoclonal antibody possessing nanomolar affinity for Met, shown to have anti-tumor growth effects in mouse models by inhibiting proliferation and angiogenesis and inducing apoptosis (Jin et al., 2008). A study in non-small cell lung cancer patients whose tumor was positive for c-Met showed that onartuzumab can prolong survival (Surati et al., 2011). Jagoda et al. (2012) labeled onartuzumab with ^{76}Br and ^{89}Zr and evaluated the ability to image c-Met-expressing tumors in mouse xenografts models. There was significant correlation between ^{89}Zr-onartuzumab or ^{76}Br-onartuzumab tumor uptake and tumor c-Met expression levels. In addition, higher tumor uptake was achieved using ^{89}Zr-onartuzumab than ^{76}Br-onartuzumab at later time points and had higher tumor-to-muscle ratios, suggesting that ^{89}Zr-onartuzumab would be better suited to image c-Met for diagnostic and prognostic purposes (Jagoda et al., 2012).

Another anti-c-Met monoclonal antibody, DN30, was labeled with ^{89}Zr and tested in mouse xenografts in vivo (Perk et al., 2008). The researchers used two human cell lines expressing different levels of c-MET, the gastric cancer line GLT-16 with high expression and the head and neck cancer line FaDu with low expression (Perk et al., 2008). ^{89}Zr-DN30 uptake in GTL-16 tumors was significantly higher than that in FaDu tumors (18.1 ± 4.5 and 7.8 ± 1.2%ID/g, respectively, at 72 hours postinjection).

An interesting assessment of HGF expression level in mice bearing glioblastoma xenografts was recently done with anti-HGF ^{89}Zr-nanobodies (Vosjan et al., 2012). ^{89}Zr-nanobodies visualized the tumors with 7.2–8.9%ID/g and had very high uptake in the kidneys. These nanobodies were also shown to be efficient theranostic substances. Treatment with these nanobodies reduced tumor growth and at a high dose eliminated the tumor in some of the mice.

The important role of c-MET in the tumor microenvironment encouraged more imaging studies aiming at the receptor using SPECT isotopes and bioluminescence (Zhao et al., 2007; Kim et al., 2009, 2010, 2011; Zhang et al., 2011a).

Imaging of tumor microenvironment is complex. Some of the processes and targets involved in the cross-talk between tumor and its environment were described here; however, the research in this field has not reached its full potential and should be further pursued. Of the tracers described above, there are clinical trials evaluating imaging of hypoxia using [^{18}F]FMISO, ^{64}Cu-ATSM, [^{18}F]HX4, and [^{18}F]FAZA and imaging using RGD peptide derivatives labeled with ^{68}Ga and ^{18}F. In addition, imaging of VEGF levels before and after treatment using ^{89}Zr-bevacizumab is ongoing.

G. Cancer Metastasis Imaging

Tumor metastasis is responsible for approximately 90% of all cancer-related deaths (Spano et al., 2012). The formation of cancer metastasis is a series of cell functions that must be gained by the cancer cells to the point where they seed at a secondary site. This cascade of events includes the following: 1) "escape" and detachment of tumor cells from the primary tumor, 2) invasion of basement membrane and ECM that surround the tumor, 3) invasion of the basement membrane supporting the endothelium and intravasation of local blood and/or lymphatic vessels, 4) adhesion to the endothelium of blood and/or lymphatic vessels of the target organ site, 5) extravasation through the endothelial cell layer and the surrounding base membrane of target organ, and finally, 6) growth within the target organ site (Spano et al., 2012; Spano and Zollo, 2012). This complex mechanism of metastasis includes multiple molecules such as MMPs, integrins, and chemokines. Some of the processes discussed above are closely connected to the metastatic process as well, and the imaging agents that were mentioned in those sections can also be used for imaging metastatic lesions. In this section we will elaborate on metastatic imaging agents that were not discussed earlier.

1. Imaging of Integrin $\alpha_4\beta_1$/Very Late Antigen-4. Integrin expression levels and cellular regulation change during tumor development (Felding-Habermann, 2003).

$\alpha_4\beta_1$ integrin, also called very late antigen-4 (VLA-4), is expressed by both blood cancers and solid tumors. Its expression can facilitate circulating tumor cells to adhere to vasculature endothelium and extravasate, thereby supporting dissemination in distal organs (Peng et al., 2006). $\alpha4\beta1$ was also suggested to play a role in preparation of the potential metastatic niche; tumor-supporting cells derived from the bone marrow express VEGFR-1 and $\alpha4\beta1$ and have been shown to form a receptive environment for tumor cells (Peng et al., 2006). Shokeen et al. (2012) reported on a potentially new application of the PET radiotracer ^{64}Cu-CBTE2A-LLP2A, which was developed primarily for imaging VLA-4-expressing tumors and VLA-4-expressing bone marrow-derived cells in premetastatic niche sites of bone metastasis in mice. LLP2A is a small peptide-based high-affinity and high-specificity peptidomimetic against $\alpha4\beta1$ integrin (Peng et al., 2006). ^{64}Cu-CBTE2A-LLP2A had higher cellular uptake in VLA-4-positive cells than VLA-4-negative cells. Thereafter, the tracer was evaluated in vivo in two of the following mouse models: 1) subcutaneous model—VLA-4-positive murine melanoma cells were subcutaneously injected into mice and 2) metastasis model — VLA-4-negative human breast carcinoma were injected intra-arterially into mice. To verify that ^{64}Cu-CBTE2A-LLP2A uptake is due to the binding to VLA-4 positive bone marrow-derived cells and not VLA-4-negative tumor cells, the negative cells were transfected with luciferase. Metastases were monitored by both BLI and micro-PET/CT. ^{64}Cu-CBTE2A-LLP2A showed accumulation in subcutaneous VLA-4-positive tumors but also high uptake in other VLA-4-expressing organs such as bone marrow and spleen (11.26 $\pm$ 2.59 and 8.36 $\pm$ 2.15%ID/g, respectively, at a 2-hour time point) (Shokeen et al., 2012).

In the metastatic model that uses VLA-4 negative tumor cells, BLI showed metastatic lesions in the leg bones. ^{64}Cu-CBTE2A-LLP2A had higher accumulation in the region of metastasis than the surrounding leg, suggesting recruitment of VLA-4 positive bone marrow-derived cells to metastatic sites (Shokeen et al., 2012). However, the actual numerical difference between the metastasis and surrounding leg was rather small, which would be very hard to detect in a clinical setting. Moreover, the researchers suggest that this agent might be suitable for imaging potential metastatic niches, but they only showed data in regions where metastatic lesions already existed. Accumulation of radioactivity increases over time in the metastasis, suggesting that recruitment of VLA-4-positive cells occur but can be detected only at least 10 days after cell injection. Nonetheless, imaging the formation of premetastatic niches might be very useful to help physicians make a more informed decision regarding appropriate therapy and should be further investigated.

*2. Imaging of Transforming Growth Factor-*β. TGF-β promotes cancer angiogenesis, migration, invasiveness, immune suppression, and metastasis and is therefore a target for the development of many anticancer drugs. Imaging TGF-β level in the tumor will have clinical impact for guiding and monitoring specific treatment (Oude Munnink et al., 2011). Fresolimumab is a human antibody that was tested for its ability to neutralize all mammalian active isoforms of TGF-β (Oude Munnink et al., 2011). Fresolimumab was conjugated to *N*-succinyldesferrioxamine-B-tetrafluorphenol chelator for ^{89}Zr labeling. The ability of ^{89}Zr-fresolimumab to evaluate TGF-β levels was tested using Chinese hamster ovary cells expressing intermediate and high levels of transfected human TGF-β1 in mouse xenograft models (Oude Munnink et al., 2011). ^{89}Zr-fresolimumab had clear uptake at 3 and 6 days postinjection by tumors expressing different levels of TGF-β1. There was no significant difference in the uptake between the two models (~6 %ID/g at 6 days postinjection) (Oude Munnink et al., 2011). Similar tumor uptake was found when nonspecific antibody was used, implicating that ^{89}Zr-Fresolimumab accumulation in the tumors was not specific (Oude Munnink et al., 2011). TGF-β1 does seem to be a very interesting target for imaging, but more specific tracers need to be developed.

3. Imaging of Chemokine Receptor CXCR4. CXCR4 is a member of the chemokine receptor subfamily of seven-transmembrane domain GPCR whose sole known natural ligand is CXCL12/stromal cell derived factor-1. CXCR4 is an unusual chemokine receptor having roles beyond leukocyte recruitment, which include fundamental processes such as the development of the hematopoietic, cardiovascular, and nervous systems during embryogenesis (Burger and Peled, 2009). CXCR4 was also found to be expressed by cancers originated from breast, prostate, lung, colon, and multiple myeloma. CXCR4 expression can be induced by a number of transcription factors important in cancer such as HIF-1, nuclear factor-κB, and oncoproteins PAX3-FKHR and RET/PTC (Furusato et al., 2010; Teicher and Fricker, 2010). A number of recent studies correlated high levels of CXCR4 expression in cancers with poor prognosis and with resistance to chemotherapy, in part through enhancing interactions between cancers and bone marrow stroma. A possible role for CXCR4 and chemokine receptors, in general, in cancer and metastasis was first suggested in studies of breast cancer, showing that the receptor plays a role in directing metastatic cells to CXCL12-expressing organs (Muller et al., 2001). More recent work has shown that CXCR4 membrane expression can be used as a prognostic marker for metastatic potential of node-negative breast tumors and patient survival (Blot et al., 2008). Similarly, locally advanced breast cancer patients receiving neoadjuvant

chemotherapy who had high expression of CXCR4, had a significantly higher incidence of recurrence and cancer death compared with patients with tumors expressing low CXCR4 (Holm et al., 2009). Collectively, the data on CXCR4 in cancer suggest that this receptor increases tumor cell survival and/or growth and/or metastasis, making it a potentially attractive therapeutic target (Wald et al., 2013; Weiss and Jacobson, 2013).

Multiple CXCR4 antagonists were developed and are being evaluated and used for stem cell mobilization and as antitumor therapy (Burger and Peled, 2009). Evaluating CXCR4 expression in whole tumors noninvasively will enable personalized treatment with CXCR4 antagonists. 4-F-benzoyl-TN14003 (T140) is a high-affinity CXCR4 peptide antagonist consisting of 14 amino acids, with one disulfide bond between Cys^4 and Cys^{13}, an amidated C terminus, and a 4-fluorobenzoyl group at the N terminus. We have labeled T140 with ^{18}F without changing its chemical structure. We found that it does bind to CXCR4 in tumors (Fig. 24A), but tumor uptake is prevented in vivo because of its binding to red blood cells (RBC) (Jacobson et al., 2010). We were able to overcome this RBC binding by injecting the tracer in low SA (coinjection with 10 μg of unlabeled peptide per mouse). This tracer did not show high uptake in the liver (~3%ID/g), and when injected in low SA, it gave high tumor-to-background ratio (>20). However, the major drawback was its long synthesis time and relatively low radiochemical yield. To shorten the synthesis, we have introduced a DOTA chelator on the lysine residues of the peptide and labeled it with ^{64}Cu (Jacobson et al., 2011) to give ^{64}Cu-T140-2D. ^{64}Cu-T140-2D showed similar binding to RBC as the fluorine-18 labeled T140, and in low SA form could be used for imaging CXCR4-positive tumors (Jacobson et al., 2011). Nevertheless, there was significantly higher activity accumulation in the liver (~20%ID/g).

In an attempt to limit undesired binding of labeled T140 to RBC, we synthesized the peptide with DOTA or NOTA chelators at the N terminus, replacing the fluoro-benzoyl group, and thereafter labeled the tracers with ^{64}Cu. Replacing the fluoro-benzoyl group with either DOTA or NOTA diminished the binding of labeled T140 to RBC, while only slightly reducing the binding to CXCR4 (Fig. 24, B and C) (Jacobson et al., 2012). These two optimized tracers, used in high SA, showed high accumulation in CXCR4-positive tumors (5–6%ID/g) but not in CXCR4-negative tumors and high tumor-to-background ratio, while having short radiosynthesis time, high radiochemical yield, and no nonspecific binding to RBC (Jacobson et al., 2012).

Another CXCR4 antagonist that was labeled for PET imaging by us and others is AMD3100 [1,1′-[1,4-phenylenebis(methylene)]bis [1,4,8,11-tetraazacyclotetradecane], plerixafor]. AMD3100 is a bicyclam that can chelate a metal ion, and it was labeled with ^{64}Cu (Jacobson et al., 2009; Nimmagadda et al., 2010; Weiss et al., 2012). ^{64}Cu-AMD3100 had rapid clearance from the blood (unlike T140) and accumulation in CXCR4 expressing organs such as the bone marrow and spleen (Jacobson et al., 2009). ^{64}Cu-AMD3100 specifically accumulated in CXCR4 expressing tumors (Fig. 24, D and E) (Nimmagadda et al., 2010; Weiss et al., 2012). However, the main drawback of the tracer was high accumulation in the liver (>40%ID/g), which was specific to the parent molecule and masked some of the adjacent organs. This phenomenon is not CXCR4 specific. In another study, a similar small molecule *N*-(4-((1,4,8,11-tetraazacyclotetradecan-1-yl)methyl)benzyl)-1-(pyridin-2-yl)methanamine hexahydrobromide (AMD3465), whose structure contains one cyclam that can chelate copper-64, was also evaluated as a PET tracer for imaging CXCR4 and showed very high accumulation in CXCR4-expressing tumor (~100%ID/g) and lower but significant (40%ID/g) accumulation in the liver (De Silva et al., 2011).

4. Imaging of Urokinase-type Plasminogen Activator Receptor. The urokinase plasminogen activator (uPA) system consists of a proteinase, its receptor (urokinase-type plasminogen activator receptor, uPAR), and plasminogen activator inhibitors, including types 1 and 2 (Atfy et al., 2012; Ma and Tao, 2012). In some cancers, uPA plays a significant role in tumor progression, including angiogenesis, tumor growth, and metastasis. uPAR expressed/overexpressed by tumor cells (Zhang et al., 2013a) binds uPA and initiates a pericellular proteolysis cascade: uPA cleaves plasminogen into active plasmin, which in turn starts a proleolytic degradation of the extracellular matrix (ECM) and activates MMPs and growth factors. This cascade also activates multiple intracellular signaling pathways (Ma and Tao, 2012).

Immunohistochemistry and in situ hybridization studies showed that uPAR is expressed in low levels by normal tissues and is upregulated in cancer lesions. Studies have shown correlation between uPAR expression and poor prognosis in several cancers including breast, colorectal, and gastric cancer. Hence, the development of molecular imaging probes for uPAR might help to identify and treat patients with high uPAR expression (Persson et al., 2012a).

AE105, a uPAR peptide antagonist in the nanomolar range, was labeled with several PET isotopes (^{68}Ga, ^{64}Cu, and ^{18}F) and evaluated in various human xenograft models expressing different levels of uPAR (Persson et al., 2012a,b; Zhang et al., 2013a). These peptide-based tracers had specific accumulation in uPAR-expressing tumor xenografts and were able to differentiate high and low uPAR.

Tumor metastasis is the main reason for cancer-associated death, and imaging of tumor metastasis is crucial for guiding therapy. Some processes and

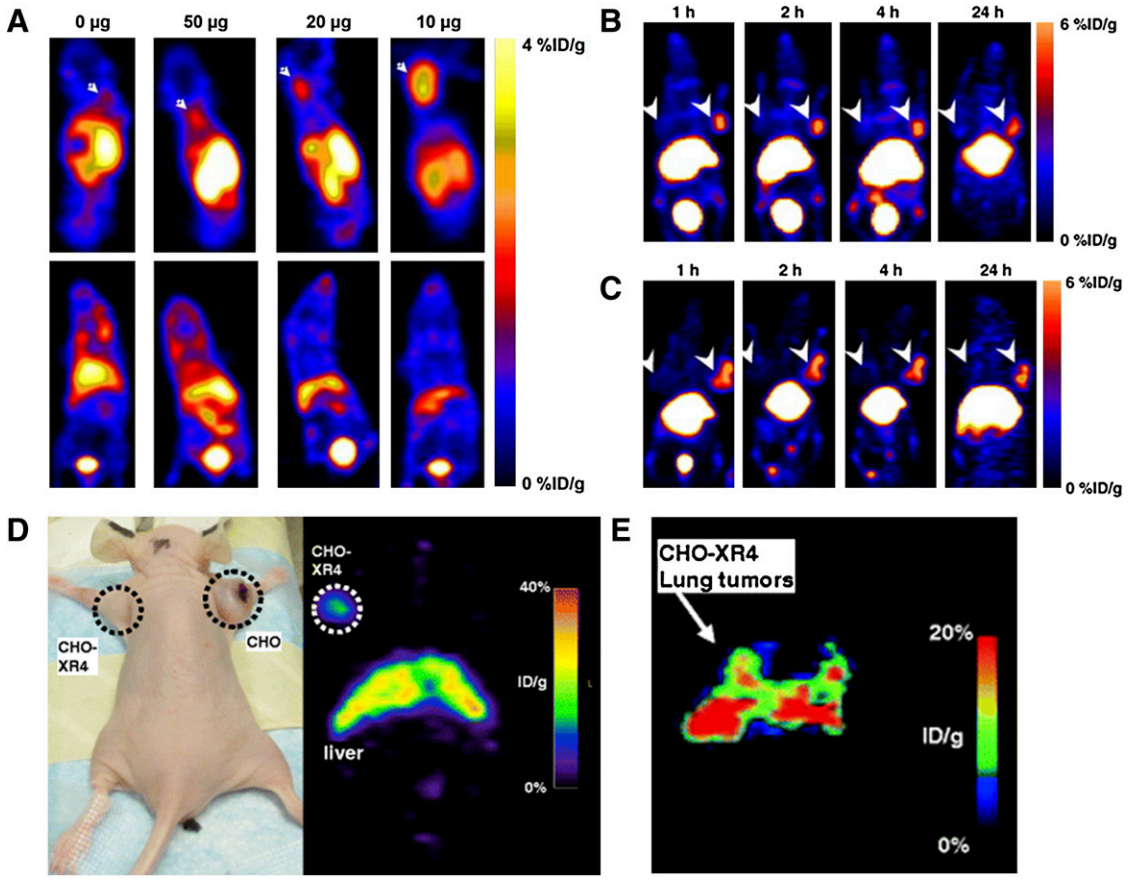

Fig. 24. (A) PET imaging of tumors of CHO cells transfected with CXCR4 (CHO-CXCR4) using CXCR4 peptide antagonist [^{18}F]T140 of different specific activity at 2 hours postinjection Upper row is dorsal slices, with arrows indicating CXCR4-CHO tumor. Lower row is ventral slices. [Adapted from Jacobson O, Weiss ID, Kiesewetter DO, Farber JM, and Chen X (2010) PET of tumor CXCR4 expression with 4-^{18}F-T140. *J Nucl Med* **51:** 1796–1804. Used with permission.] (B and C) PET imaging of tumors of CHO-CXCR4 using derivatives of CXCR4 peptide antagonist T140 after substitution of the 4F-benzyl group at the N terminus of the peptide with DOTA (B) or NOTA (C) and labeled with ^{64}Cu up to 24 hours postinjection. [Adapted from Jacobson O, Weiss ID, Szajek LP, Niu G, Ma Y, Kiesewetter DO, Peled A, Eden HS, Farber JM, and Chen X (2011) Improvement of CXCR4 tracer specificity for PET imaging. *J Control Release* **157:**216–223. Used with permission.] (D) PET imaging of CHO-CXCR4 (left) and CHO (right) tumor mice with ^{64}Cu-AMD3100 at 6 hours postinjection. (E) PET imaging of lung metastasis of CHO-CXCR4 using ^{64}Cu-AMD3100 at 1 hour postinjection. [Adapted from Weiss ID, Jacobson O, Kiesewetter DO, Jacobus JP, Szajek LP, Chen X, and Farber JM (2012) Positron emission tomography imaging of tumors expressing the human chemokine receptor CXCR4 in mice with the use of ^{64}Cu-AMD3100. *Mol Imaging Biol* **14:** 106–114. Used with permission.]

markers related to cancer metastasis were not yet addressed by the PET research community, such as molecules involved in epithelial to mesenchymal transitions. On the other hand, imaging some of the targets, such as CXCR4, has shown feasibility in multiple animal models and several tracers for this receptor have already been developed and should be further translated into clinical trials.

III. Theranostic Radiotracers

Theranostic radiotracers are "all in one" tracers that can serve as both imaging and therapy agents (Velikyan, 2012). The labeled tracers are used for evaluating target receptors in the tumor or its environment, and if the tumor is positive, the same molecule is thereafter used for therapy, either unlabeled or labeled with therapeutic radioisotopes (Baum and Kulkarni, 2012; Fani et al., 2012; Goldenberg et al., 2012; Oberg, 2012). The value of such molecules is obvious: it enables knowledge that the same molecule will reach the tumor and therefore significantly increase the rate of success of the treatment. The ability to use the same molecule for both imaging and therapy is more easily achieved when the tracer contains a chelator, which can bind imaging radioisotopes and thereafter apply radiation therapy isotopes such as ^{177}Lu and ^{90}Y.

One study on this matter was published by Gabriel et al. (2010) describing customized tumor targeting. In this study 100 cancer patients, with the majority of them having NET, were PET/CT scanned with somatostatin octreotide peptide analog ^{68}Ga-DOTA-TOC. If the PET scan was negative, the patient also underwent PET scan with a different peptide analog lanreotide (^{68}Ga-DOTA-LAN). Patients that were positive for either scan underwent dosimetry measurement with the same compound for which they were positive,

labeled with ^{111}In, for calculating appropriate dosimetry and organ exposure. Finally, the patients were treated with the same molecule labeled with ^{90}Y with the exception of patients with lesions smaller than 2 cm, who were treated with ^{177}Lu-DOTA-TATE (another SST analog). This approach resulted in response to therapy of about 33% of the patients, favoring such customized therapy for advanced tumor stage (Gabriel et al., 2010).

Another interesting study was published recently on treatment efficacy of CXCR4 antagonist, T140 peptide, against human NSCLC in mouse xenograft models. The exact peptide was previously labeled with ^{18}F, without changing its chemical structure (Jacobson et al., 2010). CXCR4/CXCL12 interactions promote NSCLC growth and metastasis and might promote NSCLC resistance to chemotherapy and/or radiotherapy (Fahham et al., 2012). The researchers first evaluated the antiproliferative effects of T140 in vitro, using five different NSCLC cell lines expressing CXCR4. Then the cell lines with the highest and lowest proliferative response to CXCL12 stimulation were further investigated in vivo. Both tumors had high CXCR4 expression, as was confirmed by immunohistochemistry. T140 was injected subcutaneously at a distant site from the tumor and significantly delayed the growth of both xenografts, with higher effect on the tumors derived from the cell line that was more responsive to CXCL12. The median tumor volume was decreased by nearly 50% in both tumor types (Fahham et al., 2012). Taken together, the two studies show that the same molecule in the labeled form can be used for imaging CXCR4 by solid tumor and in the unlabeled form for therapy.

An example for antibody imaging/therapy is the antibody ibritumomab tiuxetan (Zevalin; Spectrum Pharmaceuticals, Inc., Irvine, CA), which was approved for the treatment of patients with relapsed and refractory non-Hodgkin's lymphomas and was labeled with ^{89}Zr for imaging and ^{90}Y for treatment (Rizvi et al., 2012). Seven patients with relapsed B-cell non-Hodgkin's lymphomas underwent PET scans with ^{89}Zr-ibritumomab tiuxetan at 1 hour and 3 and 6 days postinjection and again 2 weeks after treatment with ^{90}Y-ibritumomab tiuxetan. PET images at 1 hour postinjection of ^{89}Zr-ibritumomab tiuxetan showed typical distribution for an antibody, with high activity in the blood pool and uptake in the liver, heart, spleen, bone marrow, and kidneys and almost no uptake in the tumor lesions. At 3 and 6 days postinjection, the uptake in the tumor was increased and the activity in other organs (except for liver) was decreased. The researchers compared imaging when only ^{89}Zr-ibritumomab tiuxetan was injected to the patients and when it was coinjected with therapeutic amount of ^{90}Y-ibritumomab tiuxetan and concluded that the therapeutic amount of ^{90}Y-ibritumomab tiuxetan did not influence ^{89}Zr-ibritumomab tiuxetan PET imaging distribution. Furthermore, they calculated human effective dose of ^{90}Y-ibritumomab tiuxetan based on ^{89}Zr-ibritumomab tiuxetan and suggested that ^{89}Zr-ibritumomab tiuxetan can be used in the future for calculating appropriate dosing of ^{90}Y-ibritumomab tiuxetan (Rizvi et al., 2012).

An approach that is attracting increasing attention and interest in the recent years for molecules that have both imaging capabilities and drug delivery is the use of nanoparticles (NPs). NPs including liposomes, polymeric micelles, dendrimers, superparamagnetic iron oxide crystals, and colloidal gold and many more forms can be manufactured using different chemical methods (Wang et al., 2010). The idea behind NPs is that the same particle can contain several different molecules: some will control delivery, some will direct the specificity to targets on the tumor cells or microenvironment, some will retain drugs to be released in the targeted organ, and others will enable visualization of the NPs in vivo by different imaging techniques such as MRI and PET. Targeting the tumor and its microenvironment can be done either passively, based on the abnormal vasculature of the tumor that allows enhanced permeability and retention or by active targeting that depends on ligand-directed binding to receptors expressed by tumor cells. Release of drugs retained within the NPs may be controlled in response to changes of temperature, pH, or enzymatic cleavage (Wang et al., 2010). However, targeted delivery of these NPs in vivo in animal models and patients remains to be a challenge, with high accumulation in the liver and spleen regardless of useful properties in cell culture condition. One of the benefits of using NPs for therapy is that the poor solubility, poor biodistribution, unfavorable pharmacokinetics, and lack of selectivity of chemotherapeutic drugs can be relatively easily overcome (Yang et al., 2011c).

Yang et al. (2011c) reported on the evaluation of multifunctional and water-soluble superparamagnetic iron oxide (SPIO) nanocarriers for targeted drug delivery and PET/MR imaging of glioblastoma xenografts expressing integrin $\alpha_v\beta_3$ in mice (Yang et al., 2011c). The chemotherapeutic drug doxorubicin was conjugated onto SPIO nanocarriers using a hydrazone bond, which is pH sensitive and releases the drug at lower pH, usually found in tumor microenvironment. For tumor targeting, cRGD peptide ($\alpha_v\beta_3$ antagonist) was conjugated onto SPIO nanocarriers along with NOTA chelator for ^{64}Cu PET isotope (Yang et al., 2011c). ^{64}Cu-cRGD-SPIO-nanocarriers were injected into tumor-bearing mice and evaluated up to 48 hours postinjection. Tumor targeting of ^{64}Cu-cRGD-SPIO-nanocarriers was compared with free cRGD nanocarriers (^{64}Cu-SPIO-nanocarriers; Fig. 25). ^{64}Cu-cRGD-SPIO-nanocarriers accumulated in the tumor (5.4 ± 2.1% ID/g at 48 hours postinjection). It also accumulated in the liver; however, the uptake in that organ reduced over time (6.1 ± 1.6%ID/g

at 48 hours postinjection). Other than the liver, the NPs did not have high uptake in other organs, demonstrating good targeting abilities and favorable tumor contrast (Fig. 25). Specific binding was proven by blocking experiment, done by administration of cRGD (10 mg/kg mouse body weight) with ^{64}Cu-cRGD-SPIO-nanocarriers, which significantly reduced tumor uptake at all the time points examined (Yang et al., 2011c). Unfortunately, the authors did not report on any evaluation of the NPs for drug release at the tumor site or the efficacy of antitumor treatment. However, there have been several other reports showing that NPs can be used for therapy, indicating that this technology for theranostics has a great potential (Gao et al., 2012).

The data described in this section include several technologies that enable diagnosis and treatment with the same molecule. The nanoparticle technology, although very interesting, seems to be the most remote for translation to the clinic because of undesired uptake in non–cancer-related organs. Antibodies, on the other hand, have already been used in the clinic and evaluated as tracers in clinical trials, such as the ^{89}Zr-DFO-J591, which was described in section II.D. Peptides are also being evaluated as treatment in clinical trials, and thereafter the transition of such peptides for clinical imaging should be relatively straightforward.

IV. Conclusions and Perspectives

In this review, we described various PET tracers for cancer imaging by dissecting different processes involved in tumor development and dissemination. PET is a nuclear medicine technology that uses injected bioprobes for imaging their accumulation in target organs and tissues. PET cancer diagnosis in the clinic is currently limited to the use of tracers that measure metabolic processes. However, multiple specific tracers are currently being evaluated in clinical trials. The research on development of new and improved tracers is constantly growing.

Cancer is a complex multiple process and its initiation requires cells to evade the strict regulation of proliferation, which can occur because of genetic defects or accumulation of mutation. This evasion requires both ignoring suppressive signals, as well as sustaining proliferative signals. Local tumor growth also requires tumor cells to resist apoptosis. For the tumor to grow further locally, tumor cells also have to replicate limitlessly and at some point be able to induce angiogenesis. For the tumor to spread, it will have to become more aggressive and invade the surrounding tissue, which will also enable tumor cells to reach the blood stream and form metastasis. The metastatic process requires seeding in tissues that can

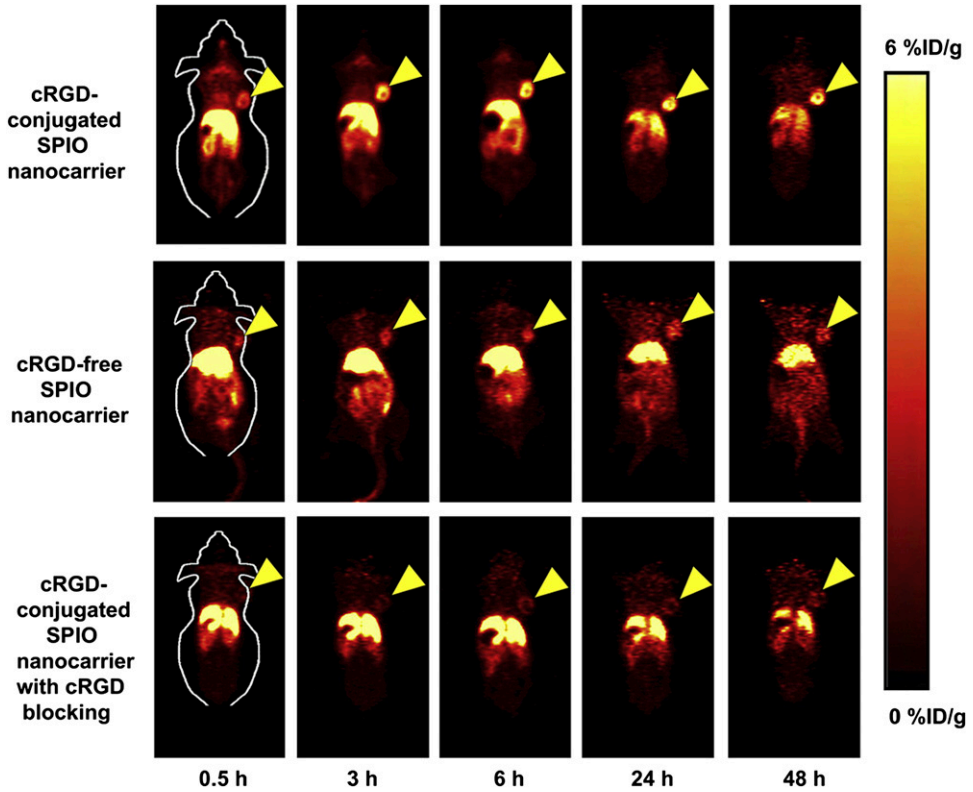

Fig. 25. Coronal PET images of tumor-bearing mice at different time points postinjection of ^{64}Cu-SPIO-nanocarriers (cRGD-conjugated, cRGD-free, and cRGD-conjugated with a blocking dose of cRGD). [Adapted from Yang X, Hong H, Grailer JJ, Rowland IJ, Javadi A, Hurley SA, Xiao Y, Yang Y, Zhang Y, Nickles RJ, Cai W, Steeber DA, and Gong S (2011) cRGD-functionalized, DOX-conjugated, and ^{64}Cu-labeled superparamagnetic iron oxide nanoparticles for targeted anticancer drug delivery and PET/MR imaging. *Biomaterials* **31:**4151–4160. Used with permission from Elsevier.]

support tumor cell proliferation. It is also important to note that during the tumor development and spread, the tumor needs to evade the immune system and sometimes harness it for its own benefits. All the processes described above involve multiple mechanisms and protein expressions, which are not the same for every type of cancer. Because of the different mechanisms used by different cancers, it is highly important to establish which mechanism takes place for each tumor type and each patient to tailor personalized therapy. Currently, the only method available for determining protein expression by tumors is by invasive biopsy. The other possible noninvasive method that might be used in the near future for some mechanisms is nuclear medicine imaging, including PET and SPECT. Herein, we tried to describe for the readers the broad spectrum of tracers that are being developed for PET imaging of cancers, divided by the main processes that occur in cancer development. The development of PET tracers will enable theranostics, which means giving specific therapy based on the exact diagnosis and thereafter monitoring the related treatment. Some PET tracers we described above can be used both as diagnostic tools and in unlabeled form or labeled with therapeutic radioisotopes can serve as therapeutics.

Nevertheless, not all the processes and markers of cancer and metastasis have been targeted yet and new tracers are expected to be developed in the future. In a broader perspective for the future of PET tracers for cancer and other pathologies, we would argue that the requirement of a cyclotron facility for the production of most PET isotopes and the expensive process of their production will drive more and more laboratories to use the less expensive and more available ^{68}Ga, which is produced using a generator. In most cases, ^{68}Ga also offers easier radiosynthesis than ^{18}F and ^{11}C, and these advantages might mitigate its disadvantage of slightly reduced image quality than that of ^{18}F and ^{11}C. The use of ^{68}Ga will dictate development of tracers that are either peptides or small molecules because of the short half-life.

Another future direction of radiochemistry that we expect to take place is the use of ^{18}F in the form of Al^{18}F, which is easily chelated by NOTA chelator and offers a shorter and easier radiosynthesis. Similar to ^{68}Ga, the short half-life of ^{18}F will limit its labeling application to peptides, small proteins (such as the affibody), and small molecules.

We would like to take this opportunity to suggest an additional class of interesting targets/tracers that might be used for imaging, which are microRNAs (miRNAs). Currently there is no PET or SPECT tracer using miRNA and most of the available tracers are fluorescent, which is very limited for whole body in vivo imaging. New insights on miRNA show that these molecules might be transferred from one cell to another, sometimes via the circulation, in microvesicles (Hunter et al., 2008). Adopting these vehicles as a method for delivering radioactivity, either by direct labeling or by labeling the miRNA within, might prove beneficial for tumor imaging.

Genomic analysis of cancers is becoming more frequent in the clinic as a means for achieving personalized treatment of cancer; however, these analyses may result in multiple targets and are not necessarily expressed on the protein level by the tumors. Development of specific tumor markers can complement genomic analysis by allowing positive gene upregulation results to be tested by protein expression, enabling a more precise personalized treatment of patients, and will assist in the evaluation of treatment.

Acknowledgments

The authors thank Dr. Ido D. Weiss and Dr. Don Ho for proofreading the manuscript.

Authorship Contributions

Wrote or contributed to the writing of the manuscript: Jacobson, Chen.

References

Abate C, Ferorelli S, Contino M, Marottoli R, Colabufo NA, Perrone R, and Berardi F (2011) Arylamides hybrids of two high-affinity σ2 receptor ligands as tools for the development of PET radiotracers. *Eur J Med Chem* **46**:4733–4741.

Abiraj K, Mansi R, Tamma ML, Fani M, Forrer F, Nicolas G, Cescato R, Reubi JC, and Maecke HR (2011) Bombesin antagonist-based radioligands for translational nuclear imaging of gastrin-releasing peptide receptor-positive tumors. *J Nucl Med* **52**:1970–1978.

Abourbeh G, Dissoki S, Jacobson O, Litchi A, Ben Daniel R, Laki D, Levitzki A, and Mishani E (2007) Evaluation of radiolabeled ML04, a putative irreversible inhibitor of epidermal growth factor receptor, as a bioprobe for PET imaging of EGFR-overexpressing tumors. *Nucl Med Biol* **34**:55–70.

Adams JM (2003) Ways of dying: multiple pathways to apoptosis. *Genes Dev* **17**: 2481–2495.

Adams JM and Cory S (2007) Bcl-2-regulated apoptosis: mechanism and therapeutic potential. *Curr Opin Immunol* **19**:488–496.

Adams MC, Turkington TG, Wilson JM, and Wong TZ (2010) A systematic review of the factors affecting accuracy of SUV measurements. *AJR Am J Roentgenol* **195**:310–320.

Aerts HJ, Dubois L, Perk L, Vermaelen P, van Dongen GA, Wouters BG, and Lambin P (2009) Disparity between in vivo EGFR expression and ^{89}Zr-labeled cetuximab uptake assessed with PET. *J Nucl Med* **50**:123–131.

Allen AM, Ben-Ami M, Reshef A, Steinmetz A, Kundel Y, Inbar E, Djaldetti R, Davidson T, Fenig E, and Ziv I (2012) Assessment of response of brain metastases to radiotherapy by PET imaging of apoptosis with ^{18}F-ML-10. *Eur J Nucl Med Mol Imaging* **39**:1400–1408.

Aloya R, Shirvan A, Grimberg H, Reshef A, Levin G, Kidron D, Cohen A, and Ziv I (2006) Molecular imaging of cell death in vivo by a novel small molecule probe. *Apoptosis* **11**:2089–2101.

Anastasi A, Erspamer V, and Bucci M (1971) Isolation and structure of bombesin and alytesin, 2 analogous active peptides from the skin of the European amphibians Bombina and Alytes. *Experientia* **27**:166–167.

Arteaga CL (2002) Epidermal growth factor receptor dependence in human tumors: more than just expression? *Oncologist* **7** (Suppl 4):31–39.

Atfy M, Eissa M, Salah HE, and El Shabrawy DA (2012) Role of urokinase plasminogen activator receptor (CD87) as a prognostic marker in acute myeloid leukemia. *Med Oncol* **29**:2063–2069.

auf dem Keller U, Bellac CL, Li Y, Lou Y, Lange PF, Ting R, Harwig C, Kappelhoff R, Dedhar S, and Adam MJ, et al. (2010) Novel matrix metalloproteinase inhibitor [^{18}F]marimastat-aryltrifluoroborate as a probe for in vivo positron emission tomography imaging in cancer. *Cancer Res* **70**:7562–7569.

Backer MV and Backer JM (2012) Imaging key biomarkers of tumor angiogenesis. *Theranostics* **2**:502–515.

Bader HL and Hsu T (2012) Systemic VHL gene functions and the VHL disease. *FEBS Lett* **586**:1562–1569.

Bagatell CJ and Bremner WJ (1996) Androgens in men—uses and abuses. *N Engl J Med* **334**:707–714.

Baum RP and Kulkarni HR (2012) THERANOSTICS: From molecular imaging using Ga-68 labeled tracers and PET/CT to personalized radionuclide therapy - The Bad Berka experience. *Theranostics* **2**:437–447.

Bauvois B (2012) New facets of matrix metalloproteinases MMP-2 and MMP-9 as cell surface transducers: outside-in signaling and relationship to tumor progression. *Biochim Biophys Acta* **1825**:29–36.

Bauwens M, De Saint-Hubert M, Devos E, Deckers N, Reutelingsperger C, Mortelmans L, Himmelreich U, Mottaghy FM, and Verbruggen A (2011) Site-specific ^{68}Ga-labeled Annexin A5 as a PET imaging agent for apoptosis. *Nucl Med Biol* **38**:381–392.

Beer AJ, Grosu AL, Carlsen J, Kolk A, Sarbia M, Stangier I, Watzlowik P, Wester HJ, Haubner R, and Schwaiger M (2007) [18F]galacto-RGD positron emission tomography for imaging of alphavbeta3 expression on the neovasculature in patients with squamous cell carcinoma of the head and neck. *Clin Cancer Res* **13**:6610–6616.

Beer AJ, Haubner R, Goebel M, Luderschmidt S, Spilker ME, Wester HJ, Weber WA, and Schwaiger M (2005) Biodistribution and pharmacokinetics of the alphavbeta3-selective tracer ^{18}F-galacto-RGD in cancer patients. *J Nucl Med* **46**:1333–1341.

Beer AJ, Kessler H, Wester HJ, and Schwaiger M (2011) PET imaging of integrin αVβ3 expression. *Theranostics* **1**:48–57.

Beheshti M, Vali R, Waldenberger P, Fitz F, Nader M, Hammer J, Loidl W, Pirich C, Fogelman I, and Langsteger W (2009) The use of F-18 choline PET in the assessment of bone metastases in prostate cancer: correlation with morphological changes on CT. *Mol Imaging Biol* **11**:446–454.

Bello L, Francolini M, Marthyn P, Zhang J, Carroll RS, Nikas DC, Strasser JF, Villani R, Cheresh DA, and Black PM (2001) α(v)β3 and α(v)β5 integrin expression in glioma periphery. *Neurosurgery* **49**:380–389, discussion 390.

Bem WT, Thomas GE, Mamone JY, Homan SM, Levy BK, Johnson FE, and Coscia CJ (1991) Overexpression of sigma receptors in nonneural human tumors. *Cancer Res* **51**:6558–6562.

Bhardwaj V, Cascone T, Cortez MA, Amini A, Evans J, Komaki RU, Heymach JV, and Welsh JW (2013) Modulation of c-Met signaling and cellular sensitivity to radiation: potential implications for therapy. *Cancer* **119**:1768–1775.

Blankenberg F (2002) To scan or not to scan, it is a question of timing: technetium-99m-annexin V radionuclide imaging assessment of treatment efficacy after one course of chemotherapy. *Clin Cancer Res* **8**:2757–2758.

Blankenberg FG (2008) In vivo detection of apoptosis. *J Nucl Med* **49** (Suppl 2): 81S–95S.

Blot E, Laberge-Le Couteulx S, Jamali H, Cornic M, Guillemet C, Duval C, Hellot MF, Pille JY, Picquenot JM, and Veyret C (2008) CXCR4 membrane expression in node-negative breast cancer. *Breast J* **14**:268–274.

Blumenschein GR Jr, Mills GB, and Gonzalez-Angulo AM (2012) Targeting the hepatocyte growth factor-cMET axis in cancer therapy. *J Clin Oncol* **30**:3287–3296.

Bögler O and Mikkelsen T (2003) Angiogenesis in glioma: molecular mechanisms and roadblocks to translation. *Cancer J* **9**:205–213.

Bonasera TA, Ortu G, Rozen Y, Krais R, Freedman NM, Chisin R, Gazit A, Levitzki A, and Mishani E (2001) Potential $^{(18)}$F-labeled biomarkers for epidermal growth factor receptor tyrosine kinase. *Nucl Med Biol* **28**:359–374.

Bonner JA, Harari PM, Giralt J, Cohen RB, Jones CU, Sur RK, Raben D, Baselga J, Spencer SA, and Zhu J, et al. (2010) Radiotherapy plus cetuximab for locoregionally advanced head and neck cancer: 5-year survival data from a phase 3 randomised trial, and relation between cetuximab-induced rash and survival. *Lancet Oncol* **11**:21–28.

Brooks PC, Clark RA, and Cheresh DA (1994a) Requirement of vascular integrin α v β 3 for angiogenesis. *Science* **264**:569–571.

Brooks PC, Montgomery AM, Rosenfeld M, Reisfeld RA, Hu T, Klier G, and Cheresh DA (1994b) Integrin αvβ3 antagonists promote tumor regression by inducing apoptosis of angiogenic blood vessels. *Cell* **79**:1157–1164.

Buchmann I, Henze M, Engelbrecht S, Eisenhut M, Runz A, Schäfer M, Schilling T, Haufe S, Herrmann T, and Haberkorn U (2007) Comparison of 68Ga-DOTATOC PET and ^{111}In-DTPAOC (Octreoscan) SPECT in patients with neuroendocrine tumours. *Eur J Nucl Med Mol Imaging* **34**:1617–1626.

Buck AK, Herrmann K, Shen C, Dechow T, Schwaiger M, and Wester HJ (2009) Molecular imaging of proliferation in vivo: positron emission tomography with [^{18}F]fluorothymidine. *Methods* **48**:205–215.

Burger JA and Peled A (2009) CXCR4 antagonists: targeting the microenvironment in leukemia and other cancers. *Leukemia* **23**:43–52.

Cai W, Chen K, He L, Cao Q, Koong A, and Chen X (2007) Quantitative PET of EGFR expression in xenograft-bearing mice using ^{64}Cu-labeled cetuximab, a chimeric anti-EGFR monoclonal antibody. *Eur J Nucl Med Mol Imaging* **34**:850–858.

Cai W, Niu G, and Chen X (2008a) Imaging of integrins as biomarkers for tumor angiogenesis. *Curr Pharm Des* **14**:2943–2973.

Cai W, Niu G, and Chen X (2008b) Multimodality imaging of the HER-kinase axis in cancer. *Eur J Nucl Med Mol Imaging* **35**:186–208.

Cantley LC (2002) The phosphoinositide 3-kinase pathway. *Science* **296**:1655–1657.

Carpenter CD, Ingraham HA, Cochet C, Walton GM, Lazar CS, Sowadski JM, Rosenfeld MG, and Gill GN (1991) Structural analysis of the transmembrane domain of the epidermal growth factor receptor. *J Biol Chem* **266**:5750–5755.

Chang JW, Chou CL, Huang SF, Wang HM, Hsieh JJ, Hsu T, and Cheung YC (2007) Erlotinib response of EGFR-mutant gefitinib-resistant non-small-cell lung cancer. *Lung Cancer* **58**:414–417.

Chappell WH, Steelman LS, Long JM, Kempf RC, Abrams SL, Franklin RA, Bäsecke J, Stivala F, Donia M, and Fagone P, et al. (2011) Ras/Raf/MEK/ERK and PI3K/PTEN/Akt/mTOR inhibitors: rationale and importance to inhibiting these pathways in human health. *Oncotarget* **2**:135–164.

Chen K and Chen X (2011) Positron emission tomography imaging of cancer biology: current status and future prospects. *Semin Oncol* **38**:70–86.

Chen L, Zhang Z, Kolb HC, Walsh JC, Zhang J, and Guan Y (2012) ^{18}F -HX4 hypoxia imaging with PET/CT in head and neck cancer: a comparison with ^{18}F-FMISO. *Nucl Med Commun* **33**:1096–1102.

Chen P, Cameron R, Wang J, Vallis KA, and Reilly RM (2003) Antitumor effects and normal tissue toxicity of ^{111}In-labeled epidermal growth factor administered to athymic mice bearing epidermal growth factor receptor-positive human breast cancer xenografts. *J Nucl Med* **44**:1469–1478.

Chen X (2006) Multimodality imaging of tumor integrin alphavbeta3 expression. *Mini Rev Med Chem* **6**:227–234.

Chen X, Liu S, Hou Y, Tohme M, Park R, Bading JR, and Conti PS (2004a) MicroPET imaging of breast cancer alphav-integrin expression with 64Cu-labeled dimeric RGD peptides. *Mol Imaging Biol* **6**:350–359.

Chen X, Tohme M, Park R, Hou Y, Bading JR, and Conti PS (2004b) Micro-PET imaging of alphavbeta3-integrin expression with ^{18}F-labeled dimeric RGD peptide. *Mol Imaging* **3**:96–104.

Cheng Q, Lu L, Grafström J, Olofsson MH, Thorell JO, Samén E, Johansson K, Ahlzén HS, Stone-Elander S, and Linder S, et al.; Sel-tag Imaging Project (2012) Combining [^{11}C]-AnxA5 PET imaging with serum biomarkers for improved detection in live mice of modest cell death in human solid tumor xenografts. *PLoS ONE* **7**:e42151.

Cheng Z, De Jesus OP, Kramer DJ, De A, Webster JM, Gheysens O, Levi J, Namavari M, Wang S, and Park JM, et al. (2010) ^{64}Cu-labeled affibody molecules for imaging of HER2 expressing tumors. *Mol Imaging Biol* **12**:316–324.

Cheng Z, De Jesus OP, Namavari M, De A, Levi J, Webster JM, Zhang R, Lee B, Syud FA, and Gambhir SS (2008) Small-animal PET imaging of human epidermal growth factor receptor type 2 expression with site-specific ^{18}F-labeled protein scaffold molecules. *J Nucl Med* **49**:804–813.

Chin FT, Shen B, Liu S, Berganos RA, Chang E, Mittra E, Chen X, and Gambhir SS (2012) First experience with clinical-grade ([^{18}F]FPP(RGD$_2$): an automated multi-step radiosynthesis for clinical PET studies. *Mol Imaging Biol* **14**:88–95.

Chipuk JE, Kuwana T, Bouchier-Hayes L, Droin NM, Newmeyer DD, Schuler M, and Green DR (2004) Direct activation of Bax by p53 mediates mitochondrial membrane permeabilization and apoptosis. *Science* **303**:1010–1014.

Choura M and Rebaï A (2011) Receptor tyrosine kinases: from biology to pathology. *J Recept Signal Transduct Res* **31**:387–394.

Cohen MH, Williams GA, Sridhara R, Chen G, and Pazdur R (2003) FDA drug approval summary: gefitinib (ZD1839) (Iressa) tablets. *Oncologist* **8**:303–306.

Comis RL (2005) The current situation: erlotinib (Tarceva) and gefitinib (Iressa) in non-small cell lung cancer. *Oncologist* **10**:467–470.

Comuzzi B, Nemes C, Schmidt S, Jasarevic Z, Lodde M, Pycha A, Bartsch G, Offner F, Culig Z, and Hobisch A (2004) The androgen receptor co-activator CBP is up-regulated following androgen withdrawal and is highly expressed in advanced prostate cancer. *J Pathol* **204**:159–166.

Corsten MF, Hofstra L, Narula J, and Reutelingsperger CP (2006) Counting heads in the war against cancer: defining the role of annexin A5 imaging in cancer treatment and surveillance. *Cancer Res* **66**:1255–1260.

Coussens LM, Fingleton B, and Matrisian LM (2002) Matrix metalloproteinase inhibitors and cancer: trials and tribulations. *Science* **295**:2387–2392.

Dalton JT, Mukherjee A, Zhu Z, Kirkovsky L, and Miller DD (1998) Discovery of nonsteroidal androgens. *Biochem Biophys Res Commun* **244**:1–4.

Daughaday WH and Deuel TF (1991) Tumor secretion of growth factors. *Endocrinol Metab Clin North Am* **20**:539–563.

Degterev A, Boyce M, and Yuan J (2003) A decade of caspases. *Oncogene* **22**: 8543–8567.

Dehdashti F, Laforest R, Gao F, Shoghi KI, Aft RL, Nussenbaum B, Kreisel FH, Bartlett NL, Cashen A, and Wagner-Johnston N, et al. (2013) Assessment of cellular proliferation in tumors by PET using ^{18}F-ISO-1. *J Nucl Med* **54**:350–357.

de Jong IJ, Pruim J, Elsinga PH, Jongen MM, Mensink HJ, and Vaalburg W (2002) Visualisation of bladder cancer using (^{11})C-choline PET: first clinical experience. *Eur J Nucl Med Mol Imaging* **29**:1283–1288.

Deng Y and Chang S (2007) Role of telomeres and telomerase in genomic instability, senescence and cancer. *Lab Invest* **87**:1071–1076.

De Silva RA, Peyre K, Pullambhatla M, Fox JJ, Pomper MG, and Nimmagadda S (2011) Imaging CXCR4 expression in human cancer xenografts: evaluation of monocyclam ^{64}Cu-AMD3465. *J Nucl Med* **52**:986–993.

Deri MA, Zeglis BM, Francesconi LC, and Lewis JS (2013) PET imaging with ^{89}Zr: from radiochemistry to the clinic. *Nucl Med Biol* **40**:3–14.

Dijkers EC, Oude Munnink TH, Kosterink JG, Brouwers AH, Jager PL, de Jong JR, van Dongen GA, Schröder CP, Lub-de Hooge MN, and de Vries EG (2010) Biodistribution of ^{89}Zr-trastuzumab and PET imaging of HER2-positive lesions in patients with metastatic breast cancer. *Clin Pharmacol Ther* **87**:586–592.

Doss M, Kolb HC, Zhang JJ, Bélanger MJ, Stubbs JB, Stabin MG, Hostetler ED, Alpaugh RK, von Mehren M, and Walsh JC, et al. (2012) Biodistribution and radiation dosimetry of the integrin marker ^{18}F-RGD-K5 determined from whole-body PET/CT in monkeys and humans. *J Nucl Med* **53**:787–795.

Egeblad M and Werb Z (2002) New functions for the matrix metalloproteinases in cancer progression. *Nat Rev Cancer* **2**:161–174.

Eiblmaier M, Meyer LA, Watson MA, Fracasso PM, Pike LJ, and Anderson CJ (2008) Correlating EGFR expression with receptor-binding properties and internalization of ^{64}Cu-DOTA-cetuximab in 5 cervical cancer cell lines. *J Nucl Med* **49**:1472–1479.

Elsinga PH (2002) Radiopharmaceutical chemistry for positron emission tomography. *Methods* **27**:208–217.

Enslow MS, Zollinger LV, Morton KA, Butterfield RI, Kadrmas DJ, Christian PE, Boucher KM, Heilbrun ME, Jensen RL, and Hoffman JM (2012) Comparison of ^{18}F-fluorodeoxyglucose and ^{18}F-fluorothymidine PET in differentiating radiation necrosis from recurrent glioma. *Clin Nucl Med* **37**:854–861.

Essmann F and Schulze-Osthoff K (2012) Translational approaches targeting the p53 pathway for anti-cancer therapy. *Br J Pharmacol* **165**:328–344.

Fahham D, Weiss ID, Abraham M, Beider K, Hanna W, Shlomai Z, Eizenberg O, Zamir G, Izhar U, and Shapira OM, et al. (2012) In vitro and in vivo therapeutic efficacy of CXCR4 antagonist BKT140 against human non-small cell lung cancer. *J Thorac Cardiovasc Surg* **144**:1167–1175.

Fan Z, Masui H, Altas I, and Mendelsohn J (1993) Blockade of epidermal growth factor receptor function by bivalent and monovalent fragments of 225 anti-epidermal growth factor receptor monoclonal antibodies. *Cancer Res* **53**:4322–4328.

Fani M, Maecke HR, and Okarvi SM (2012) Radiolabeled peptides: valuable tools for the detection and treatment of cancer. *Theranostics* **2**:481–501.

Fantl WJ, Johnson DE, and Williams LT (1993) Signalling by receptor tyrosine kinases. *Annu Rev Biochem* **62**:453–481.

Felding-Habermann B (2003) Integrin adhesion receptors in tumor metastasis. *Clin Exp Metastasis* **20**:203–213.

Felding-Habermann B, Mueller BM, Romerdahl CA, and Cheresh DA (1992) Involvement of integrin alpha V gene expression in human melanoma tumorigenicity. *J Clin Invest* **89**:2018–2022.

Feng J, Funk WD, Wang SS, Weinrich SL, Avilion AA, Chiu CP, Adams RR, Chang E, Allsopp RC, and Yu J, et al. (1995) The RNA component of human telomerase. *Science* **269**:1236–1241.

Ferretti G, Felici A, Papaldo P, Fabi A, and Cognetti F (2007) HER2/neu role in breast cancer: from a prognostic foe to a predictive friend. *Curr Opin Obstet Gynecol* **19**:56–62.

Fiechter M, Gebhard C, Ghadri JR, Fuchs TA, Pazhenkottil AP, Nkoulou RN, Herzog BA, Altorfer U, Gaemperli O, and Kaufmann PA (2013) Myocardial perfusion imaging with (^{13})N-Ammonia PET is a strong predictor for outcome. *Int J Cardiol* **167**:1023–1026.

Fiechter M, Ghadri JR, Gebhard C, Fuchs TA, Pazhenkottil AP, Nkoulou RN, Herzog BA, Wyss CA, Gaemperli O, and Kaufmann PA (2012) Diagnostic value of ^{13}N-ammonia myocardial perfusion PET: added value of myocardial flow reserve. *J Nucl Med* **53**:1230–1234.

Fulda S (2009) Apoptosis pathways and their therapeutic exploitation in pancreatic cancer. *J Cell Mol Med* **13**:1221–1227.

Furumoto S, Takashima K, Kubota K, Ido T, Iwata R, and Fukuda H (2003) Tumor detection using ^{18}F-labeled matrix metalloproteinase-2 inhibitor. *Nucl Med Biol* **30**:119–125.

Furusato B, Mohamed A, Uhlén M, and Rhim JS (2010) CXCR4 and cancer. *Pathol Int* **60**:497–505.

Gabriel M, Andergassen U, Putzer D, Kroiss A, Waitz D, Von Guggenberg E, Kendler D, and Virgolini IJ (2010) Individualized peptide-related-radionuclide-therapy concept using different radiolabelled somatostatin analogs in advanced cancer patients. *Q J Nucl Med Mol Imaging* **54**:92–99.

Gaertner FC, Kessler H, Wester HJ, Schwaiger M, and Beer AJ (2012) Radiolabelled RGD peptides for imaging and therapy. *Eur J Nucl Med Mol Imaging* **39** (Suppl 1):S126–S138.

Gao F, Li L, Liu T, Hao N, Liu H, Tan L, Li H, Huang X, Peng B, and Yan C, et al. (2012) Doxorubicin loaded silica nanorattles actively seek tumors with improved anti-tumor effects. *Nanoscale* **4**:3365–3372.

Gartel AL (2009) p21(WAF1/CIP1) and cancer: a shifting paradigm? *Biofactors* **35**: 161–164.

Gauchez AS, Du Moulinet D'Hardemare A, Lunardi J, Vuillez JP, and Fagret D (1999) Potential use of radiolabeled antisense oligonucleotides in oncology. *Anticancer Res* **19** (6B):4989–4997.

Gil-da-Costa R, Braun A, and Martin A (2006) Using PET H_2O^{15} brain imaging to study the functional-anatomical correlates of non-human primate communication. *Methods* **38**:221–226.

Goel S, Duda DG, Xu L, Munn LL, Boucher Y, Fukumura D, and Jain RK (2011) Normalization of the vasculature for treatment of cancer and other diseases. *Physiol Rev* **91**:1071–1121.

Gofrit ON, Mishani E, Orevi M, Klein M, Freedman N, Pode D, Shapiro A, Katz R, Libson E, and Chisin R (2006) Contribution of ^{11}C-choline positron emission tomography/computerized tomography to preoperative staging of advanced transitional cell carcinoma. *J Urol* **176**:940–944, discussion 944.

Goldenberg DM, Chang CH, Rossi EA, J W, McBride, and Sharkey RM (2012) Pretargeted molecular imaging and radioimmunotherapy. *Theranostics* **2**:523–540.

Greer SN, Metcalf JL, Wang Y, and Ohh M (2012) The updated biology of hypoxia-inducible factor. *EMBO J* **31**:2448–2460.

Groot-Wassink T, Aboagye EO, Wang Y, Lemoine NR, Keith WN, and Vassaux G (2004) Noninvasive imaging of the transcriptional activities of human telomerase promoter fragments in mice. *Cancer Res* **64**:4906–4911.

Grosu AL, Souvatzoglou M, Röper B, Dobritz M, Wiedenmann N, Jacob V, Wester HJ, Reischl G, Machulla HJ, and Schwaiger M, et al. (2007) Hypoxia imaging with FAZA-PET and theoretical considerations with regard to dose painting for individualization of radiotherapy in patients with head and neck cancer. *Int J Radiat Oncol Biol Phys* **69**:541–551.

Grüner JM, Paamand R, Højgaard L, and Law I (2011) Brain perfusion CT compared with^{15}O-H_2O-PET in healthy subjects. *EJNMMI Res* **1**:28–38.

Hamers-Casterman C, Atarhouch T, Muyldermans S, Robinson G, Hamers C, Songa EB, Bendahman N, and Hamers R (1993) Naturally occurring antibodies devoid of light chains. *Nature* **363**:446–448.

Hanahan D and Weinberg RA (2000) The hallmarks of cancer. *Cell* **100**:57–70.

Hanahan D and Weinberg RA (2011) Hallmarks of cancer: the next generation. *Cell* **144**:646–674.

Hansen AE, Kristensen AT, Jørgensen JT, McEvoy FJ, Busk M, van der Kogel AJ, Bussink J, Engelholm SA, and Kjær A (2012) (^{64})Cu-ATSM and (18)FDG PET uptake and (^{64})Cu-ATSM autoradiography in spontaneous canine tumors: comparison with pimonidazole hypoxia immunohistochemistry. *Radiat Oncol* **7**:89–99.

Hara T, Inagaki K, Kosaka N, and Morita T (2000) Sensitive detection of mediastinal lymph node metastasis of lung cancer with ^{11}C-choline PET. *J Nucl Med* **41**: 1507–1513.

Haubner R, Weber WA, Beer AJ, Vabuliene E, Reim D, Sarbia M, Becker KF, Goebel M, Hein R, and Wester HJ, et al. (2005) Noninvasive visualization of the activated alphavbeta3 integrin in cancer patients by positron emission tomography and [18F]Galacto-RGD. *PLoS Med* **2**:e70.

Haug AR, Cindea-Drimus R, Auernhammer CJ, Reincke M, Wängler B, Uebleis C, Schmidt GP, Göke B, Bartenstein P, and Hacker M (2012) The role of ^{68}Ga-DOTATATE PET/CT in suspected neuroendocrine tumors. *J Nucl Med* **53**: 1686–1692.

Havelund BM, Holdgaard PC, Rafaelsen SR, Mortensen LS, Theil J, Bender D, Pløen J, Spindler KL, and Jakobsen A (2013) Tumour hypoxia imaging with ^{18}F-fluoroazomycinarabinofuranoside PET/CT in patients with locally advanced rectal cancer. *Nucl Med Commun* **34**:155–161.

Heinlein CA and Chang C (2004) Androgen receptor in prostate cancer. *Endocr Rev* **25**:276–308.

Heiss WD, Wienhard K, Wagner R, Lanfermann H, Thiel A, Herholz K, and Pietrzyk U (1996) F-Dopa as an amino acid tracer to detect brain tumors. *J Nucl Med* **37**:1180–1182.

Herbst RS (2003) Erlotinib (Tarceva): an update on the clinical trial program. *Semin Oncol* **30**(3, Suppl 7)34–46.

Herbst RS and Kies MS (2003) Gefitinib: current and future status in cancer therapy. *Clin Adv Hematol Oncol* **1**:466–472.

Hiyama E and Hiyama K (2003) Telomerase as tumor marker. *Cancer Lett* **194**: 221–233.

Ho Jin Cho JDL, Park JY, Yun M, Kang WJ, Walsh JC, Kolb H, and Zhang JJ (2009) First in human evaluation of a newly developed integrin binding PET tracer, ^{18}F-RGD-K5 in patients with breast cancer: Comparison with ^{18}F-FDG uptake pattern and microvessel density. *J Nucl Med* **50(Suppl. 2)**:1910.

Hofland LJ and Lamberts SW (2003) The pathophysiological consequences of somatostatin receptor internalization and resistance. *Endocr Rev* **24**:28–47.

Höglund J, Shirvan A, Antoni G, Gustavsson SA, Långström B, Ringheim A, Sörensen J, Ben-Ami M, and Ziv I (2011) ^{18}F-ML-10, a PET tracer for apoptosis: first human study. *J Nucl Med* **52**:720–725.

Holland JP, Divilov V, Bander NH, Smith-Jones PM, Larson SM, and Lewis JS (2010) ^{89}Zr-DFO-J591 for immunoPET of prostate-specific membrane antigen expression in vivo. *J Nucl Med* **51**:1293–1300.

Holm NT, Abreo F, Johnson LW, Li BD, and Chu QD (2009) Elevated chemokine receptor CXCR4 expression in primary tumors following neoadjuvant chemotherapy predicts poor outcomes for patients with locally advanced breast cancer (LABC). *Breast Cancer Res Treat* **113**:293–299.

Hornick JR, Spitzer D, Goedegebuure P, Mach RH, and Hawkins WG (2012) Therapeutic targeting of pancreatic cancer utilizing sigma-2 ligands. *Surgery* **152**(3, Suppl 1)S152–S156.

Hu S, Kiesewetter DO, Zhu L, Guo N, Gao H, Liu G, Hida N, Lang L, Niu G, and Chen X (2012) Longitudinal PET imaging of doxorubicin-induced cell death with ^{18}F-Annexin V. *Mol Imaging Biol* **14**:762–770.

Hua H, Li M, Luo T, Yin Y, and Jiang Y (2011) Matrix metalloproteinases in tumorigenesis: an evolving paradigm. *Cell Mol Life Sci* **68**:3853–3868.

Hunter MP, Ismail N, Zhang X, Aguda BD, Lee EJ, Yu L, Xiao T, Schafer J, Lee ML, and Schmittgen TD, et al. (2008) Detection of microRNA expression in human peripheral blood microvesicles. *PLoS ONE* **3**:e3694.

Hunter T (1984) The epidermal growth factor receptor gene and its product. *Nature* **311**:414–416.

Hwang R and Varner J (2004) The role of integrins in tumor angiogenesis. *Hematol Oncol Clin North Am* **18**:991–1006, vii.

Hyde R, Taylor PM, and Hundal HS (2003) Amino acid transporters: roles in amino acid sensing and signalling in animal cells. *Biochem J* **373**:1–18.

Ichihara E, Kiura K, and Tanimoto M (2011) Targeting angiogenesis in cancer therapy. *Acta Med Okayama* **65**:353–362.

Inubushi M, Saga T, Koizumi M, Takagi R, Hasegawa A, Koto M, Wakatuki M, Morikawa T, Yoshikawa K, and Tanimoto K, et al. (2013) Predictive value of 3′-deoxy-3′-[^{18}F]fluorothymidine positron emission tomography/computed tomography for outcome of carbon ion radiotherapy in patients with head and neck mucosal malignant melanoma. *Ann Nucl Med* **27**:1–10.

Ishida Y, Kawai K, Magata Y, Takeda R, Hashiguchi H, Abe H, Mukai T, and Saji H (2004) Changes in dopamine D2 receptors and 6-[^{18}F]fluoro-L-3,4-dihydroxyphenylalanine uptake in the brain of 6-hydroxydopamine-lesioned rats. *Neurodegener Dis* **1**:109–112.

Jackowski S (1994) Coordination of membrane phospholipid synthesis with the cell cycle. *J Biol Chem* **269**:3858–3867.

Jacobson O and Chen X (2010) PET designated flouride-18 production and chemistry. *Curr Top Med Chem* **10**:1048–1059.

Jacobson O, Weiss ID, Kiesewetter DO, Farber JM, and Chen X (2010) PET of tumor CXCR4 expression with 4-^{18}F-T140. *J Nucl Med* **51**:1796–1804.

Jacobson O, Weiss ID, Szajek L, Farber JM, and Kiesewetter DO (2009) ^{64}Cu-AMD3100—a novel imaging agent for targeting chemokine receptor CXCR4. *Bioorg Med Chem* **17**:1486–1493.

Jacobson O, Weiss ID, Szajek LP, Niu G, Ma Y, Kiesewetter DO, Farber JM, and Chen X (2011) PET imaging of CXCR4 using copper-64 labeled peptide antagonist. *Theranostics* **1**:251–262.

Jacobson O, Weiss ID, Szajek LP, Niu G, Ma Y, Kiesewetter DO, Peled A, Eden HS, Farber JM, and Chen X (2012) Improvement of CXCR4 tracer specificity for PET imaging. *J Control Release* **157**:216–223.

Jadvar H (2012) Can choline PET tackle the challenge of imaging prostate cancer? *Theranostics* **2**:331–332.

Jager PL, de Korte MA, Lub-de Hooge MN, van Waarde A, Koopmans KP, Perik PJ and de Vries EG (2005) Molecular imaging: what can be used today. Cancer Imaging 5 Spec No A:S27–32.

Jagoda EM, Lang L, Bhadrasetty V, Histed S, Williams M, Kramer-Marek G, Mena E, Rosenblum L, Marik J, and Tinianow JN, et al. (2012) Immuno-PET of the hepatocyte growth factor receptor Met using the 1-armed antibody onartuzumab. *J Nucl Med* **53**:1592–1600.

Jhanwar YS and Straus DJ (2006) The role of PET in lymphoma. *J Nucl Med* **47**: 1326–1334.

Jin H, Yang R, Zheng Z, Romero M, Ross J, Bou-Reslan H, Carano RA, Kasman I, Mai E, and Young J, et al. (2008) MetMAb, the one-armed 5D5 anti-c-Met antibody, inhibits orthotopic pancreatic tumor growth and improves survival. *Cancer Res* **68**: 4360–4368.

Jora C, Mattakarottu JJ, Aniruddha PG, Mudalsha R, Singh DK, Pathak HC, Sharma N, Sarin A, Prince A, and Singh G (2011) Comparative evaluation of ^{18}F-FDOPA, ^{13}N-AMMONIA, ^{18}F-FDG PET/CT and MRI in primary brain tumors - A pilot study. *Indian J Nucl Med* **26**:78–81.

Jungbluth AA, Stockert E, Huang HJ, Collins VP, Coplan K, Iversen K, Kolb D, Johns TJ, Scott AM, and Gullick WJ, et al. (2003) A monoclonal antibody recognizing human cancers with amplification/overexpression of the human epidermal growth factor receptor. *Proc Natl Acad Sci USA* **100**:639–644.

Kabolizadeh P, Kubicek GJ, Heron DE, Ferris RL, and Gibson MK (2012) The role of cetuximab in the management of head and neck cancers. *Expert Opin Biol Ther* **12**: 517–528.

Kaira K, Oriuchi N, Shimizu K, Ishikita T, Higuchi T, Imai H, Yanagitani N, Sunaga N, Hisada T, and Ishizuka T, et al. (2009) Correlation of angiogenesis with ^{18}F-FMT and ^{18}F-FDG uptake in non-small cell lung cancer. *Cancer Sci* **100**:753–758.

Kang L, Wang RF, Yan P, Liu M, Zhang CL, Yu MM, Cui YG, and Xu XJ (2010) Noninvasive visualization of RNA delivery with ^{99m}Tc-radiolabeled small-interference RNA in tumor xenografts. *J Nucl Med* **51**:978–986.

Kawamura K, Yamasaki T, Yui J, Hatori A, Konno F, Kumata K, Irie T, Fukumura T, Suzuki K, and Kanno I, et al. (2009) In vivo evaluation of P-glycoprotein and breast cancer resistance protein modulation in the brain using [(^{11})C]gefitinib. *Nucl Med Biol* **36**:239–246.

Kenny L, Coombes RC, Vigushin DM, Al-Nahhas A, Shousha S, and Aboagye EO (2007) Imaging early changes in proliferation at 1 week post chemotherapy: a pilot study in breast cancer patients with 3′-deoxy-3′-[^{18}F]fluorothymidine positron emission tomography. *Eur J Nucl Med Mol Imaging* **34**:1339–1347.

Kenny LM, Coombes RC, Oulie I, Contractor KB, Miller M, Spinks TJ, McParland B, Cohen PS, Hui AM, and Palmieri C, et al. (2008) Phase I trial of the positron-emitting Arg-Gly-Asp (RGD) peptide radioligand ^{18}F-AH111585 in breast cancer patients. *J Nucl Med* **49**:879–886.

Kenny LM, Vigushin DM, Al-Nahhas A, Osman S, Luthra SK, Shousha S, Coombes RC, and Aboagye EO (2005) Quantification of cellular proliferation in tumor and normal tissues of patients with breast cancer by [^{18}F]fluorothymidine-positron emission tomography imaging: evaluation of analytical methods. *Cancer Res* **65**: 10104–10112.

Kim EM, Jeong MH, Kim DW, Jeong HJ, Lim ST, and Sohn MH (2011) Iodine 125-labeled mesenchymal-epithelial transition factor binding peptide-click-cRGDyk heterodimer for glioma imaging. *Cancer Sci* **102**:1516–1521.

Kim EM, Joung MH, Lee CM, Jeong HJ, Lim ST, Sohn MH, and Kim DW (2010) Synthesis of Tc-99m labeled 1,2,3-triazole-4-yl c-met binding peptide as a potential c-met receptor kinase positive tumor imaging agent. *Bioorg Med Chem Lett* **20**: 4240–4243.

Kim EM, Park EH, Cheong SJ, Lee CM, Kim DW, Jeong HJ, Lim ST, Sohn MH, Kim K, and Chung J (2009) Characterization, biodistribution and small-animal SPECT of I-125-labeled c-Met binding peptide in mice bearing c-Met receptor tyrosine kinase-positive tumor xenografts. *Nucl Med Biol* **36**:371–378.

Kishino T, Hoshikawa H, Nishiyama Y, Yamamoto Y, and Mori N (2012) Usefulness of 3′-deoxy-3′-^{18}F-fluorothymidine PET for predicting early response to chemoradiotherapy in head and neck cancer. *J Nucl Med* **53**:1521–1527.

Koch CJ, Scheuermann JS, Divgi C, Judy KD, Kachur AV, Freifelder R, Reddin JS, Karp J, Stubbs JB, and Hahn SM, et al. (2010) Biodistribution and dosimetry of (^{18})F-EF5 in cancer patients with preliminary comparison of (^{18})F-EF5 uptake versus EF5 binding in human glioblastoma. *Eur J Nucl Med Mol Imaging* **37**: 2048–2059.

Komar G, Oikonen V, Sipilä H, Seppänen M, and Minn H (2012) Noninvasive parametric blood flow imaging of head and neck tumours using [^{15}O]H_2O and PET/CT. *Nucl Med Commun* **33**:1169–1178.

Koopmans KP, Neels ON, Kema IP, Elsinga PH, Links TP, de Vries EG, and Jager PL (2009) Molecular imaging in neuroendocrine tumors: molecular uptake mechanisms and clinical results. *Crit Rev Oncol Hematol* **71**:199–213.

Kramer-Marek G, Kiesewetter DO, and Capala J (2009) Changes in HER2 expression in breast cancer xenografts after therapy can be quantified using PET and (^{18})F-labeled affibody molecules. *J Nucl Med* **50**:1131–1139.

Kramer-Marek G, Shenoy N, Seidel J, Griffiths GL, Choyke P, and Capala J (2011) ^{68}Ga-DOTA-affibody molecule for in vivo assessment of HER2/neu expression with PET. *Eur J Nucl Med Mol Imaging* **38**:1967–1976.

Krausz Y, Freedman N, Rubinstein R, Lavie E, Orevi M, Tshori S, Salmon A, Glaser B, Chisin R, and Mishani E, et al. (2011) 68Ga-DOTA-NOC PET/CT imaging of neuroendocrine tumors: comparison with 111In-DTPA-octreotide (OctreoScan®). *Mol Imaging Biol* **13**:583–593.

Krausz Y, Rubinstein R, Appelbaum L, Mishani E, Orevi M, Fraenkel M, Tshori S, Glaser B, Bocher M, and Salmon A, et al. (2012) Ga-68 DOTA-NOC uptake in the pancreas: pathological and physiological patterns. *Clin Nucl Med* **37**:57–62.

Kumar U (2011) Cross-talk and modulation of signaling between somatostatin and growth factor receptors. *Endocrine* **40**:168–180.

la Fougère C, Suchorska B, Bartenstein P, Kreth FW, and Tonn JC (2011) Molecular imaging of gliomas with PET: opportunities and limitations. *Neuro-oncol* **13**: 806–819.

Lamberts SW, de Herder WW, and Hofland LJ (2002) Somatostatin analogs in the diagnosis and treatment of cancer. *Trends Endocrinol Metab* **13**:451–457.

Lappano R and Maggiolini M (2011) G protein-coupled receptors: novel targets for drug discovery in cancer. *Nat Rev Drug Discov* **10**:47–60.

Larson SM, Morris M, Gunther I, Beattie B, Humm JL, Akhurst TA, Finn RD, Erdi Y, Pentlow K, and Dyke J, et al. (2004) Tumor localization of 16β-^{18}F-fluoro-5alpha-dihydrotestosterone versus ^{18}F-FDG in patients with progressive, metastatic prostate cancer. *J Nucl Med* **45**:366–373.

Larsson LG (2011) Oncogene- and tumor suppressor gene-mediated suppression of cellular senescence. *Semin Cancer Biol* **21**:367–376.

Laverman P, Boerman OC, Corstens FH, and Oyen WJ (2002) Fluorinated amino acids for tumour imaging with positron emission tomography. *Eur J Nucl Med Mol Imaging* **29**:681–690.

Lears KA, Ferdani R, Liang K, Zheleznyak A, Andrews R, Sherman CD, Achilefu S, Anderson CJ, and Rogers BE (2011) In vitro and in vivo evaluation of ^{64}Cu-labeled SarAr-bombesin analogs in gastrin-releasing peptide receptor-expressing prostate cancer. *J Nucl Med* **52**:470–477.

Lee DC, Fenton SE, Berkowitz EA, and Hissong MA (1995) Transforming growth factor alpha: expression, regulation, and biological activities. *Pharmacol Rev* **47**: 51–85.

Lee ST and Scott AM (2007) Hypoxia positron emission tomography imaging with ^{18}f-fluoromisonidazole. *Semin Nucl Med* **37**:451–461.

Leonard JP, LaCasce AS, Smith MR, Noy A, Chirieac LR, Rodig SJ, Yu JQ, Vallabhajosula S, Schoder H, and English P, et al. (2012) Selective CDK4/6 inhibition with tumor responses by PD0332991 in patients with mantle cell lymphoma. *Blood* **119**:4597–4607.

Leu JI, Dumont P, Hafey M, Murphy ME, and George DL (2004) Mitochondrial p53 activates Bak and causes disruption of a Bak-Mcl1 complex. *Nat Cell Biol* **6**: 443–450.

Lewis JS, Laforest R, Dehdashti F, Grigsby PW, Welch MJ, and Siegel BA (2008) An imaging comparison of ^{64}Cu-ATSM and ^{60}Cu-ATSM in cancer of the uterine cervix. *J Nucl Med* **49**:1177–1182.

Li DY, Sorensen LK, Brooke BS, Urness LD, Davis EC, Taylor DG, Boak BB, and Wendel DP (1999) Defective angiogenesis in mice lacking endoglin. *Science* **284**:1534–1537.

Li H, Xu D, Toh BH, and Liu JP (2006) TGF-beta and cancer: is Smad3 a repressor of hTERT gene? *Cell Res* **16**:169–173.

Li W, Niu G, Lang L, Guo N, Ma Y, Kiesewetter DO, Backer JM, Shen B, and Chen X (2012a) PET imaging of EGF receptors using [^{18}F]FBEM-EGF in a head and neck squamous cell carcinoma model. *Eur J Nucl Med Mol Imaging* **39**:300–308.

Li X, Link JM, Stekhova S, Yagle KJ, Smith C, Krohn KA, and Tait JF (2008) Site-specific labeling of annexin V with F-18 for apoptosis imaging. *Bioconjug Chem* **19**: 1684–1688.

Li Z, Graf NA, Herrmann K, Jünger A, Aichler M, Feuchtinger A, Baumgart A, Walch A, Peschel C, and Schwaiger M, et al. (2012b) FLT-PET is superior to FDG-PET for very early response prediction in NPM-ALK-positive lymphoma treated with targeted therapy. *Cancer Res* **72**:5014–5024.

Lin HH (2012) Adhesion family of G protein-coupled receptors and cancer. *Chang Gung Med J* **35**:15–27.

Lin LL, Silvoniemi A, Stubbs JB, Rengan R, Suilamo S, Solin O, Divgi C, Eskola O, Sorger JM, and Stabin MG, et al. (2012) Radiation dosimetry and biodistribution of the hypoxia tracer (^{18})F-EF5 in oncologic patients. *Cancer Biother Radiopharm* **27**: 412–419.

Lingner J, Cooper JP, and Cech TR (1995) Telomerase and DNA end replication: no longer a lagging strand problem? *Science* **269**:1533–1534.

Liu A, Dence CS, Welch MJ, and Katzenellenbogen JA (1992) Fluorine-18-labeled androgens: radiochemical synthesis and tissue distribution studies on six fluorine-substituted androgens, potential imaging agents for prostatic cancer. *J Nucl Med* **33**:724–734.

Liu M, Wang RF, Zhang CL, Yan P, Yu MM, Di LJ, Liu HJ, and Guo FQ (2007) Noninvasive imaging of human telomerase reverse transcriptase (hTERT) messenger RNA with ^{99m}Tc-radiolabeled antisense probes in malignant tumors. *J Nucl Med* **48**:2028–2036.

Liu N, Li M, Li X, Meng X, Yang G, Zhao S, Yang Y, Ma L, Fu Z, and Yu J (2009) PET-based biodistribution and radiation dosimetry of epidermal growth factor receptor-selective tracer ^{11}C-PD153035 in humans. *J Nucl Med* **50**:303–308.

Liu S (2006) Radiolabeled multimeric cyclic RGD peptides as integrin alphavbeta3 targeted radiotracers for tumor imaging. *Mol Pharm* **3**:472–487.

Lopci E, Piccardo A, Nanni C, Altrinetti V, Garaventa A, Pession A, Cistaro A, Chiti A, Villavecchia G, and Fanti S (2012) ^{18}F-DOPA PET/CT in neuroblastoma: comparison of conventional imaging with CT/MR. *Clin Nucl Med* **37**:e73–e78.

Ma YY and Tao HQ (2012) Role of urokinase plasminogen activator receptor in gastric cancer: a potential therapeutic target. *Cancer Biother Radiopharm* **27**: 285–290.

Maddika S, Ande SR, Panigrahi S, Paranjothy T, Weglarczyk K, Zuse A, Eshraghi M, Manda KD, Wiechec E, and Los M (2007) Cell survival, cell death and cell cycle pathways are interconnected: implications for cancer therapy. *Drug Resist Updat* **10**:13–29.

Mankoff DA, Shields AF, Graham MM, Link JM, Eary JF, and Krohn KA (1998) Kinetic analysis of 2-[carbon-11]thymidine PET imaging studies: compartmental model and mathematical analysis. *J Nucl Med* **39**:1043–1055.

Martínez-Rumayor A, Arrieta O, Guevara P, Escobar E, Rembao D, Salina C, and Sotelo J (2004) Coexpression of hepatocyte growth factor/scatter factor (HGF/SF) and its receptor cMET predict recurrence of meningiomas. *Cancer Lett* **213**: 117–124.

McCall KC, Humm JL, Bartlett R, Reese M, and Carlin S (2012) Copper-64-diacetyl-bis($N(_4)$-methylthiosemicarbazone) pharmacokinetics in FaDu xenograft tumors and correlation with microscopic markers of hypoxia. *Int J Radiat Oncol Biol Phys* **84**:e393–e399.

McCubrey JA, Milella M, Tafuri A, Martelli AM, Lunghi P, Bonati A, Cervello M, Lee JT, and Steelman LS (2008a) Targeting the Raf/MEK/ERK pathway with small-molecule inhibitors. *Curr Opin Investig Drugs* **9**:614–630.

McCubrey JA, Steelman LS, Abrams SL, Bertrand FE, Ludwig DE, Bäsecke J, Libra M, Stivala F, Milella M, and Tafuri A, et al. (2008b) Targeting survival cascades induced by activation of Ras/Raf/MEK/ERK, PI3K/PTEN/Akt/mTOR and Jak/STAT pathways for effective leukemia therapy. *Leukemia* **22**:708–722.

McKeague M and Derosa MC (2012) Challenges and opportunities for small molecule aptamer development. *J Nucleic Acids* **2012**:748913.

Mease RC, Dusich CL, Foss CA, Ravert HT, Dannals RF, Seidel J, Prideaux A, Fox JJ, Sgouros G, and Kozikowski AP, et al. (2008) N-[N-[(S)-1,3-Dicarboxypropyl] carbamoyl]-4-[^{18}F]fluorobenzyl-L-cysteine, [^{18}F]DCFBC: a new imaging probe for prostate cancer. *Clin Cancer Res* **14**:3036–3043.

Memon AA, Jakobsen S, Dagnaes-Hansen F, Sorensen BS, Keiding S, and Nexo E (2009) Positron emission tomography (PET) imaging with [^{11}C]-labeled erlotinib: a micro-PET study on mice with lung tumor xenografts. *Cancer Res* **69**:873–878.

Memon AA, Weber B, Winterdahl M, Jakobsen S, Meldgaard P, Madsen HH, Keiding S, Nexo E, and Sorensen BS (2011) PET imaging of patients with non-small cell lung cancer employing an EGF receptor targeting drug as tracer. *Br J Cancer* **105**: 1850–1855.

Mendelsohn J and Baselga J (2003) Status of epidermal growth factor receptor antagonists in the biology and treatment of cancer. *J Clin Oncol* **21**:2787–2799.

Meng X, Loo BW Jr, Ma L, Murphy JD, Sun X, and Yu J (2011) Molecular imaging with ^{11}C-PD153035 PET/CT predicts survival in non-small cell lung cancer treated with EGFR-TKI: a pilot study. *J Nucl Med* **52**:1573–1579.

Meric-Bernstam F and Hung MC (2006) Advances in targeting human epidermal growth factor receptor-2 signaling for cancer therapy. *Clin Cancer Res* **12**: 6326–6330.

Miao Z, Ren G, Liu H, Jiang L, and Cheng Z (2010) Small-animal PET imaging of human epidermal growth factor receptor positive tumor with a ^{64}Cu labeled affibody protein. *Bioconjug Chem* **21**:947–954.

Miao Z, Ren G, Liu H, Qi S, Wu S, and Cheng Z (2012) PET of EGFR expression with an ^{18}F-labeled affibody molecule. *J Nucl Med* **53**:1110–1118.

Mihara M, Erster S, Zaika A, Petrenko O, Chittenden T, Pancoska P, and Moll UM (2003) p53 has a direct apoptogenic role at the mitochondria. *Mol Cell* **11**:577–590.

Milenic DE, Wong KJ, Baidoo KE, Nayak TK, Regino CA, Garmestani K, and Brechbiel MW (2010) Targeting HER2: a report on the in vitro and in vivo preclinical data supporting trastuzumab as a radioimmunoconjugate for clinical trials. *MAbs* **2**:550–564.

Miles D, Harbeck N, Escudier B, Hurwitz H, Saltz L, Van Cutsem E, Cassidy J, Mueller B, and Sirzén F (2011) Disease course patterns after discontinuation of bevacizumab: pooled analysis of randomized phase III trials. *J Clin Oncol* **29**: 83–88.

Mishani E and Abourbeh G (2007) Cancer molecular imaging: radionuclide-based biomarkers of the epidermal growth factor receptor (EGFR). *Curr Top Med Chem* **7**: 1755–1772.

Mishani E, Abourbeh G, Eiblmaier M, and Anderson CJ (2008) Imaging of EGFR and EGFR tyrosine kinase overexpression in tumors by nuclear medicine modalities. *Curr Pharm Des* **14**:2983–2998.

Mittra ES, Goris ML, Iagaru AH, Kardan A, Burton L, Berganos R, Chang E, Liu S, Shen B, and Chin FT,, et al. (2011) Pilot pharmacokinetic and dosimetric studies of (^{18})F-FPPRGD2: a PET radiopharmaceutical agent for imaging α(v)β(3) integrin levels. *Radiology* **260**:182–191.

Montgomery AJ, Lingford-Hughes AR, Egerton A, Nutt DJ, and Grasby PM (2007) The effect of nicotine on striatal dopamine release in man: A [^{11}C]raclopride PET study. *Synapse* **61**:637–645.

Morris MJ, Divgi CR, Pandit-Taskar N, Batraki M, Warren N, Nacca A, Smith-Jones P, Schwartz L, Kelly WK, and Slovin S, et al. (2005) Pilot trial of unlabeled and indium-111-labeled anti-prostate-specific membrane antigen antibody J591 for castrate metastatic prostate cancer. *Clin Cancer Res* **11**:7454–7461.

Morris MJ, Pandit-Taskar N, Divgi CR, Bender S, O'Donoghue JA, Nacca A, Smith-Jones P, Schwartz L, Slovin S, and Finn R, et al. (2007) Phase I evaluation of J591 as a vascular targeting agent in progressive solid tumors. *Clin Cancer Res* **13**: 2707–2713.

Mortensen LS, Johansen J, Kallehauge J, Primdahl H, Busk M, Lassen P, Alsner J, Sørensen BS, Toustrup K, and Jakobsen S, et al. (2012) FAZA PET/CT hypoxia imaging in patients with squamous cell carcinoma of the head and neck treated with radiotherapy: results from the DAHANCA 24 trial. *Radiother Oncol* **105**: 14–20.

Müller A, Homey B, Soto H, Ge N, Catron D, Buchanan ME, McClanahan T, Murphy E, Yuan W, and Wagner SN, et al. (2001) Involvement of chemokine receptors in breast cancer metastasis. *Nature* **410**:50–56.

Nagengast WB, de Korte MA, Oude Munnink TH, Timmer-Bosscha H, den Dunnen WF, Hollema H, de Jong JR, Jensen MR, Quadt C, and Garcia-Echeverria C, et al. (2010) ^{89}Zr-bevacizumab PET of early antiangiogenic tumor response to treatment with HSP90 inhibitor NVP-AUY922. *J Nucl Med* **51**:761–767.

Nakamura TM, Morin GB, Chapman KB, Weinrich SL, Andrews WH, Lingner J, Harley CB, and Cech TR (1997) Telomerase catalytic subunit homologs from fission yeast and human. *Science* **277**:955–959.

Nanda PK, Pandey U, Bottenus BN, Rold TL, Sieckman GL, Szczodroski AF, Hoffman TJ, and Smith CJ (2012) Bombesin analogues for gastrin-releasing peptide receptor imaging. *Nucl Med Biol* **39**:461–471.

Nayak TK, Garmestani K, Baidoo KE, Milenic DE, and Brechbiel MW (2011) PET imaging of tumor angiogenesis in mice with VEGF-A-targeted (^{86})Y-CHX-A″-DTPA-bevacizumab. *Int J Cancer* **128**:920–926.

Nayak TK, Garmestani K, Milenic DE, and Brechbiel MW (2012) PET and MRI of metastatic peritoneal and pulmonary colorectal cancer in mice with human epidermal growth factor receptor 1-targeted ^{89}Zr-labeled panitumumab. *J Nucl Med* **53**:113–120.

Nguyen QD, Smith G, Glaser M, Perumal M, Arstad E, and Aboagye EO (2009) Positron emission tomography imaging of drug-induced tumor apoptosis with a caspase-3/7 specific [^{18}F]-labeled isatin sulfonamide. *Proc Natl Acad Sci USA* **106**:16375–16380.

Niemeyer MG, Kuijper AF, Gerhards LJ, D'Haene EG, and van der Wall EE (1993) Nitrogen-13 ammonia perfusion imaging: relation to metabolic imaging. *Am Heart J* **125**:848–854.

Nimmagadda S, Pullambhatla M, Stone K, Green G, Bhujwalla ZM, and Pomper MG (2010) Molecular imaging of CXCR4 receptor expression in human cancer xenografts with [^{64}Cu]AMD3100 positron emission tomography. *Cancer Res* **70**: 3935–3944.

Nishimura K, Hida S, Nishio Y, Ohishi K, Okada Y, Okada K, Yoshida O, Nishimura K, and Nishibuchi S (1988) The validity of magnetic resonance imaging (MRI) in the staging of bladder cancer: comparison with computed tomography (CT) and transurethral ultrasonography (US). *Jpn J Clin Oncol* **18**:217–226.

Niu G, Cai W, and Chen X (2008) Molecular imaging of human epidermal growth factor receptor 2 (HER-2) expression. *Front Biosci* **13**:790–805.

Niu G, Li Z, Xie J, Le QT, and Chen X (2009) PET of EGFR antibody distribution in head and neck squamous cell carcinoma models. *J Nucl Med* **50**:1116–1123.

Niu G, Murad YM, Gao H, Hu S, Guo N, Jacobson O, Nguyen TD, Zhang J, and Chen X (2012) Molecular targeting of CEACAM6 using antibody probes of different sizes. *J Control Release* **161**:18–24.

Niu G, Zhu L, Ho DN, Zhang F, Gao H, Quan Q, Hida N, Ozawa T, Liu G, and Chen X (2013) Longitudinal bioluminescence imaging of the dynamics of Doxorubicin induced apoptosis. *Theranostics* **3**:190–200.

Oberg K (2012) Molecular imaging radiotherapy: theranostics for personalized patient management of neuroendocrine tumors (NETs). *Theranostics* **2**:448–458.

Oliveira S, Schiffelers RM, van der Veeken J, van der Meel R, Vongpromek R, van Bergen En Henegouwen PM, Storm G, and Roovers RC (2010) Downregulation of EGFR by a novel multivalent nanobody-liposome platform. *J Control Release* **145**: 165–175.

Olsson AK, Dimberg A, Kreuger J, and Claesson-Welsh L (2006) VEGF receptor signalling - in control of vascular function. *Nat Rev Mol Cell Biol* **7**:359–371.

Orevi M, Klein M, Mishani E, Chisin R, Freedman N, and Gofrit ON (2012) ^{11}C-Acetate PET/CT in bladder urothelial carcinoma: intraindividual comparison with ^{11}C-choline. *Clin Nucl Med* **37**:e67–e72.

Otrock ZK, Hatoum HA, Awada AH, Ishak RS, and Shamseddine AI (2009) Hypoxia-inducible factor in cancer angiogenesis: structure, regulation and clinical perspectives. *Crit Rev Oncol Hematol* **70**:93–102.

Oude Munnink TH, Arjaans ME, Timmer-Bosscha H, Schröder CP, Hesselink JW, Vedelaar SR, Walenkamp AM, Reiss M, Gregory RC, and Lub-de Hooge MN, et al. (2011) PET with the 89Zr-labeled transforming growth factor-β antibody fresolimumab in tumor models. *J Nucl Med* **52**:2001–2008.

Oude Munnink TH, Korte MA, Nagengast WB, Timmer-Bosscha H, Schröder CP, Jong JR, Dongen GA, Jensen MR, Quadt C, and Hooge MN, et al. (2010) (^{89})Zr-trastuzumab PET visualises HER2 downregulation by the HSP90 inhibitor NVP-AUY922 in a human tumour xenograft. *Eur J Cancer* **46**:678–684.

Parma J, Duprez L, Van Sande J, Cochaux P, Gervy C, Mockel J, Dumont J, and Vassart G (1993) Somatic mutations in the thyrotropin receptor gene cause hyperfunctioning thyroid adenomas. *Nature* **365**:649–651.

Paudyal B, Paudyal P, Oriuchi N, Hanaoka H, Tominaga H, and Endo K (2011) Positron emission tomography imaging and biodistribution of vascular endothelial growth factor with ^{64}Cu-labeled bevacizumab in colorectal cancer xenografts. *Cancer Sci* **102**:117–121.

Paudyal P, Paudyal B, Hanaoka H, Oriuchi N, Iida Y, Yoshioka H, Tominaga H, Watanabe S, Watanabe S, and Ishioka NS, et al. (2010) Imaging and biodistribution of Her2/neu expression in non-small cell lung cancer xenografts with Cu-labeled trastuzumab PET. *Cancer Sci* **101**:1045–1050.

Peng L, Liu R, Marik J, Wang X, Takada Y, and Lam KS (2006) Combinatorial chemistry identifies high-affinity peptidomimetics against α4β1 integrin for in vivo tumor imaging. *Nat Chem Biol* **2**:381–389.

Pérez-Gómez E, Del Castillo G, Juan Francisco S, López-Novoa JM, Bernabéu C, and Quintanilla M (2010) The role of the TGF-β coreceptor endoglin in cancer. *ScientificWorldJournal* **10**:2367–2384.

Perk LR, Stigter-van Walsum M, Visser GW, Kloet RW, Vosjan MJ, Leemans CR, Giaccone G, Albano R, Comoglio PM, and van Dongen GA (2008) Quantitative PET imaging of Met-expressing human cancer xenografts with ^{89}Zr-labelled monoclonal antibody DN30. *Eur J Nucl Med Mol Imaging* **35**:1857–1867.

Persson M, Madsen J, Østergaard S, Jensen MM, Jørgensen JT, Juhl K, Lehmann C, Ploug M, and Kjaer A (2012a) Quantitative PET of human urokinase-type plasminogen activator receptor with ^{64}Cu-DOTA-AE105: implications for visualizing cancer invasion. *J Nucl Med* **53**:138–145.

Persson M, Madsen J, Østergaard S, Ploug M, and Kjaer A (2012b) ^{68}Ga-labeling and in vivo evaluation of a uPAR binding DOTA- and NODAGA-conjugated peptide for PET imaging of invasive cancers. *Nucl Med Biol* **39**:560–569.

Pfeifer A, Knigge U, Mortensen J, Oturai P, Berthelsen AK, Loft A, Binderup T, Rasmussen P, Elema D, and Klausen TL, et al. (2012) Clinical PET of neuroendocrine tumors using ^{64}Cu-DOTATATE: first-in-humans study. *J Nucl Med* **53**:1207–1215.

Picchio M and Castellucci P (2012) Clinical indications of C-choline PET/CT in prostate cancer patients with biochemical relapse. *Theranostics* **2**:313–317.

Polager S and Ginsberg D (2008) E2F - at the crossroads of life and death. *Trends Cell Biol* **18**:528–535.

Polager S and Ginsberg D (2009) p53 and E2f: partners in life and death. *Nat Rev Cancer* **9**:738–748.

Porter AC and Vaillancourt RR (1998) Tyrosine kinase receptor-activated signal transduction pathways which lead to oncogenesis. *Oncogene* **17** (11 Reviews): 1343–1352.

Prenzel N, Fischer OM, Streit S, Hart S, and Ullrich A (2001) The epidermal growth factor receptor family as a central element for cellular signal transduction and diversification. *Endocr Relat Cancer* **8**:11–31.

Prigent SA and Lemoine NR (1992) The type 1 (EGFR-related) family of growth factor receptors and their ligands. *Prog Growth Factor Res* **4**:1–24.

Rahmim A and Zaidi H (2008) PET versus SPECT: strengths, limitations and challenges. *Nucl Med Commun* **29**:193–207.

Rajendran JG and Krohn KA (2005) Imaging hypoxia and angiogenesis in tumors. *Radiol Clin North Am* **43**:169–187.

Ramos-Suzarte M, Rodríguez N, Oliva JP, Iznaga-Escobar N, Perera A, Morales A, Gonzalez N, Cordero M, Torres L, and Pimentel G, et al. (1999) ^{99m}Tc-labeled antihuman epidermal growth factor receptor antibody in patients with tumors of epithelial origin: Part III. Clinical trials safety and diagnostic efficacy. *J Nucl Med* **40**:768–775.

Rasey JS, Koh WJ, Evans ML, Peterson LM, Lewellen TK, Graham MM, and Krohn KA (1996) Quantifying regional hypoxia in human tumors with positron emission tomography of [^{18}F]fluoromisonidazole: a pretherapy study of 37 patients. *Int J Radiat Oncol Biol Phys* **36**:417–428.

Reubi JC and Waser B (2003) Concomitant expression of several peptide receptors in neuroendocrine tumours: molecular basis for in vivo multireceptor tumour targeting. *Eur J Nucl Med Mol Imaging* **30**:781–793.

Ritter CA and Arteaga CL (2003) The epidermal growth factor receptor-tyrosine kinase: a promising therapeutic target in solid tumors. *Semin Oncol* **30**(1, Suppl 1) 3–11.

Rizvi SN, Visser OJ, Vosjan MJ, van Lingen A, Hoekstra OS, Zijlstra JM, Huijgens PC, van Dongen GA, and Lubberink M (2012) Biodistribution, radiation dosimetry and scouting of ^{90}Y-ibritumomab tiuxetan therapy in patients with relapsed B-cell

non-Hodgkin's lymphoma using 89Zr-ibritumomab tiuxetan and PET. *Eur J Nucl Med Mol Imaging* **39**:512–520.
Robinson SD, Reynolds LE, Wyder L, Hicklin DJ, and Hodivala-Dilke KM (2004) Beta3-integrin regulates vascular endothelial growth factor-A-dependent permeability. *Arterioscler Thromb Vasc Biol* **24**:2108–2114.
Rodari M, Lopci E, Pepe G, Antunovic L, and Chiti A (2011) [^{11}C]-choline PET/CT in imaging locally advanced prostate cancer. *Nucl Med Rev Cent East Eur* **14**: 118–119.
Rosen LS, Hurwitz HI, Wong MK, Goldman J, Mendelson DS, Figg WD, Spencer S, Adams BJ, Alvarez D, and Seon BK, et al. (2012) A phase I first-in-human study of TRC105 (Anti-Endoglin Antibody) in patients with advanced cancer. *Clin Cancer Res* **18**:4820–4829.
Rundhaug JE (2003) Matrix metalloproteinases, angiogenesis, and cancer: commentary re: A. C. Lockhart et al., Reduction of wound angiogenesis in patients treated with BMS-275291, a broad spectrum matrix metalloproteinase inhibitor. Clin. Cancer Res., 9: 00-00, 2003. *Clin Cancer Res* **9**:551–554.
Ryu JS, Kim JS, Moon DH, Kim SM, Shin MJ, Chang JS, Park SK, Han DJ, and Lee HK (2002) Bone SPECT is more sensitive than MRI in the detection of early osteonecrosis of the femoral head after renal transplantation. *J Nucl Med* **43**: 1006–1011.
Sakurai T and Kudo M (2011) Signaling pathways governing tumor angiogenesis. *Oncology* **81** (Suppl 1):24–29.
Saleem A, Charnley N, and Price P (2006) Clinical molecular imaging with positron emission tomography. *Eur J Cancer* **42**:1720–1727.
Santos AF, Huang H, and Tindall DJ (2004) The androgen receptor: a potential target for therapy of prostate cancer. *Steroids* **69**:79–85.
Scher HI, Beer TM, Higano CS, Anand A, Taplin ME, Efstathiou E, Rathkopf D, Shelkey J, Yu EY, and Alumkal J, et al.; Prostate Cancer Foundation/Department of Defense Prostate Cancer Clinical Trials Consortium (2010) Antitumour activity of MDV3100 in castration-resistant prostate cancer: a phase 1-2 study. *Lancet* **375**: 1437–1446.
Schillaci O and Simonetti G (2004) Fusion imaging in nuclear medicine—applications of dual-modality systems in oncology. *Cancer Biother Radiopharm* **19**:1–10.
Schnell O, Krebs B, Carlsen J, Miederer I, Goetz C, Goldbrunner RH, Wester HJ, Haubner R, Pöpperl G, and Holtmannspötter M, et al. (2009) Imaging of integrin α(v)β(3) expression in patients with malignant glioma by [^{18}F] Galacto-RGD positron emission tomography. *Neuro-oncol* **11**:861–870.
Schuetz M, Schmid MP, Pötter R, Kommata S, Georg D, Lukic D, Dudczak R, Kletter K, Dimopoulos J, and Karanikas G, et al. (2010) Evaluating repetitive ^{18}F-fluoroazomycin-arabinoside (^{18}FAZA) PET in the setting of MRI guided adaptive radiotherapy in cervical cancer. *Acta Oncol* **49**:941–947.
Schuster DM, Votaw JR, Nieh PT, Yu W, Nye JA, Master V, Bowman FD, Issa MM, and Goodman MM (2007) Initial experience with the radiotracer anti-1-amino-3-^{18}F-fluorocyclobutane-1-carboxylic acid with PET/CT in prostate carcinoma. *J Nucl Med* **48**:56–63.
Schuurbiers OC, Kaanders JH, van der Heijden HF, Dekhuijzen RP, Oyen WJ, and Bussink J (2009) The PI3-K/AKT-pathway and radiation resistance mechanisms in non-small cell lung cancer. *J Thorac Oncol* **4**:761–767.
Schwarzenböck S, Souvatzoglou M, and Krause BJ (2012) Choline PET and PET/CT in primary diagnosis and staging of prostate cancer. *Theranostics* **2**:318–330.
Seidman AD, Berry D, Cirrincione C, Harris L, Muss H, Marcom PK, Gipson G, Burstein H, Lake D, and Shapiro CL, et al. (2008) Randomized phase III trial of weekly compared with every-3-weeks paclitaxel for metastatic breast cancer, with trastuzumab for all HER-2 overexpressors and random assignment to trastuzumab or not in HER-2 nonoverexpressors: final results of Cancer and Leukemia Group B protocol 9840. *J Clin Oncol* **26**:1642–1649.
Semenza GL (2012) Hypoxia-inducible factors: mediators of cancer progression and targets for cancer therapy. *Trends Pharmacol Sci* **33**:207–214.
Shang B, Cao Z, and Zhou Q (2012) Progress in tumor vascular normalization for anticancer therapy: challenges and perspectives. *Fr Medecine* **6**:67–78.
Shay JW and Bacchetti S (1997) A survey of telomerase activity in human cancer. *Eur J Cancer* **33**:787–791.
Shenker A, Laue L, Kosugi S, Merendino JJ Jr, Minegishi T, and Cutler GB Jr (1993) A constitutively activating mutation of the luteinizing hormone receptor in familial male precocious puberty. *Nature* **365**:652–654.
Shi J, Kim YS, Zhai S, Liu Z, Chen X, and Liu S (2009) Improving tumor uptake and pharmacokinetics of $^{(64)}$Cu-labeled cyclic RGD peptide dimers with Gly$_{(3)}$ and PEG $_{(4)}$ linkers. *Bioconjug Chem* **20**:750–759.
Shi Y (2006) Mechanical aspects of apoptosome assembly. *Curr Opin Cell Biol* **18**: 677–684.
Shields AF, Grierson JR, Dohmen BM, Machulla HJ, Stayanoff JC, Lawhorn-Crews JM, Obradovich JE, Muzik O, and Mangner TJ (1998a) Imaging proliferation in vivo with [F-18]FLT and positron emission tomography. *Nat Med* **4**:1334–1336.
Shields AF, Mankoff DA, Link JM, Graham MM, Eary JF, Kozawa SM, Zheng M, Lewellen B, Lewellen TK, and Grierson JR, et al. (1998b) Carbon-11-thymidine and FDG to measure therapy response. *J Nucl Med* **39**:1757–1762.
Shiue CY and Welch MJ (2004) Update on PET radiopharmaceuticals: life beyond fluorodeoxyglucose. *Radiol Clin North Am* **42**:1033–1053, viii.
Shokeen M, Zheleznyak A, Wilson JM, Jiang M, Liu R, Ferdani R, Lam KS, Schwarz JK, and Anderson CJ (2012) Molecular imaging of very late antigen-4 (α4β1 integrin) in the premetastatic niche. *J Nucl Med* **53**:779–786.
Siegel PM and Massagué J (2003) Cytostatic and apoptotic actions of TGF-beta in homeostasis and cancer. *Nat Rev Cancer* **3**:807–821.
Smith TA (2010) Towards detecting the HER-2 receptor and metabolic changes induced by HER-2-targeted therapies using medical imaging. *Br J Radiol* **83**: 638–644.
Soloviev D, Lewis D, Honess D, and Aboagye E (2012) [(^{18})F]FLT: an imaging biomarker of tumour proliferation for assessment of tumour response to treatment. *Eur J Cancer* **48**:416–424.
Spanaki MV, Spencer SS, Corsi M, MacMullan J, Seibyl J, and Zubal IG (1999) Sensitivity and specificity of quantitative difference SPECT analysis in seizure localization. *J Nucl Med* **40**:730–736.
Spano D, Heck C, De Antonellis P, Christofori G, and Zollo M (2012) Molecular networks that regulate cancer metastasis. *Semin Cancer Biol* **22**:234–249.
Spano D and Zollo M (2012) Tumor microenvironment: a main actor in the metastasis process. *Clin Exp Metastasis* **29**:381–395.
Spiegelberg BD and Hamm HE (2007) Roles of G-protein-coupled receptor signaling in cancer biology and gene transcription. *Curr Opin Genet Dev* **17**:40–44.
Sprague JE, Li WP, Liang K, Achilefu S, and Anderson CJ (2006) In vitro and in vivo investigation of matrix metalloproteinase expression in metastatic tumor models. *Nucl Med Biol* **33**:227–237.
Staller P, Sulitkova J, Lisztwan J, Moch H, Oakeley EJ, and Krek W (2003) Chemokine receptor CXCR4 downregulated by von Hippel-Lindau tumour suppressor pVHL. *Nature* **425**:307–311.
Stanelle J and Pützer BM (2006) E2F1-induced apoptosis: turning killers into therapeutics. *Trends Mol Med* **12**:177–185.
Steelman LS, Abrams SL, Whelan J, Bertrand FE, Ludwig DE, Bäsecke J, Libra M, Stivala F, Milella M, and Tafuri A, et al. (2008) Contributions of the Raf/MEK/ERK, PI3K/PTEN/Akt/mTOR and Jak/STAT pathways to leukemia. *Leukemia* **22**: 686–707.
Su H, Seimbille Y, Ferl GZ, Bodenstein C, Fueger B, Kim KJ, Hsu YT, Dubinett SM, Phelps ME, and Czernin J, et al. (2008) Evaluation of [(^{18})F]gefitinib as a molecular imaging probe for the assessment of the epidermal growth factor receptor status in malignant tumors. *Eur J Nucl Med Mol Imaging* **35**:1089–1099.
Sun H, Mangner TJ, Collins JM, Muzik O, Douglas K, and Shields AF (2005a) Imaging DNA synthesis in vivo with ^{18}F-FMAU and PET. *J Nucl Med* **46**:292–296.
Sun H, Sloan A, Mangner TJ, Vaishampayan U, Muzik O, Collins JM, Douglas K, and Shields AF (2005b) Imaging DNA synthesis with [^{18}F]FMAU and positron emission tomography in patients with cancer. *Eur J Nucl Med Mol Imaging* **32**: 15–22.
Sun X, Niu G, Chan N, Shen B, and Chen X (2011) Tumor hypoxia imaging. *Mol Imaging Biol* **13**:399–410.
Surati M, Patel P, Peterson A, and Salgia R (2011) Role of MetMAb (OA-5D5) in c-MET active lung malignancies. *Expert Opin Biol Ther* **11**:1655–1662.
Tafti BA, Shaba W, Li Y, Yevdayev E, and Berenji GR (2012) Staging and follow-up of lacrimal gland carcinomas by ^{18}F-FDG PET/CT imaging. *Clin Nucl Med* **37**: e249–252.
Takeuchi K and Ito F (2011) Receptor tyrosine kinases and targeted cancer therapeutics. *Biol Pharm Bull* **34**:1774–1780.
Tan H, Chen L, Guan Y, and Lin X (2011) Comparison of MRI, F-18 FDG, and ^{11}C-choline PET/CT for their potentials in differentiating brain tumor recurrence from brain tumor necrosis following radiotherapy. *Clin Nucl Med* **36**:978–981.
Tateishi K, Tateishi U, Sato M, Yamanaka S, Kanno H, Murata H, Inoue T, and Kawahara N (2013) Application of ^{62}Cu-diacetyl-bis (N^4-methylthiosemicarbazone) PET imaging to predict highly malignant tumor grades and hypoxia-inducible factor-1α expression in patients with glioma. *AJNR Am J Neuroradiol* **34**:92–99.
te Beek ET, de Boer P, Moerland M, Schmidt ME, Hoetjes NJ, Windhorst AD, van Berckel BN, Cohen AF, van Gerven JM, and Lammertsma AA (2012) In vivo quantification of striatal dopamine D2 receptor occupancy by JNJ-37822681 using [^{11}C]raclopride and positron emission tomography. *J Psychopharmacol* **26**: 1128–1135.
Teicher BA and Fricker SP (2010) CXCL12 (SDF-1)/CXCR4 pathway in cancer. *Clin Cancer Res* **16**:2927–2931.
Ter-Pogossian MM and Herscovitch P (1985) Radioactive oxygen-15 in the study of cerebral blood flow, blood volume, and oxygen metabolism. *Semin Nucl Med* **15**: 377–394.
Thorwarth D, Eschmann SM, Holzner F, Paulsen F, and Alber M (2006) Combined uptake of [^{18}F]FDG and [^{18}F]FMISO correlates with radiation therapy outcome in head-and-neck cancer patients. *Radiother Oncol* **80**:151–156.
Tsai CM, Chang KT, Perng RP, Mitsudomi T, Chen MH, Kadoyama C, and Gazdar AF (1993) Correlation of intrinsic chemoresistance of non-small-cell lung cancer cell lines with HER-2/neu gene expression but not with ras gene mutations. *J Natl Cancer Inst* **85**:897–901.
Turpeenniemi-Hujanen T (2005) Gelatinases (MMP-2 and -9) and their natural inhibitors as prognostic indicators in solid cancers. *Biochimie* **87**:287–297.
Ujula T, Huttunen M, Luoto P, Peräkylä H, Simpura I, Wilson I, Bergman M, and Roivainen A (2010) Matrix metalloproteinase 9 targeting peptides: syntheses, ^{68}Ga-labeling, and preliminary evaluation in a rat melanoma xenograft model. *Bioconjug Chem* **21**:1612–1621.
Urban NB, Slifstein M, Thompson JL, Xu X, Girgis RR, Raheja S, Haney M, and Abi-Dargham A (2012) Dopamine release in chronic cannabis users: a [^{11}c]raclopride positron emission tomography study. *Biol Psychiatry* **71**:677–683.
Vanhaesebroeck B and Alessi DR (2000) The PI3K-PDK1 connection: more than just a road to PKB. *Biochem J* **346**:561–576.
van Waarde A, Rybczynska AA, Ramakrishnan N, Ishiwata K, Elsinga PH, and Dierckx RA (2010) Sigma receptors in oncology: therapeutic and diagnostic applications of sigma ligands. *Curr Pharm Des* **16**:3519–3537.
Vanzetta I (2006) Hemodynamic responses in cortex investigated with optical imaging methods. Implications for functional brain mapping. *J Physiol Paris* **100**: 201–211.
Vävere AL, Kridel SJ, Wheeler FB, and Lewis JS (2008) 1-^{11}C-Acetate as a PET radiopharmaceutical for imaging fatty acid synthase expression in prostate cancer. *J Nucl Med* **49**:327–334.
Velikyan I (2012) Molecular imaging and radiotherapy: theranostics for personalized patient management. *Theranostics* **2**:424–426.
Vilner BJ, John CS, and Bowen WD (1995) Sigma-1 and sigma-2 receptors are expressed in a wide variety of human and rodent tumor cell lines. *Cancer Res* **55**: 408–413.

Vivanco I and Sawyers CL (2002) The phosphatidylinositol 3-Kinase AKT pathway in human cancer. *Nat Rev Cancer* **2**:489–501.

Vogel CL, Cobleigh MA, Tripathy D, Gutheil JC, Harris LN, Fehrenbacher L, Slamon DJ, Murphy M, Novotny WF, and Burchmore M, et al. (2002) Efficacy and safety of trastuzumab as a single agent in first-line treatment of HER2-overexpressing metastatic breast cancer. *J Clin Oncol* **20**:719–726.

Vosjan MJ, Vercammen J, Kolkman JA, Stigter-van Walsum M, Revets H, and van Dongen GA (2012) Nanobodies targeting the hepatocyte growth factor: potential new drugs for molecular cancer therapy. *Mol Cancer Ther* **11**:1017–1025.

Wald O, Shapira OM, and Izhar U (2013) CXCR4/CXCL12 axis in non small cell lung cancer (NSCLC) pathologic roles and therapeutic potential. *Theranostics* **3**:26–33.

Wan W, Guo N, Pan D, Yu C, Weng Y, Luo S, Ding H, Xu Y, Wang L, and Lang L, et al. (2013) First experience of ^{18}F-alfatide in lung cancer patients using a new lyophilized kit for rapid radiofluorination. *J Nucl Med* **54**:691–698.

Wang C and Youle RJ (2009) The role of mitochondria in apoptosis. *Annu Rev Genet* **43**:95–118.

Wang H, Cai W, Chen K, Li ZB, Kashefi A, He L, and Chen X (2007a) A new PET tracer specific for vascular endothelial growth factor receptor 2. *Eur J Nucl Med Mol Imaging* **34**:2001–2010.

Wang H, Gao H, Guo N, Niu G, Ma Y, Kiesewetter DO, and Chen X (2012) Site-specific labeling of scVEGF with fluorine-18 for positron emission tomography imaging. *Theranostics* **2**:607–617.

Wang H, Yu JM, Yang GR, Song XR, Sun XR, Zhao SQ, Wang XW, and Zhao W (2007b) Further characterization of the epidermal growth factor receptor ligand ^{11}C-PD153035. *Chin Med J (Engl)* **120**:960–964.

Wang J and Maurer L (2005) Positron emission tomography: applications in drug discovery and drug development. *Curr Top Med Chem* **5**:1053–1075.

Wang J, Sui M, and Fan W (2010) Nanoparticles for tumor targeted therapies and their pharmacokinetics. *Curr Drug Metab* **11**:129–141.

Weber WA, Wester HJ, Grosu AL, Herz M, Dzewas B, Feldmann HJ, Molls M, Stöcklin G, and Schwaiger M (2000) O-(2-[^{18}F]fluoroethyl)-L-tyrosine and L-[methyl-^{11}C]methionine uptake in brain tumours: initial results of a comparative study. *Eur J Nucl Med* **27**:542–549.

Weiss ID and Jacobson O (2013) Molecular imaging of chemokine receptor CXCR4. *Theranostics* **3**:76–84.

Weiss ID, Jacobson O, Kiesewetter DO, Jacobus JP, Szajek LP, Chen X, and Farber JM (2012) Positron emission tomography imaging of tumors expressing the human chemokine receptor CXCR4 in mice with the use of ^{64}Cu-AMD3100. *Mol Imaging Biol* **14**:106–114.

Wirth T, Kühnel F, and Kubicka S (2005) Telomerase-dependent gene therapy. *Curr Mol Med* **5**:243–251.

Wu FC (1992) Testicular steroidogenesis and androgen use and abuse. *Baillieres Clin Endocrinol Metab* **6**:373–403.

Xie X, Li L, Xiao X, Guo J, Kong Y, Wu M, Liu W, Gao G, Hsu JL, and Wei W, et al. (2012) Targeted expression of BikDD eliminates breast cancer with virtually no toxicity in noninvasive imaging models. *Mol Cancer Ther* **11**:1915–1924.

Yang M, Gao H, Sun X, Yan Y, Quan Q, Zhang W, Mohamedali KA, Rosenblum MG, Niu G, and Chen X (2011a) Multiplexed PET probes for imaging breast cancer early response to VEGF$_{121}$/rGel treatment. *Mol Pharm* **8**:621–628.

Yang M, Gao H, Zhou Y, Ma Y, Quan Q, Lang L, Chen K, Niu G, Yan Y, and Chen X (2011b) ^{18}F-labeled GRPR agonists and antagonists: A comparative study in prostate cancer imaging. *Theranostics* **1**:220–229.

Yang X, Hong H, Grailer JJ, Rowland IJ, Javadi A, Hurley SA, Xiao Y, Yang Y, Zhang Y, and Nickles RJ, et al. (2011c) cRGD-functionalized, DOX-conjugated, and ^{64}Cu-labeled superparamagnetic iron oxide nanoparticles for targeted anticancer drug delivery and PET/MR imaging. *Biomaterials* **32**:4151–4160.

Yarden Y and Sliwkowski MX (2001) Untangling the ErbB signalling network. *Nat Rev Mol Cell Biol* **2**:127–137.

Yeh HH, Ogawa K, Balatoni J, Mukhapadhyay U, Pal A, Gonzalez-Lepera C, Shavrin A, Soghomonyan S, Flores L 2nd, and Young D, et al. (2011) Molecular imaging of active mutant L858R EGF receptor (EGFR) kinase-expressing nonsmall cell lung carcinomas using PET/CT. *Proc Natl Acad Sci USA* **108**:1603–1608.

Yhee JY, Kim SA, Koo H, Son S, Ryu JH, Youn IC, Choi K, Kwon IC, and Kim K (2012) Optical imaging of cancer-related proteases using near-infrared fluorescence matrix metalloproteinase-sensitive and cathepsin B-sensitive probes. *Theranostics* **2**:179–189.

Yin D, He Y, Perera MA, Hong SS, Marhefka C, Stourman N, Kirkovsky L, Miller DD, and Dalton JT (2003) Key structural features of nonsteroidal ligands for binding and activation of the androgen receptor. *Mol Pharmacol* **63**:211–223.

Yoshimoto M, Waki A, Yonekura Y, Sadato N, Murata T, Omata N, Takahashi N, Welch MJ, and Fujibayashi Y (2001) Characterization of acetate metabolism in tumor cells in relation to cell proliferation: acetate metabolism in tumor cells. *Nucl Med Biol* **28**:117–122.

Yu EY, Muzi M, Hackenbracht JA, Rezvani BB, Link JM, Montgomery RB, Higano CS, Eary JF, and Mankoff DA (2011) C11-acetate and F-18 FDG PET for men with prostate cancer bone metastases: relative findings and response to therapy. *Clin Nucl Med* **36**:192–198.

Yu ST, Yang YB, Liang GP, Li C, Chen L, Shi CM, Tang XD, Li CZ, Li L, and Wang GZ, et al. (2010) An optimized telomerase-specific lentivirus for optical imaging of tumors. *Cancer Res* **70**:2585–2594.

Yu XF and Han ZC (2006) Matrix metalloproteinases in bone marrow: roles of gelatinases in physiological hematopoiesis and hematopoietic malignancies. *Histol Histopathol* **21**:519–531.

Yuan H, Schroeder T, Bowsher JE, Hedlund LW, Wong T, and Dewhirst MW (2006) Intertumoral differences in hypoxia selectivity of the PET imaging agent ^{64}Cu(II)-diacetyl-bis(N^4-methylthiosemicarbazone). *J Nucl Med* **47**:989–998.

Yun M, Bang SH, Kim JW, Park JY, Kim KS, and Lee JD (2009) The importance of acetyl coenzyme A synthetase for ^{11}C-acetate uptake and cell survival in hepatocellular carcinoma. *J Nucl Med* **50**:1222–1228.

Zhang L, Virani S, Zhang Y, Bhojani MS, Burgess TL, Coxon A, Galban CJ, Ross BD, and Rehemtulla A (2011a) Molecular imaging of c-Met tyrosine kinase activity. *Anal Biochem* **412**:1–8.

Zhang MR, Kumata K, Hatori A, Takai N, Toyohara J, Yamasaki T, Yanamoto K, Yui J, Kawamura K, and Koike S, et al. (2010) [^{11}C]Gefitinib ([^{11}c]Iressa): radiosynthesis, in vitro uptake, and in vivo imaging of intact murine fibrosarcoma. *Mol Imaging Biol* **12**:181–191.

Zhang W, Ling D, Tan J, Zhang J, and Li L (2013a) Expression of urokinase plasminogen activator and plasminogen activator inhibitor type-1 in ovarian cancer and its clinical significance. *Oncol Rep* **29**:637–645.

Zhang X, Paule MG, Newport GD, Zou X, Sadovova N, Berridge MS, Apana SM, Hanig JP, Slikker W Jr, and Wang C (2009) A minimally invasive, translational biomarker of ketamine-induced neuronal death in rats: microPET Imaging using ^{18}F-annexin V. *Toxicol Sci* **111**:355–361.

Zhang X, Xiong Z, Wu Y, Cai W, Tseng JR, Gambhir SS, and Chen X (2006) Quantitative PET imaging of tumor integrin alphavbeta3 expression with ^{18}F-FRGD2. *J Nucl Med* **47**:113–121.

Zhang Y, Hong H, and Cai W (2011b) PET tracers based on Zirconium-89. *Curr Radiopharm* **4**:131–139.

Zhang Y, Hong H, Engle JW, Bean J, Yang Y, Leigh BR, Barnhart TE, and Cai W (2011c) Positron emission tomography imaging of CD105 expression with a 64Cu-labeled monoclonal antibody: NOTA is superior to DOTA. *PLoS ONE* **6**: e28005.

Zhang Y, Hong H, Orbay H, Valdovinos HF, Nayak TR, Theuer CP, Barnhart TE, and Cai W (2013b) PET imaging of CD105/endoglin expression with a $^{61/64}$Cu -labeled Fab antibody fragment. *Eur J Nucl Med Mol Imaging* **40**:759–767.

Zhang Y, Hong H, Severin GW, Engle JW, Yang Y, Goel S, Nathanson AJ, Liu G, Nickles RJ, and Leigh BR, et al. (2012) ImmunoPET and near-infrared fluorescence imaging of CD105 expression using a monoclonal antibody dual-labeled with (^{89})Zr and IRDye 800CW. *Am J Transl Res* **4**:333–346.

Zhao J, Lu Y, and Shen HM (2012) Targeting p53 as a therapeutic strategy in sensitizing TRAIL-induced apoptosis in cancer cells. *Cancer Lett* **314**:8–23.

Zhao P, Grabinski T, Gao C, Skinner RS, Giambernardi T, Su Y, Hudson E, Resau J, Gross M, and Vande Woude GF, et al. (2007) Identification of a met-binding peptide from a phage display library. *Clin Cancer Res* **13**:6049–6055.

Zheng QH, Fei X, DeGrado TR, Wang JQ, Stone KL, Martinez TD, Gay DJ, Baity WL, Mock BH, and Glick-Wilson BE, et al. (2003) Synthesis, biodistribution and micro-PET imaging of a potential cancer biomarker carbon-11 labeled MMP inhibitor (2R)-2-[[4-(6-fluorohex-1-ynyl)phenyl]sulfonylamino]-3-methylbutyric acid [^{11}C] methyl ester. *Nucl Med Biol* **30**:753–760.

Zheng QH, Fei X, Liu X, Wang JQ, Stone KL, Martinez TD, Gay DJ, Baity WL, Miller KD, and Sledge GW, et al. (2004) Comparative studies of potential cancer biomarkers carbon-11 labeled MMP inhibitors (S)-2-(4′-[^{11}C]methoxybiphenyl-4-sulfonylamino)-3-methylbutyric acid and N-hydroxy-(R)-2-[[(4′-[^{11}C]methoxyphenyl)sulfonyl]benzylamino]-3-methylbutanamide. *Nucl Med Biol* **31**:77–85.

Zhu L, Zhang F, Ma Y, Liu G, Kim K, Fang X, Lee S, and Chen X (2011) In vivo optical imaging of membrane-type matrix metalloproteinase (MT-MMP) activity. *Mol Pharm* **8**:2331–2338.

Zimny M, Gagel B, DiMartino E, Hamacher K, Coenen HH, Westhofen M, Eble M, Buell U, and Reinartz P (2006) FDG—a marker of tumour hypoxia? A comparison with [^{18}F]fluoromisonidazole and pO_2-polarography in metastatic head and neck cancer. *Eur J Nucl Med Mol Imaging* **33**:1426–1431.